Title
COHERENCE IN MULTILEVEL SYSTEMS

Author
Breiland, William George.

Publication Date
1975-07-01

LBL-3917
c.1

COHERENCE IN MULTILEVEL SYSTEMS

William George Breiland
(Ph. D. thesis)

July 1975

Prepared for the U. S. Energy Research and
Development Administration under Contract W-7405-ENG-48

LBL-3917
c.1

I dedicate this work to my parents. To my father I owe any ability to look at the world and see simple basic forms, and to my mother I owe the patience to deal with the world as it really is.

One does not learn from failures, but from the new attempts that are made after the failures.

(From a Fortune Cookie)

Table of Contents

COHERENCE IN MULTILEVEL SYSTEMS

William George Breiland

Inorganic Materials Research Division, Lawrence Berkeley Laboratory
and Department of Chemistry; University of California,
Berkeley, California 94720

ABSTRACT

Mathematical descriptions of an excited state multilevel system are developed to include progressively the effects of coherent coupling, feeding, decay and relaxation, and the expressions are illustrated with several pulse coherence experiments utilizing zero field optically detected magnetic resonance of excited triplet states.

A new method is described in which the time development of the coherent components in a multilevel system is monitored by using an observable that can measure only relative populations between the levels. The method is illustrated with zero field magnetic resonance experiments, and extension of the method to optical frequency pulse experiments is discussed.

By treating a coherently driven excited state system as two levels in contact with a population reservoir, exact expressions are obtained for both transient and steady-state behavior in the presence of transverse and spin lattice relaxation, constant incoherent pumping, spontaneous emission between the two levels, and also decay back into the reservoir. The development reveals that a substantial steady-state coherent component may be maintained by the application of a high power off resonance driving field, and in many cases this component could be orders of magnitude larger than the component that is maintained by applying an on resonance driving field. In view of the possible significance that this may have in the optical frequency region, experimental verification of the steady-state component for zero field triplet states is presented.

After formulating the general mathematical development, it is applied specifically to zero field microwave phosphorescence double resonance. Experimental methods and apparatus are discussed in detail and results of optically detected transient nutations, spin echoes, and Fourier transform spectroscopy are presented. In addition, the effects of allowedness, molecular orientation, and driving field inhomogeneities are described and methods for either eliminating these effects or utilizing them to gain further information are discussed.

Note on the References Cited

The text of this work references either the original paper, or, where references would be too numerous, a review article or text, in the hope that the reader is led to the most pertinent source. In addition to these fundamental works, the reference section contains a selected list of related papers that have been the most helpful to me.

SUMMARY OF FREQUENTLY USED SYMBOLS

F	feeding matrix (45) or vector (77)
F_x	constant feeding rate into lower level
F_y	constant feeding rate into upper level
f	allowedness or transition dipole moment factor $0 \leqslant f \leqslant 1$
$g(\omega_o - \bar{\omega}_o)$	inhomogeneous distribution function centered at an average frequency, $\bar{\omega}_o$
$\gamma(\omega_1)$	inhomogeneous driving field distribution function
K	decay matrix (43)
k_A	average of decay constants $\frac{k_x + k_y}{2}$
k_D	difference of decay constants $\frac{k_x - k_y}{2}$
k_x	decay rate constant from lower level
k_y	decay rate constant from upper level
N	total population $r_y + r_x$
N^o	total population in absence of a driving field under steady-state conditions $r_y^o + r_x^o$
N^s	total population in presence of a driving field under steady-state conditions $r_y^s + r_x^s$
Q	non-unitary "evolution operator" (49) and (51)
r_j	$j = 1,2,3,x,y$ vector model components (4), (7), (50)
r_j^o	components in absence of a driving field under steady-state conditions (54) or (73)
$r_j(o)$	initial value of components
r_j^s	components in presence of a driving field under steady-state conditions (56) or (73)
S	time evolution operator (20) in absence of relaxation
σ_j	$j = 1,2,3$ Pauli spin matricies (8)

T	effective transverse relaxation time (73)
T_e	effective transverse relaxation time (73)
T_x	spin-lattice relaxation time for lower to upper level transition
T_y	spin-lattice relaxation time for upper to lower level transition
T_1	total spin-lattice relaxation time (71)
T_2	homogeneous relaxation time
T_{2e}	homogeneous relaxation time along applied field direction
T_2^*	inhomogeneous relaxation time
t_1	effective relaxation time (55)
t_2	effective relaxation time (55)
τ	effective relaxation time (73)
U	rotating frame unitary operator (15), (91)
ω	driving field frequency
ω_o	$\hbar\omega_o$ = energy level splitting in two-level system
ω_1	driving field amplitude
$\bar{\omega}$	$\sqrt{\omega_1^2 + \Delta\omega^2}$ (21) nutation frequency
$\bar{\omega}_o$	central frequency of inhomogeneous line
$\Delta\omega$	$\omega_o - \omega$ off-resonance frequency
$\overline{\Delta\omega}$	$\bar{\omega}_o - \omega$ off-resonance frequency for inhomogeneous line

I. INTRODUCTION

A. Introductory Remarks

This work resulted and grew largely from a desire by the author to find a rigorous and fundamental mathematical description for the optical detection of magnetic resonance in zero field, particularly as it applies to the effects of feeding and decay in the presence of a coherent driving field. As new experiments and techniques were being developed to measure coherence in the excited states of molecular crystals, it became quite apparent that the well-known formalism of conventional magnetic resonance coherence experiments had limited applicability to the excited state problem, owing to the fact that the total population is not conserved in such a situation. Investigation resulted in a problem that deals with the basic nature of a two level system, and rediscovery of the fascinating link between magnetic resonance, optical spectroscopy, and maser systems that evolves from such a study has been most rewarding.

The aim of the formal development presented in the following chapters is not to concoct "high-powered" mathematical solutions to a very general problem. The models and resulting expressions are purposefully kept as simple as possible, in the hope that the physics of the problem is never hidden in complicated equations. The state of experimental development in this field has just begun to evolve, and at this stage it is far more important to gain a semiquantitative understanding of basic effects before an attempt is made to "fit" a given set of data to a realistic mathematical model. In this way the full range of experimental possibilities may be realized by utilizing a basic and easily visualized theory that has sufficient mathematical rigor to set the principles firmly. Much of the material presented here is a collection of facts, each of which may be well-known in some specific field, but they are not necessarily well-known by all. These formalisms are presented in order to convince both the reader and the author that they may indeed be carried over from their respective fields, and, with the proper considerations and additions, form a reasonable description of observed experimental data.

The author has endeavored to include within the formalism all the basic quantum mechanics that is relevent to the problem, and this effort would therefore be considered successful if any observed deviations from the ideal expressions presented here actually contain information relating to the molecular dynamics or excited state structure of a particular system, and are not simply trivial oversights dealing with results that are characteristic of all two-level systems. In addition, it is hoped that some of the new viewpoints presented here, such as the probe pulse method, will in turn prove to be useful and lend additional insight to the fields from which the basics were taken.

B. Historical Context

The first double resonance experiments measured changes in Zeeman level populations induced by radio frequency fields by monitoring the fluorescence emission from these levels.[1,2] The method, which was originally done for gas phase atomic systems, was adapted to inorganic solids by Geschwind et al.,[3,4] and was applied considerably later to triplet state molecular solids.[5,6] This delay was perhaps due largely to the fact that conventional EPR of excited triplet state organic solids remained an elusive problem until it was firmly established by Hutchison and Mangum in 1961.[7,8] Immediately following the high field double resonance experiments, optically detected magnetic resonance (ODMR) was observed in zero field.[9] Following these preliminary experiments, a profusion of techniques related to zero field ODMR appeared, the major contributions being phosphorescence-microwave double resonance (PMDR),[10] and the optical detection of ENDOR[11] and EEDOR.[12] The relavent Hamiltonians that contribute to the hyperfine structure of the triplet state energy levels were elucidated as fast as the experimental techniques were developed, and are now very well documented in a number of review articles[13-15] and books.[16-18]

It became rapidly apparent that ODMR could provide a vast wealth of information dealing with the excited state that was unattainable by other methods. Since optical frequency photons are used to monitor the resonance, the sensitivity can be increased by a factor of 10^4 over conventional methods of detection. In addition excited states whose lifetimes were far too short for conventional detection could easily be monitored by double resonance techniques.

The triplet states of organic molecules are nondegenerate in zero field owing to the anisotropic distribution of electron spin density and the dipolar interaction between the electrons. This fact has opened equally wide vistas for the investigation of organic excited states through the use of zero field ODMR. This field has the following advantages.

1.) Optical detection allows one to eliminate the application of an external field.[13] The increased splitting of the triplet state levels is negligible compared to optical frequencies and affords no increase in sensitivity.

In fact, an external field becomes a hinderance since it tends to broaden EPR lines, increase spin-lattice relaxation, and decrease the natural spin alignment that occurs in zero field. In zero field the system is left to itself and the resulting measurements that are obtained reflect more directly the actual properties of the molecule.

2.) Magnetic resonance may be done on randomly oriented molecules[13] since the transition moment of the microwave transition merely "takes the projection" of the magnetic component of the oscillating microwave field. The triplet state splittings are determined intrinsically and do not depend on the orientation of the molecule.

3.) At sufficiently low temperatures sensitivity is enhanced even further by the fact that most organic molecules possess "preferential" or unequal populating mechanisms to the triplet state spin sublevels that may result in highly non-Boltzman population distributions.[19]

All the above features make zero field ODMR a particularly unique tool, and studies that have utilized this technique have revealed such diverse phenomena[13,15] as zero field splittings, internal and external hyperfine interactions, excited and ground state nuclear quadrapole coupling constants, relative radiative, non-radiative, and intersystem crossing rates, steady-state relative populations, individual triplet spin sublevel lifetimes, energy migration and trapping times, symmetry assignments for excited states and vibronic progressions, energy level anticrossing, and can be used to measure subtle effects related to radiationless relaxation theory.[20]

Despite the rapid advance of this field as outlined above, one major aspect of magnetic resonance was lacking in zero-field ODMR, namely coherence experiments. This situation existed simply because the standard experiments such as a spin echo could not be monitored directly with the double resonance technique. The first ramifications of coherent coupling in triplet states were considered by Harris[21] and optically detected transient nutations were observed subsequently.[22] Schmidt[23] observed the first spin echo in the excited triplet state by conventional techniques. In 1973 a new method[24] for observing coherence by means of the double resonance technique was developed and provided a means to introduce the highly informative field of relaxation measurements to zero-field ODMR. It was at this point that explicit expressions were required to help formulate a working model that could deal with the effects of feeding and decay on a coherently driven excited state system, and provided a basis for the work presented in this thesis.

C. Basis for the Treatment

The rigid restrictions placed on the interaction of light with matter by the resonance condition allows one in many cases to treat a complicated spectroscopy problem as the superposition of responses from a large number of two-level systems having different properties. This situation is particularly advantageous for a number of reasons. First, the time evolution of a two-level system may be solved exactly for all strengths of the driving field, and the standard textbook approach utilizing first order perturbation theory follows as a special case of very low driving-field strength. Second, the exact time evolution of the two-level system may be easily visualized in terms of a three dimensional vector that precesses about a well defined direction that is determined by the conditions of the experiment. This feature is perhaps the most important since the experimentalist may invent a sophisticated pulse sequence that requires a rather formidable set of analytical expressions to describe, but nonetheless, the sequence can be easily visualized by "wagging his fingers" according to the geometrical picture. Third, the applicability of the formalism is perfectly general for practically all regions of the electromagnetic spectrum and provides a satisfying link between magnetic resonance, in which coherence effects have been observed since its beginnings, and the optical region where a rich variety of coherence effects have only begun to be observed.

By assuming only that the triplet state can be made insensitive to the effects of spin-lattice relaxation, one may neglect the "odd" level and treat the problem as a two-level system. The formalism presented in Chapters II, III, and IV assumes this condition from the outset. The solutions are applicable to all regions of the spectrum, although care must be exercised when applying the results to the optical region, as will be discussed.

The development is arranged in order of increasing complexity, partially for pedagogical reasons and also to present a series of solutions, the simplest one of which may then be appropriately applied to a specific problem. Chapter II treats the coherently driven two-level system in the absence of relaxation. Chapter III presents a new method for monitoring coherence by means of a double resonance experiment and demonstrates the near equivalence between the new and conventional methods. The effects of feeding and decay are considered in Chapter IV, and, with the addition of relaxation, complete solutions are obtained for both steady-state and transients. Chapter V deals with the specific applications of these results to zero-field ODMR experiments and a detailed account is given of the experimental methods and apparatus that are utilized to perform coherence experiments on zero-field excited triplet states.

II. BASIC THEORY

This chapter deals with the basic considerations of coherent coupling between two well defined eigenstates in the absence of relaxation or lifetime considerations. Although the problem is easily soluble by a direct Schrödinger equation approach, a density matrix[25,26] solution will be presented here in order to lay a foundation for the more complicated treatments to follow. In addition, the density matrix provides the most direct link between mathematical formalism and the geometrical picture. This particular problem has been solved since the beginnings of quantum theory, but since it forms the base of what is to follow, the formalism will be presented again in an approach that represents contemporary concepts of a two-level system.

The equations developed in Chapters II-IV apply to an ensemble of a large number of weakly interacting two-level systems. A semiclassical approach is taken for the driving field which implies that the field is not quantized, and it is assumed that the wavelength of the radiation is large compared to the size of each two-level system, allowing the usual dipole approximation to be used. Furthermore, the wavelength of the radiation is assumed at first to be large compared to the entire ensemble, allowing the spatial effects of the driving field to be ignored. These spatial effects will be dealt with at the end of Chapter IV. Finally, fields that are produced by the ensemble itself are assumed to be negligible compared to the driving field strength. All these approximations are quite valid, except the last, which must be assumed in order to avoid the inclusion of a complicated set of non-linear coupled Schrödinger and Maxwell equations that are generally insoluable. This inclusion not only complicates the situation beyond intuition, but also deals with a problem that is quite removed from the original purpose of this work, and the treatment given here will thus be restricted to "thin samples".

A. Coherent Coupling and the Geometrical Representation

Consider an ensemble of two-level systems characterized by the non-degenerate states $|y\rangle$ and $|x\rangle$, with Eigenvalues $\hbar\omega_0/2$ and $-\hbar\omega_0/2$, respectively that result from a time independent Hamiltonian $\mathcal{H}_0$. At time t=o the entire ensemble is subjected to the <u>same</u> perturbation, V(t), and the density matrix[25,26] will evolve in time according to the relation (The use of primed notation is necessary for the next section).

$$i\hbar\, \dot{\rho}'(t) = \left[\mathcal{H}_0 + V(t),\ \rho'(t)\right] \tag{1}$$

If the ensemble consists of N independent systems all experiencing the same V(t), the ensemble average that is implied for $\rho'(t)$ becomes a trivial multiplicative factor, N/N, and Eq(1) reduces to the equation of motion for a single two-level system. If this situation can be made to occur, V(t) couples the two levels <u>coherently</u>. Experimentally one needs only to apply a perturbation of sufficient strength (compared to the interactions coupling the individual members of the ensemble) in order to observe the manifestations of coherent coupling.

For a single system the density matrix is just the projection operator for the state at time t, $|t\rangle$. In terms of the usual time-dependent coefficients, the state $|t\rangle$ is given by

$$|t\rangle = y|y\rangle + x|x\rangle \tag{2}$$

so that in the y-x basis an explicit form for the density matrix is given by

$$\rho'(t) = |t\rangle\langle t| = \begin{bmatrix} yy^* & yx^* \\ xy^* & xx^* \end{bmatrix} \tag{3}$$

The geometrical interpretation of Eq(1) was first introduced by Feynman, Vernon, and Hellwarth (FVH).[27] A vector may be constructed from linear combinations of the time-dependent coefficients

$$\begin{aligned} r_1 &= yx^* + xy^* \\ r_2 &= i(yx^* - xy^*) \\ r_3 &= yy^* - xx^* \end{aligned} \tag{4}$$

and, in terms of the vector $\vec{r}$, Eq(1) takes the form

$$\dot{\vec{r}} = \vec{\Omega} \times \vec{r} \tag{5}$$

where the components of Ω are given by

$$\begin{aligned} \Omega_1 &= (V_{yx} + V_{xy})/\hbar \\ \Omega_2 &= (V_{yx} - V_{xy})/\hbar \\ \Omega_3 &= \omega_o \end{aligned} \tag{6}$$

The particular forms for Eqs(4) may be justified by a result from group theory.[28] Since the vector rotation group has a two dimensional irreducible representation, it follows that a three dimensional vector may be represented by a two dimensional matrix. One choice is the well-known vector identity for <u>any</u> 2X 2 matrix, ρ,

$$\rho = 1/2(I + \vec{r}\cdot\vec{\sigma}) = 1/2 \begin{bmatrix} 1 + r_3 & r_1 - ir_2 \\ r_1 + ir_2 & 1 - r_3 \end{bmatrix} \tag{7}$$

Where I is the identity matrix and $\vec{\sigma}$ is the Pauli spin matrix vector with components

$$\begin{aligned} \sigma_1 &= \begin{pmatrix} o & 1 \\ 1 & o \end{pmatrix} \\ \sigma_2 &= \begin{pmatrix} o & -i \\ i & o \end{pmatrix} \\ \sigma_3 &= \begin{pmatrix} 1 & o \\ o & -1 \end{pmatrix} \end{aligned} \tag{8}$$

Note that Eq(7) is consistent with Eqs (3) and (4).

By representing $\rho'(t)$ as the matrix ρ in Eq(7), the total Hamiltonian $\mathcal{H}' = \mathcal{H}_o + V(t)$ as $\hbar\vec{\Omega}\cdot\vec{\sigma}/2$, and from Eq(1) and the identity

$$[\vec{\Omega}\cdot\vec{\sigma},\ \vec{r}\cdot\vec{\sigma}] = 2i(\vec{\Omega} \times \vec{r})\cdot\vec{\sigma} \qquad (9)$$

Eq(5) follows.

In terms of Fano's operational approach to the density matrix,[25] Eq(7) describes the density matrix as a minimum information term, I/2, plus three matricies whose expectation values provide a simple geometrical interpretation of the equation of motion. These three parameters serve to completely describe the system.

The true value of the geometrical representation lies in the simply visualized equation of motion for r described in Eq(5) as a precession of the r-vector about a direction defined by Ω. The fact that Eq(5) is identical in form to the torque equation of magnetic resonance[29] is, of course, not a coincidence since the Zeeman spin 1/2 system is a special case of this general treatment. This similarity in form allows one to visualize experiments based on magnetic resonance analogies that would not be readily apparent from a straightforward density matrix or Schrödinger equation approach, the "photon echo" experiment[30,31] perhaps being the best example of such an extension. The experiments described in the following chapters are all based on this concept.

B. Rotating Frame Transformation

By far the most common form of perturbation term V(t) that is used to couple the two levels in question is a linearly polarized electromagnetic field given in general by (semiclassical approximation)

$$V(t) = \hbar\, \omega_1\, \mu \cos(\omega t + \phi) \qquad (10)$$

where ω_1 is proportional to the strength of the applied field, μ is the quantum mechanical operator that contains off-diagonal elements in the y-x basis and is usually related to an electric or magnetic dipole transition, ω is the frequency of the driving field, and ϕ is the phase of the applied field. Without loss of generality μ may be considered to have real matrix elements (complex matrix elements cause only a trivial phase shift) and one may thus either incorporate the "allowedness" of the transition into ω_1 or leave it in an explicit form $f\omega_1$, $0 \leqslant f \leqslant 1$, and set $\mu = \sigma_1$ (Eq(8)). The "f value" becomes an important consideration when one is attempting to coherently couple a multiplet structure that contains lines of different allowedness, or f values, as is often the case in excited triplet states.

If ω is near the resonance frequency, ω_o, only one circularly polarized component of V(t) is important,[32,33] resulting in a total Hamiltonian $\mathcal{H}'$ given by

$$\mathcal{H}' = \mathcal{H}_o + V(t) \tag{11}$$

$$\mathcal{H}' \cong \frac{\hbar\omega_o}{2}\sigma_3 + \frac{\hbar f\omega_1}{2} e^{\frac{-i\sigma_3(\omega t + \phi)}{2}} \sigma_1 e^{\frac{i\sigma_3(\omega t + \phi)}{2}} \tag{12}$$

The second term in Eq(12) comes from the rotating field approximation

$$\begin{aligned} \omega_1 \sigma_1 \cos(\omega t + \phi) &\cong \omega_1 \Bigg(\frac{\sigma_1}{2}\cos(\omega t + \phi) + \frac{\sigma_2}{2}\sin(\omega t + \phi) \\ \text{ignore:} \qquad &\qquad + \frac{\sigma_1}{2}\cos(\omega t + \phi) - \frac{\sigma_2}{2}\sin(\omega t + \phi)\Bigg) \end{aligned} \tag{13}$$

and the exponential operator identity

$$\frac{\omega_1}{2}\Big(\sigma_1 \cos(\omega t + \phi) + \sigma_2 \sin(\omega t + \phi)\Big) = \frac{\omega_1}{2} e^{\frac{-i\sigma_3(\omega t + \phi)}{2}} \sigma_1 e^{\frac{i\sigma_3(\omega t + \phi)}{2}} \tag{14}$$

The time-dependent terms in Eq(12) make the solution of Eq(1) difficult, but this problem may be eliminated by a suitable unitary transformation that looks very much like the interaction picture. Let U be given by

$$U = \exp\left(\frac{-i\omega\mathcal{H}_o t}{\hbar\omega_o}\right) = e^{\frac{-i\sigma_3\omega t}{2}} \tag{15}$$

and define a transformed density matrix

$$\rho(t) = U^{-1}\,\rho'(t)\,U \tag{16}$$

This transformed matrix obeys an equation of motion similar to Eq(1)

$$i\hbar\dot{\rho}(t) = [\mathcal{H},\ \rho(t)] \tag{17}$$

Except that $\mathcal{H}$ is a time independent Hamiltonian given by

$$\mathcal{H} = \frac{\hbar}{2}\,(\omega_o-\omega)\sigma_3 + \frac{\hbar f\omega_1}{2}\,e^{\frac{-i\sigma_3\phi}{2}}\,\sigma_1\,e^{\frac{i\sigma_3\phi}{2}} \tag{18}$$

The Hamiltonian in Eq(18) is time-independent for any value of the driving field frequency, ω, and reduces to the interaction picture for "on-resonance" experiments, $\omega=\omega_o$. The unitary transformation given by Eq(16) amounts to transforming to a rotating-frame[34] coordinate system that is rotating about the r_3 axis with a frequency ω. This may be verified by performing the indicated transformation on generic components of $\rho'(t)$ and noting that the result is the same as if a 3X3 rotation matrix were applied to the components of $\vec{r}$. From analogy to magnetic resonance, it should prove much more convenient to remain in the rotating frame, bearing in mind that stationary in-plane components r_1 and r_2 in the rotating frame correspond to rotating components in the lab frame. Since the in-plane components generally represent the expectation value of a macroscopic dipole moment, stationary components in the rotating frame correspond to the amplitude of the signal that could be generated by such oscillating moments.

Since $\mathcal{H}$ in Eq(18) is time independent the solution to Eq(17) is obtained from a simple unitary transformation

$$\rho(t) = S^{-1}\rho(o)S \tag{19}$$

Where $\rho(o)$ is the initial value of the density matrix in the rotating frame. The time evolution operator

$$S^{-1} = \exp(-i\mathcal{H}t/\hbar) \tag{20a}$$

is given explicitly by

$$S^{-1} = \begin{bmatrix} \cos\frac{\bar{\omega}t}{2} - \frac{i\Delta\omega}{\bar{\omega}}\sin\frac{\bar{\omega}t}{2} & \frac{-if\omega_1}{\bar{\omega}}e^{-i\phi}\sin\frac{\bar{\omega}t}{2} \\ \frac{-if\omega_1}{\bar{\omega}}e^{i\phi}\sin\frac{\bar{\omega}t}{2} & \cos\frac{\bar{\omega}t}{2} + \frac{i\Delta\omega}{\bar{\omega}}\sin\frac{\bar{\omega}t}{2} \end{bmatrix} \tag{20b}$$

where the following definitions have been used

$$\begin{aligned} \Delta\omega &= \omega_o - \omega \\ \bar{\omega} &= (f^2\omega_1^2 + \Delta\omega^2)^{1/2} \end{aligned} \tag{21}$$

Eq(19) may be used to calculate the time evolution of the density matrix, or, equivalently, the r-vector for any series of imposed conditions (1,2,3...n) by constructing an appropriate S-matrix for each condition and performing successive unitary transformations. It is useful to expand Eq(19) in terms of the r-vector components. Since the phase, ϕ, serves only to determine about what relative direction in the r_1-r_2 plane the r-vector will precess it is simpler to set ϕ=0 in the equations of motion and to include phase shifts in the applied field by first rotating the initial value in-plane coordinates through an angle ϕ, i.e. a

90° phase shift results in $r_1(o) \rightarrow r_2(o)$ and $r_2(o) \rightarrow -r_1(o)$. In this way the r vector always precesses about some direction in the r_1-r_3 plane. With these considerations, the r-vector components are given, in terms of the initial values $r_1(o)$, $r_2(o)$, $r_3(o)$ by

$$r_1(t) = \frac{1}{\bar{\omega}^2}\{r_1(o)\ [f^2\omega_1^2 + \Delta\omega^2 \cos\bar{\omega}t] - r_2(o)\bar{\omega}\Delta\omega \sin\bar{\omega}t + r_3(o) f\omega_1\Delta\omega[1-\cos\bar{\omega}t]\}$$

$$r_2(t) = \frac{1}{\bar{\omega}^2}\{r_2(o)\bar{\omega}^2 \cos\bar{\omega}t - r_3(o)\bar{\omega}f\omega_1 \sin\bar{\omega}t + r_1(o)\bar{\omega}\Delta\omega \sin\bar{\omega}t\} \qquad (22)$$

$$r_3(t) = \frac{1}{\bar{\omega}^2}\{r_3(o)[\Delta\omega^2 + f^2\omega_1^2 \cos\bar{\omega}t] + r_1(o) f\omega_1\Delta\omega[1-\cos\bar{\omega}t] + r_2(o) f\bar{\omega}\omega_1 \sin\bar{\omega}t\}$$

C. Manifestations of Coherent Coupling

An important special case of Eq(22) is the following. Before the application of the perturbation, V(t), the ensemble is assumed to be incoherent, and therefore $r_1(o) = r_2(o) = 0$. $r_3(o)$ corresponds to the initial population difference between the $|y\rangle$ and $|x\rangle$ levels. Under these conditions Eq(22) simplifies considerably.

$$r_1(t) = r_3(o)\ \frac{f\omega_1\Delta\omega}{\bar{\omega}^2}[1-\cos\bar{\omega}t]$$

$$r_2(t) = -r_3(o)\ \frac{f\omega_1}{\bar{\omega}} \sin\bar{\omega}t \qquad (23)$$

$$r_3(t) = r_3(o)\ \frac{1}{\bar{\omega}^2}\ [\Delta\omega^2 + f^2\omega_1^2 \cos\bar{\omega}t]$$

Eq(23), which corresponds to the "transient nutation,"[35] represents the simplest form of coherent coupling and is therefore the easiest experiment to perform in order to determine whether the applied field is able to dominate relaxation terms. In general, all three components undergo sinusoidal oscillations reflecting the highly non-linear response of the system to the applied field. Figures 1 and 2 give the response, $r_3(t)$, as a function of time and of frequency. It is important to note that the response of the system as a function of $\Delta\omega$ is not simply the "frequency domain" response to a "time domain" impulse as would be predicted from linear response theory. The dramatic difference between the two predictions is illustrated in Fig. 3, which is the frequency response from a δ function spectral line, centered at ω_o, under the influence of a short pulse applied at a frequency ω with strength ω_1. If the system were to respond to the various Fourier components of a pulse as the applied field was swept slowly through resonance, the waveform (a) would be observed, independent of the magnitude of ω_1. Curve (b) illustrates $r_3(t)$ for a pulse where $\omega_1 t = \pi$. Doubling the pulse time yields curve (c) for a linear response, and curve (d) for the true coherent coupling response. The "hole" in curve (d) at ω_o results from the fact that $\omega_1 t = 2\pi$ resulting in a complete rotation of the r-vector. Experimental results that very closely follow this type of behavior are given in Ref. 36. The analytical expressions for (a) and (c) are obtained by assuming that the δ function line yields an absorption signal that is proportional to the power (i.e. ω_1^2) of the Fourier component of the pulse whose frequency matches the resonance condition, $\omega(\text{Fourier}) = \omega_o$. Thus, as the frequency of the applied field is swept through resonance, the δ function response will effectively "map-out" the square of the frequency Fourier transform of the pulse shape, f(t). Explicitly, if f(t) is a simple square wave modulation lasting a time t, the frequency response of the δ function

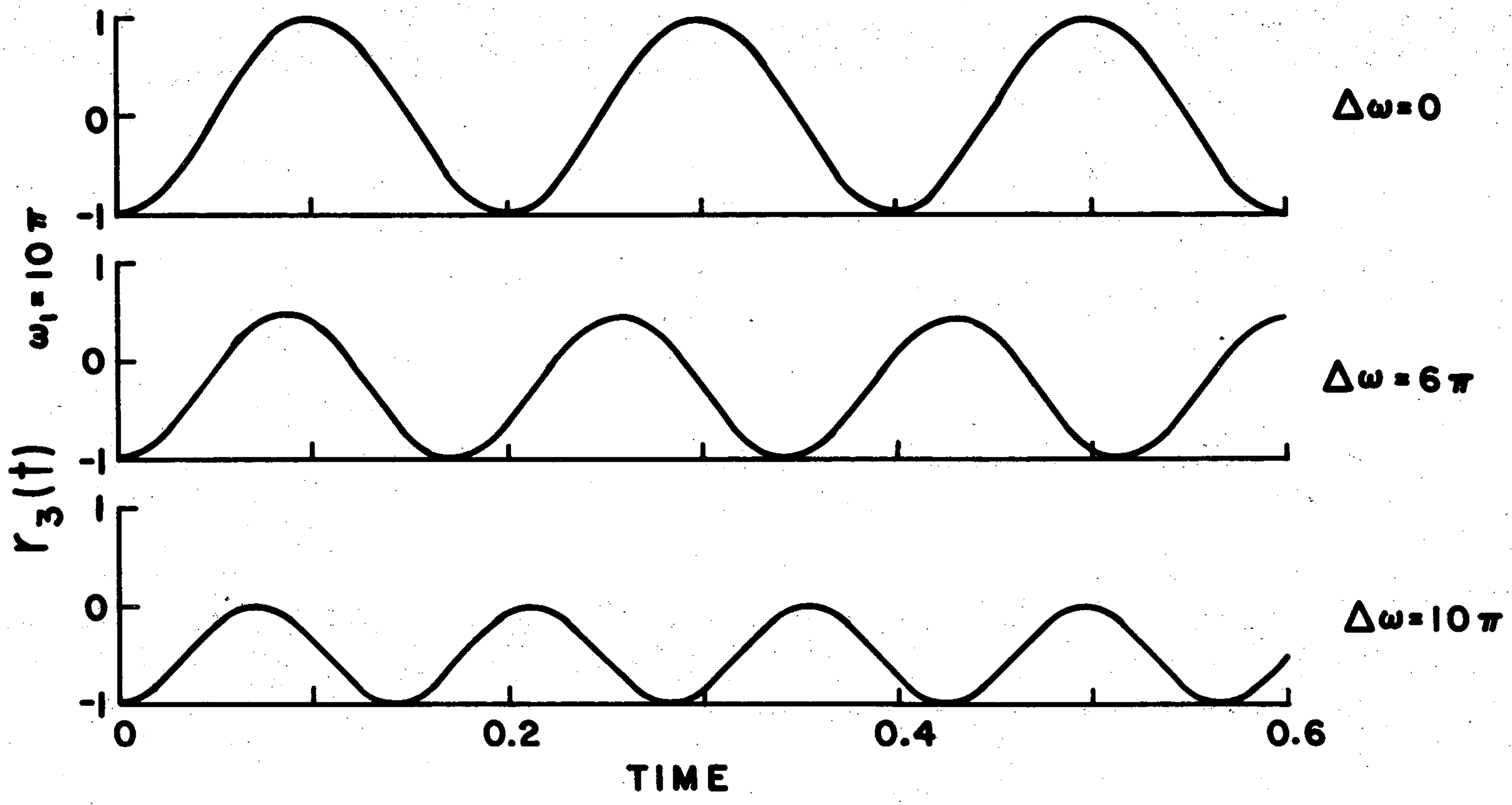

XBL 755-6297

Fig. 1. Response of the r_3 component for various values of $\Delta\omega$, as a function of time.

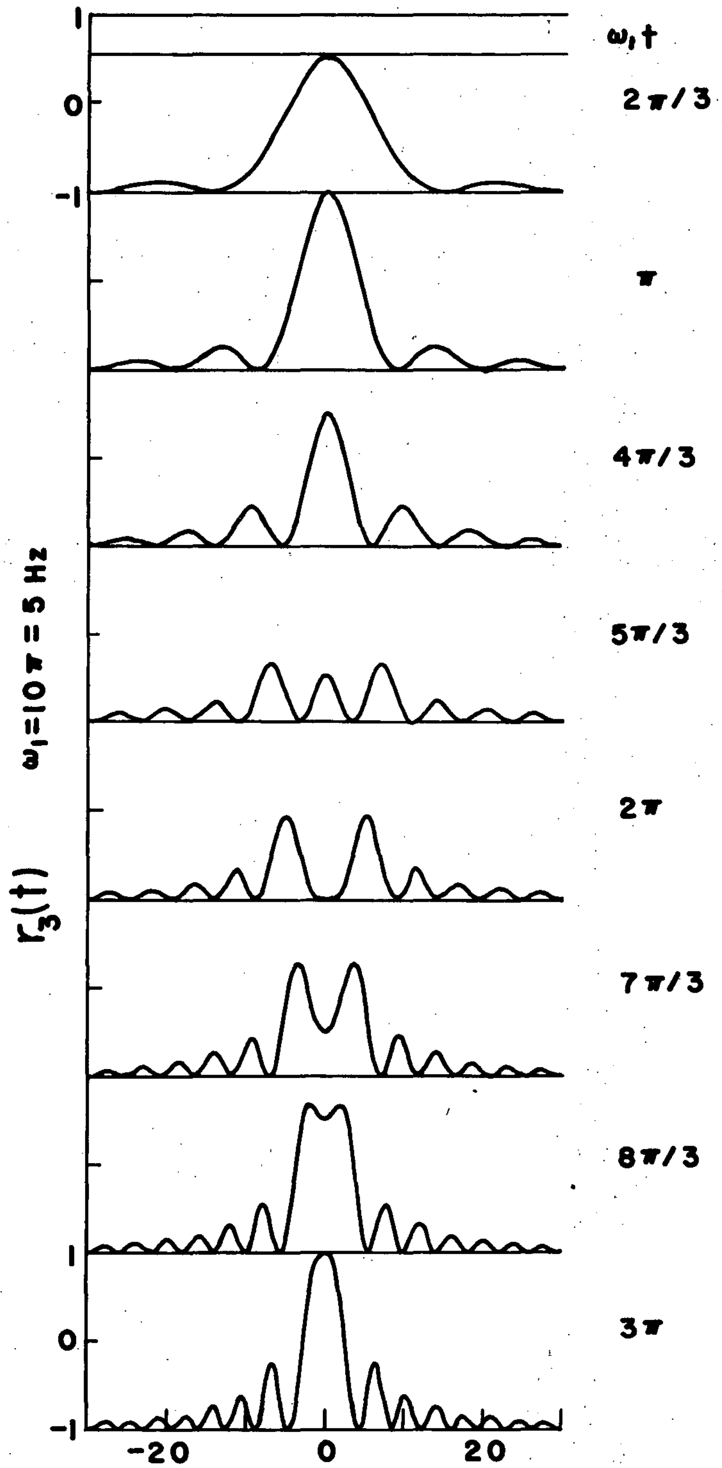

XBL 755-6282

Fig. 2. Response of the r_3 component for various values of $f\omega_1 t$, as a function of $\Delta\omega$.

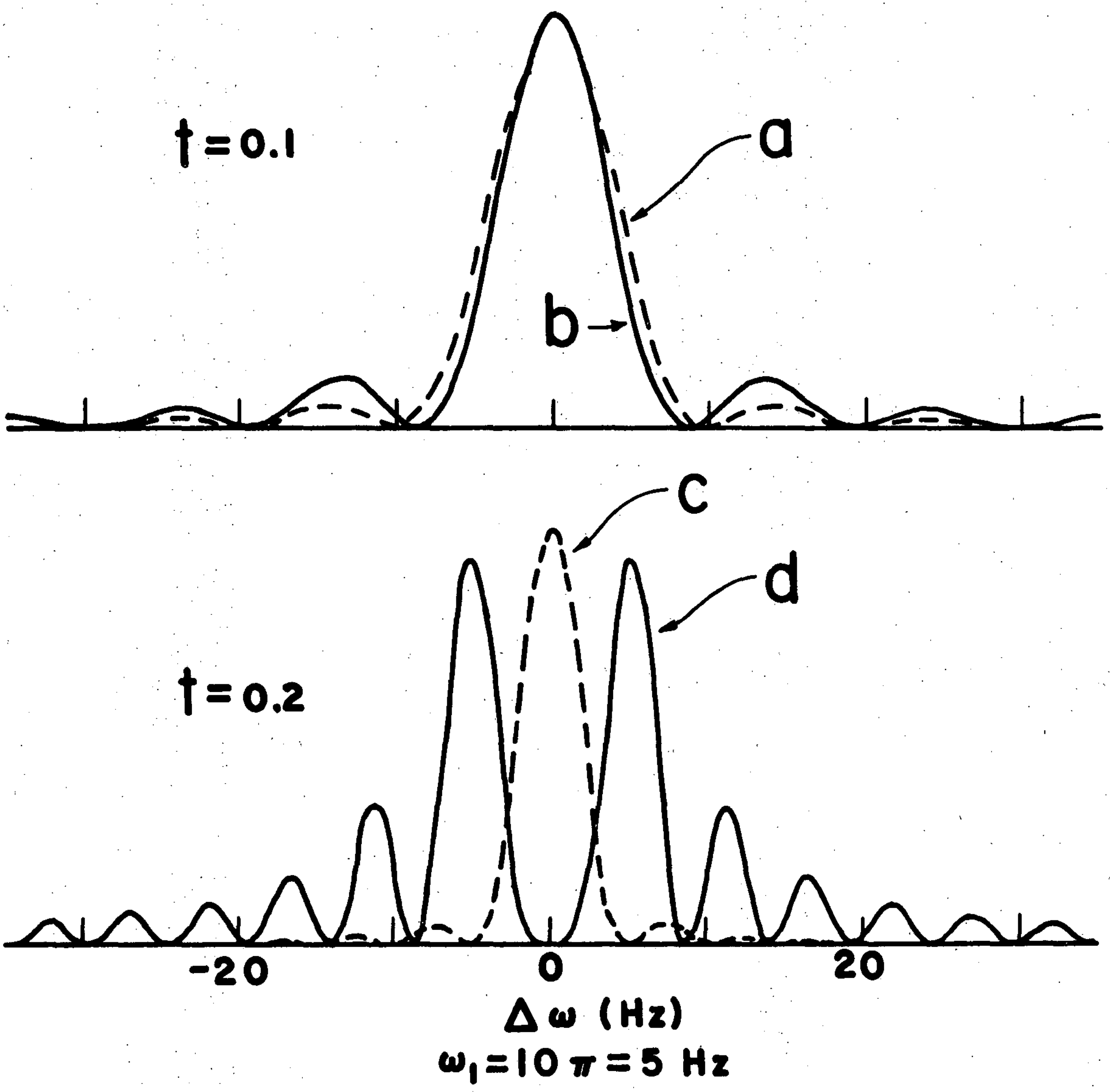

XBL 755-6296

Fig. 3. Comparison of the true nonlinear response, b and d, with a linear response a and c. Curve c has been scaled down by a factor of eight for comparison with d. a and b were purposely chosen to be as similar as possible, but in general the nonlinear response bears no resemblance to the linear response except for very short times or low power.

line will be proportional to

$$F(\omega')\propto\left[\int_{-\infty}^{\infty} e^{-i\omega' t'} f(t')dt'\right]^2=\left[\int_{-t/2}^{t/2} e^{-i\omega' t'}\,\frac{f\omega_1}{2}\,e^{i\omega t'}\,dt'\right]^2$$

$$F(\omega')\propto\frac{f^2\omega_1^2\sin^2(\omega-\omega')t/2}{(\omega-\omega')^2} \tag{24}$$

and changing variables to correspond to the previously defined term $\Delta\omega = \omega_o - \omega$

$$F(\Delta\omega)\propto f^2\omega_1^2\,\frac{\sin^2\Delta\omega t/2}{\Delta\omega^2} \tag{25}$$

Eq(25) is identical to the waveform that would result if first order time dependent perturbation theory were used to solve Eq(17). The assumptions that must be used to obtain Eq(25) from perturbation theory are $\omega_1 t \ll 1$, $x(o)=0$, $y(o)=1$, and Eq(25) is the probability, $P_{x\leftarrow y}$ of a transition from the state $|y>$ to the state $|x>$. It is gratifying to note that this expression may also be obtained from Eq(23). Since $P_{x\leftarrow y} = xx^*$ if $x(o)=0$, then $P_{x\leftarrow y} = \frac{1}{2}(1-r_3(t))$ if $r_3(o) = 1$. From Eq(23)

$$\frac{1}{2}(1-r_3(t)) = \frac{1}{2\bar{\omega}^2}\left[f^2\omega_1^2 + \Delta\omega^2 - \Delta\omega^2 - f^2\omega_1^2\cos\bar{\omega}t\right]$$

$$P_{x\leftarrow y} = f^2\omega_1^2\,\frac{\sin^2\bar{\omega}\,\frac{t}{2}}{\bar{\omega}^2} \tag{26}$$

and Eq(25) results only if $\omega_1 t \ll 1$. The "hole" at ω_o will of course not appear owing to the fact that the vector never approaches a single revolution.

III. THE PROBE PULSE METHOD

In the following sections a new method for monitoring the loss of coherence in a two level system will be presented and applied to a number of experiments that have been developed by other workers in the field of magnetic resonance. Since the technique does not utilize the conventional "in-plane" components to monitor coherence, experimental difficulties associated with cavity overload or sensitivity problems may be solved in some cases by the use of this method, and, owing to the general applicability of the approach, this method should prove valuable in a wide variety of fields that possess a "two-level" nature. In addition to being an alternative method for performing coherence experiments, this technique may prove to be the only method for many excited state systems in which the lifetimes of the levels are far too short to provide a sufficient number of spins for conventional detection and should prove most valuable in this respect.

A. Description of the Method

The geometrical picture is useful not only in terms of a simple visualization of the equation of motion for a two-level system, but also because it is strongly linked with the density matrix, the macroscopic observables associated with the ensemble are simply visualized in terms of r-vector components as well. It is just this link between a complete set of independent observables and the density matrix that led Fano to deduce in his "operator approach", that the formalism for a two level system may be extended to an n-level system in which the density matrix is expressed as a "multipole expansion" $k=0,1,2...$, in terms of k^{th} rank tensorial operators.[25,37] The elements of these tensors are given by special forms of the Clebsch-Gordon coefficients and thus represent purely geometrical considerations, as in the two-level case. It is unfortunate that Fano's work, which was done before FVH in a more general form, has not received the attention that it deserves from workers in the fields of spectroscopy and laser physics.

For a two-level system, the r_3 component is proportional to the difference in populations between the two levels and is also proportional the expectation value of $\mathcal{H}_0$ and σ_3. The expectation value of the total Hamiltonian $\mathcal{H}'$ is given by

$$\langle\mathcal{H}'\rangle = \frac{\hbar}{2}(r_1\Omega_1 + r_2\Omega_2 + r_3\Omega_3) \tag{27}$$

The in-plane components r_1 and r_2 are proportional to the expectation value of a complex dipole moment $\langle\mu\rangle$, magnetic or electric, provided that dipolar coupling is used to perturb the system and are also related to the expectation value of the quantum mechanical operator responsible for coupling the two levels, e.g. $\langle S_z\rangle \propto r_2$ for zero-field triplet states coupled by the spin operator S_z. In addition $r_1 \propto \langle\sigma_1\rangle$ and $r_2 \propto \langle\sigma_2\rangle$. The coherence information represented by the off-diagonal terms in the density matrix [r_1 and r_2 in Eq(7)] cannot be monitored directly by means of an observable that monitors r_3. This situation is unfortunate in view of the large number of double resonance techniques that provide an enormous increase in sensitivity for the experimenter, but attain this increase in sensitivity by virtue of the fact that they effectively monitor the energy level populations (r_3). Thus, one is apparently faced with the dilemma that in order to increase sensitivity, one must relinquish those measurements of relaxation phenomena that are based on coherence effects. This problem is exemplified explicitly by Eq(23). Coherence may be introduced into the ensemble by the application of a $\pi/2$ pulse ($\omega_1 t = \pi/2$, $\Delta\omega = 0$). In this case the components take on the values

$$\begin{aligned} r_1(\pi/2) &= 0 \\ r_2(\pi/2) &= -r_3(o) \\ r_3(\pi/2) &= 0 \end{aligned} \tag{28}$$

The time evolution of the system after the $\pi/2$ pulse is obtained from Eq(22) for $\Delta\omega = \omega_1 = 0$, $r_1(o) = 0$, $r_2(o) = -r_3(o)$, and $r_3(o) = 0$, and it is readily seen that the components retain the values given in Eq(28) unless some relaxation mechanism causes $r_2(\pi/2,t)$ to decay. Since $r_3(\pi/2,t)$ remains zero, which means that the energy levels appear to be equally populated, the decay of r_2 cannot be observed directly. This situation can be remedied, however, by applying an additional $\pi/2$ pulse that rotates the coherent component into the r_3 direction where the loss of coherence can then be monitored point-by-point in time. In terms of the components, the decay of the coherence is given by (assuming the standard exponential form)

$$\begin{aligned} r_1(\pi/2,t) &= 0 \\ r_2(\pi/2,t) &= -r_3(o)e^{-t/T_2} \\ r_3(\pi/2,t) &= 0 \end{aligned} \tag{29}$$

The coherence may then be monitored at any time, t, by applying a $\pi/2$ probe pulse, yielding from Eq(22)

$$\begin{aligned} r_1(\pi/2,t,\pi/2) &= 0 \\ r_2(\pi/2,t,\pi/2) &= 0 \\ r_3(\pi/2,t,\pi/2) &= -r_3(o)e^{-t/T_2} \end{aligned} \tag{30}$$

Eq(30) demonstrates that if very little decay in the coherence occurred during the time t, then the $\pi/2$ probe pulse will cause a population inversion between $|y\rangle$ and $|x\rangle$, and the observable (e.g. emission) that is used to monitor the energy level populations will show a corresponding change. On the other hand, if all the coherence in the ensemble has decayed at time t, $r_2(\pi/2,t) = 0$ and the probe pulse will not bring about any further change in r_3. The final value of r_3 would range from an inversion to saturation as the coherence decays, and the probe pulse would thus sample the coherence remaining in the ensemble in a well-defined quantitative fashion. A pictorial representation of the probe pulse method is given in Fig. 4.

Before obtaining expressions for some specific coherence experiments, a brief discussion of relaxation is appropriate in order to discuss real systems.

B. Relaxation

The effects of relaxation on an ensemble of two-level systems may be included in a simple phenomenological manner by including Bloch-type relaxation terms[38] in the equation of motion for r. Expanding Eq(5) and adding the appropriate terms yields.

$$\begin{aligned}\dot{r}_1 &= -\Delta\omega r_2 - r_1/T_{2e}\\ \dot{r}_2 &= \Delta\omega r_1 - f\omega_1 r_3 - r_2/T_2\\ \dot{r}_3 &= f\omega_1 r_2 + (r_3^S - r_3)/T_1\end{aligned} \tag{31}$$

Eq(31) expresses the modified form of the Bloch equations that was suggested by Redfield[39] in order to include the fact that "spin-spin" relaxation along the r_1 direction requires that work be done against the oscillating field. T_{2e} will thus be a function of ω_1 and could range from T_2 to ∞

Fig. 4. Optically detected free precession in excited triplet states: A diagrammatical representation of the time development of the interaction representation r vector and the laboratory frame spin sublevel populations. (a) For simplicity, consider a case where intersystem crossing occurs only to the middle sublevel, and only emission from the lower sublevel is monitored. Before the application of microwaves coupling the lower two sublevels, the r vector points along the positive z axis. (b) A $\pi/2$ pulse applied along the rotating frame x axis tips the r vector along y and the populations of the lower two sublevels are equalized. The phosphorescence intensity now corresponds to saturation. (c), (d) With the microwaves off, the in-plane y component decays to zero due to variations in local fields within the sample and homogeneous dephasing processes. The laboratory frame sublevel populations remain constant, however, so that the decay of the coherence is not directly manifested as a change in phosphorescence. (e^0), (e^1), (e^2) The decay of the coherence can be detected optically, however, by the application of an additional $\pi/2$ pulse. This probe pulse, applied along x, tips the coherent component down along z, producing an additional change in the sublevel populations and consequently in the phosphorescence intensity. The phosphorescence change induced by the probe pulse is proportional to the coherence remaining in the ensemble at the time the probe pulse is applied. This is shown in (e^0), (e^1), (e^2), which demonstrate the behavior of the r vectors and the laboratory frame sublevel populations when the probe pulse is applied at times corresponding to (b), (c), and (d), respectively. The probe at $t=0$ results in population inversion [relative to (a)] but the probe at $t=\tau''$, after complete decay of the coherence, produces no further change in population.

OPTICALLY DETECTED FREE PRECESSION IN EXCITED TRIPLET STATES
(Relationship between the laboratory frame and the interaction representation)

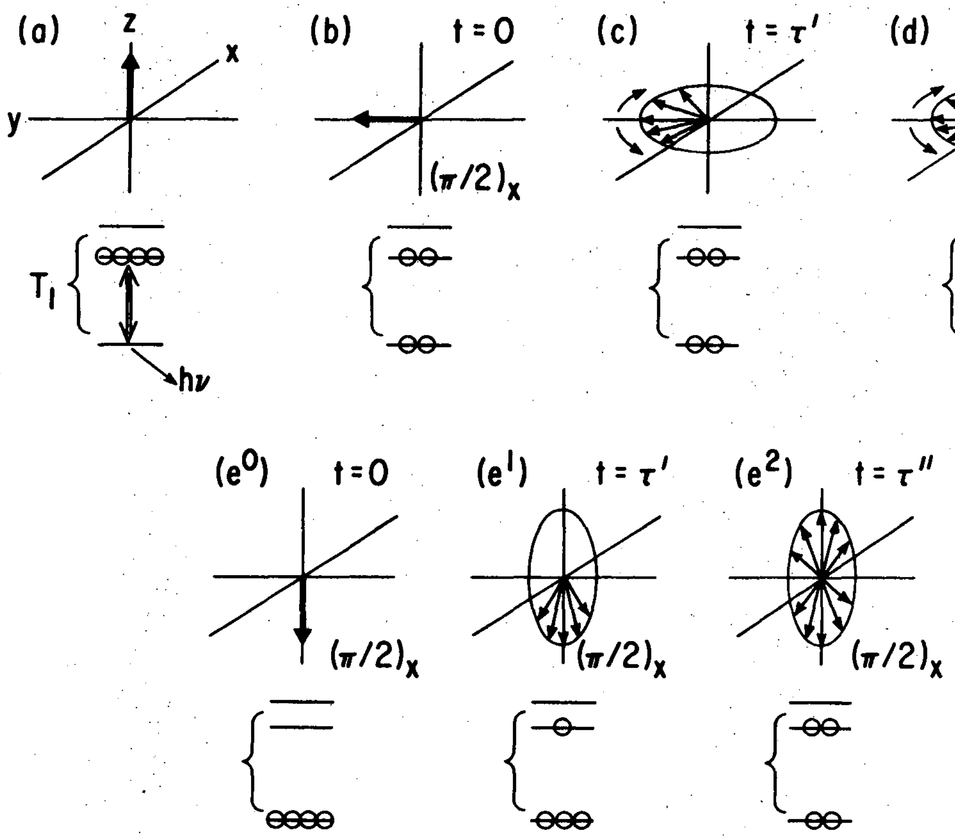

XBL 734-395

Fig. 4.

as the magnitude of ω_1 is increased from 0 to ∞.

Of course there is no a priori inference that justifies the extension of Eq(31), which was formulated to describe magnetic resonance phenomena, to the general case, but these equations should at least form a basis for semiquantitative descriptions of real two level systems. Specific relaxation mechanisms in the form of randomly varying external fields may then be included in a proper density matrix treatment in order to explain quantitative deviations from the simple expressions, but for the purposes of discussion, Eq(31) is adequate for describing specific experiments that are designed to monitor relaxation.

Complete solutions to Eq(31) will be included in the more general treatment of Chapter IV. However, several special cases are considered in the remaining sections of this chapter in order to illustrate the new method for measuring coherence and to demonstrate that the expressions obtained by monitoring energy level populations are identical in form to those obtained by measuring the in-plane components of the r vector as is done in conventional magnetic resonance spectroscopy.

In order to discuss spin echoes it is necessary to introduce inhomogeneous relaxation in the form of subensembles, each obeying Eq(31) but having a distribution of Larmor frequencies ω_o that may be described in terms of a normalized distribution function $g(\omega_o-\bar{\omega}_o)$ that is centered about an average Larmor frequency $\bar{\omega}_o$. A great number of systems exhibit a Lorentzian lineshape for $g(\omega_o-\bar{\omega}_o)$, and since Lorentzian functions are easier to integrate than Gaussian lineshapes, they will be used in this discussion to illustrate the examples.

C. On Resonance Transient Nutation

For $\Delta\omega = 0$ and the initial conditions $r_1(o) = r_2(o) = 0$, Eq(31) may be solved easily by Laplace transform techniques yielding

$$r_1(t) = 0$$

$$\begin{aligned} r_2(t) = e^{-1/2(1/T_1 + 1/T_2)t} & \left\{ \left(\frac{r_3^S}{2} \left(1/T_1 + 1/T_2\right) \frac{f\omega_1 T_2}{1+f^2\omega_1^2 T_1 T_2} - r_3(o) f\omega_1 \right) \frac{\sin\alpha t}{\alpha} \right. \\ & \left. + \frac{r_3^S f\omega_1 T_2}{1+f^2\omega_1^2 T_1 T_2} \cos\alpha t \right\} - \frac{r_3^S f\omega_1 T_2}{1+f^2\omega_1^2 T_1 T_2} \qquad (32) \end{aligned}$$

$$\begin{aligned} r_3(t) = e^{-1/2(1/T_1+1/T_2)t} & \left\{ \left(r_3(o) - \frac{r_3^S}{1 + f^2\omega_1^2 T_1 T_2} \right) \cos\alpha t + \left[\frac{r_2(o)}{2} \left(1/T_2 - 1/T_1\right) + \right. \right. \\ & \left. \left. r_3^S \left(1/T_1 - 1/2\left(1/T_1 + 1/T_2\right) \left(\frac{1}{1+f^2\omega_1^2 T_1 T_2} \right)\right) \right] \frac{\sin\alpha t}{\alpha} \right\} + \frac{r_3^S}{1+f^2\omega_1^2 T_1 T_2} \end{aligned}$$

where $\alpha = \left(f^2\omega_1^2 - 1/4\ (1/T_1 + 1/T_2)^2\right)^{1/2}$

Often T_2 is very much shorter than T_1, and Eq(32) simplifies considerably in the limit $T_1 \to \infty$

$$r_1(t) = 0$$

$$r_2(t) = -r_3(o) \frac{f\omega_1}{\beta} e^{\frac{-t}{2T_2}} \sin\beta t \qquad (33)$$

$$r_3(t) = r_3(o)\ e^{\frac{-t}{2T_2}} \left(\cos\beta t + \frac{1}{2\beta T_2} \sin\beta t \right)$$

where $\beta = (f^2\omega_1^2 - 1/4T_2^2)^{1/2}$.

In the limit of strong coherent coupling, $(f\omega_1 T_2)^2 >> 1$, Eq(33) reduces to the form

$$r_1(t) = 0$$

$$r_2(t) = -r_3(o)\, e^{\frac{-t}{2T_2}} \sin f\omega_1 t \qquad (34)$$

$$r_3(t) = r_3(o)\ e^{\frac{-t}{2T_2}} \cos\left(f\omega_1 t - \frac{1}{2\omega_1 T_2}\right)$$

For sufficiently high power and short times Eq(34) reduces to Eq(23) ($\Delta\omega = 0$).

1. Inhomogeneous Driving Field

Equation (34) represents the waveforms that would be expected from an ensemble of interacting two-level systems under the influence of a strong, homogeneous resonant field, where spin-lattice relaxation may be neglected. For an inhomogeneous resonant field, the transient nutation will die away faster owing to the fact that a range of nutation frequencies are summed to produce the signal. This may be expressed as the integral

$$\langle r_i \rangle = \int_0^{\infty} \gamma(\omega_1)\ r_i(t|f\omega_1) d\omega_1 \qquad i = 1,2,3 \qquad (35)$$

Where the parametric dependence of $r_i(t)$ on the oscillating field strength has been indicated in the integrand. The distribution function $\gamma(\omega_1)$ will be strongly dependent on actual experimental conditions and in general will be complicated and incalculable. Thus the transient nutation experiment is not particularly useful for relaxation measurements, but it is essential for verifying strong coherent coupling and for determining the times of $\pi/2$, π, etc. pulses in order to set up other pulse sequences.

2. Allowedness or f value considerations

It is important to note that the nutation frequency in the strong coherent coupling limit, Eq(34), is determined by the product $f\omega_1$. Thus if two closely spaced spectral lines having different f values are driven by the field, the transient nutation signal will be the sum of two frequencies, $\omega_1 f_1$ and $\omega_1 f_2$, and will exhibit a characteristic "beat" pattern that depends not only on the f values but also on the relative number of systems that contribute to each line. This "allowedness" consideration, which is not encountered in nuclear magnetic resonance, becomes a problem in specific applications to zero-field optically detected magnetic resonance as will be shown in Chapter V.

3. Orientation Effects

One particular form of Eq(35) merits additional attention and arises from the possible polarized nature of the coupling matrix elements from the perturbation V(t) given by Eq(10). If a homogeneous linearly polarized driving field is applied to an ensemble of molecules whose transition moments are polarized along a certain direction of the molecular coordinates, $<r_i>$ will reflect the actual spatial orientation of the molecules and is therefore not as trivial as the inhomogeneous $\gamma(\omega_1)$ discussed earlier. Again this problem does not occur in conventional magnetic resonance, for in this case the static high field serves to effectively define a polarization direction independent of the actual orientation of the molecules. Thus in zero-field optical or microwave experiments, the transient nutation will reflect a combination of driving field inhomogeneity, multiplet f values, and molecular orientation with respect to the direction of the driving field. In principle, inhomogeneity may be eliminated by better instrument design, and the orientational effects and multiplet f values are calculable, but all three effects can complicate analysis under specific applications.

It is worthwhile to consider one specific orientational effect that arises from the response of a randomly oriented array of molecules to a homogeneous linearly polarized driving field. Each molecule is assumed to have a polarization direction defined in terms of the molecular axis system. This particular situation corresponds to many physically realizable situations such as gases, liquids, polycrystaline solids, and guest molecules in a rigid glass matrix. All these examples display random orientation, and if they are not placed in some static external field, the strength of the driving field at each molecule will be determined by the local projection of the linearly polarized driving field on the molecular transition moment direction. The projection onto the transition moment is given in terms of the angle θ

$$\omega_1 = |\overset{\circ}{\omega}_1 \cos\theta| \tag{36}$$

where $\overset{\circ}{\omega}_1$ is the strength of the homogeneous driving field. We consider the simplest form of on-resonance transient nutation in the absence of relaxation, Eq(23) $\Delta\omega = 0$, where $r_3(t)$ is a cosine function. Equation (36) implies that the range of integration is from zero to $\overset{\circ}{\omega}_1$ as θ ranges from $\pi/2$ to zero. Since the driving field is assumed to be homogeneous, the distribution function $\gamma(\omega_1)$ is constant over the range of integration and is given simply by the normalization constant $1/\overset{\circ}{\omega}_1$. Equation (35) then becomes the simple relation

$$\langle r_3 \rangle = \frac{r_3(o)}{\overset{\circ}{\omega}_1} \int_0^{\overset{\circ}{\omega}_1} \cos(\omega_1 t)\, d\omega_1 = r_3(o) \frac{\sin \overset{\circ}{\omega}_1 t}{\overset{\circ}{\omega}_1 t} \tag{37}$$

Comparison of Eq(37) and Eq(23) is given in Fig. 5. Note that since the nutation frequencies range from zero to $\overset{\circ}{\omega}_1$, it is meaningless to talk about $\pi/2$ pulses, etc in an ensemble of randomly oriented molecules in zero field, and coherence experiments are severely limited in this situation.

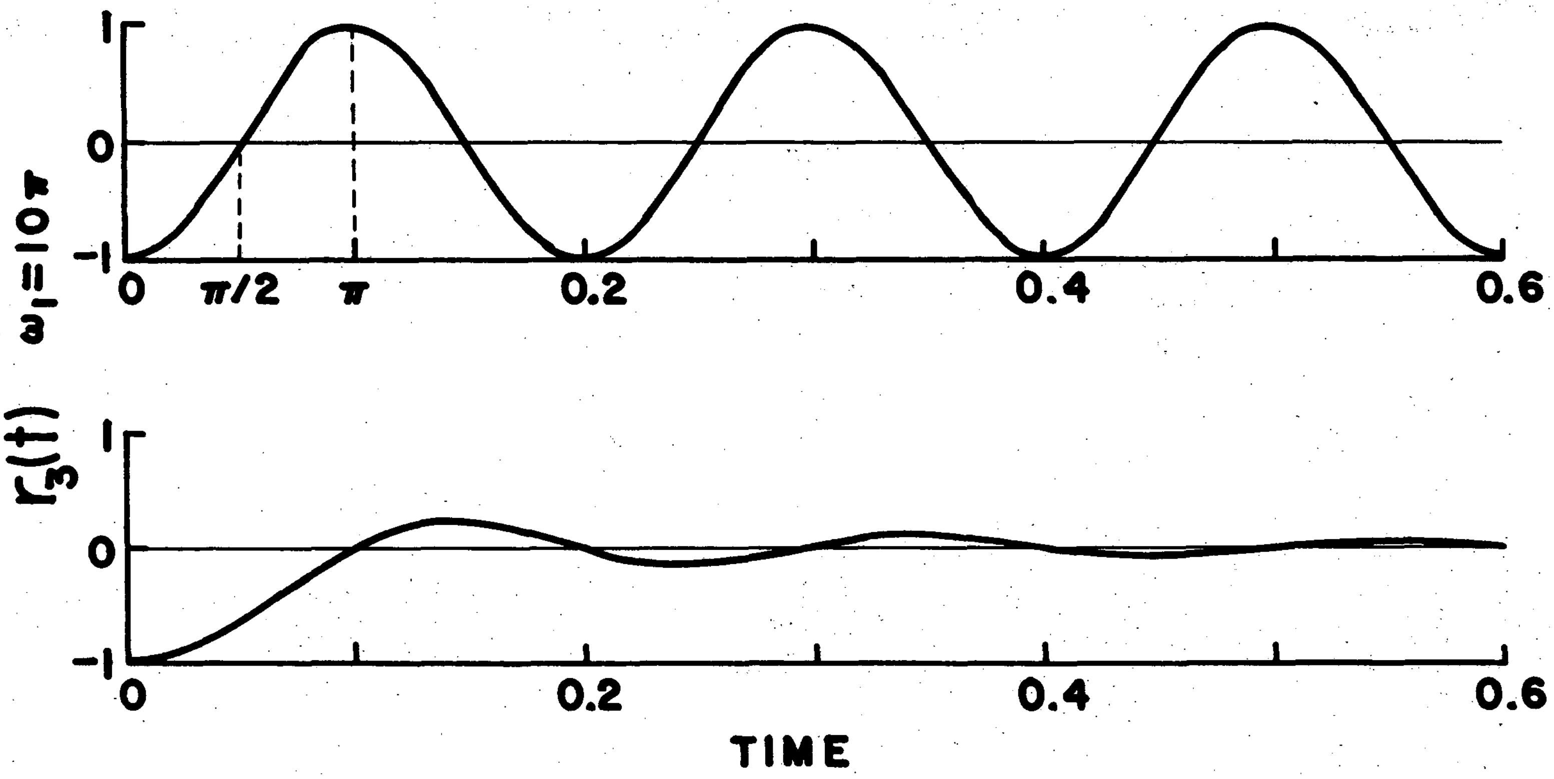

XBL 755-6295

Fig. 5. Top: Normal transient nutation in the absence of relaxation. The times that produce $\pi/2$ and π pulses are indicated. Bottom: Nutation resulting from a random array of molecules in a linearly polarized driving field also in the absence of relaxation.

Under ideal conditions, i.e. minimum driving field inhomogeneity, a single strong (f=1) transition, and sufficiently long relaxation times, the intermolecular angular correlation function for a distribution of molecules with well defined polarized transition moments could be obtained from the Fourier transform of a series of $<r_i>$ and Eq(36). Since the transient nutation may be obtained on rather rapid time scales, this feature could be used to monitor angular reorientations of intrinsic or "tagged" molecular systems to study low temperature phase transitions or possibly reorientations of liquid crystal systems. Zero field PMDR techniques may be particularly useful in this respect, owing to the very narrow EPR transitions that may be obtained from very broad optical lines, indicating that this type of experiment could be performed at elevated (>4°K) temperatures as well.

Another specific application of Eq(35) to an orientational situation is given in Chapter V in which the crystal structure of a molecular solid is used to predict the possible transient nutation waveforms resulting from the application of a linearly polarized driving field.

D. Free Induction Decay

The conventional sequence for a free induction decay consists of a single high-power $\pi/2$ pulse. Following the pulse, the r_1 and r_2 components will decay as the individual isochromats in the distribution $g(\omega_o-\bar{\omega}_o)$ fan out in the rotating frame plane (see Fig. 4). The behavior of the system is obtained from the time evolution operator $S = S(\omega_1 t=\pi/2)S_\tau$ Eq(20), where S_τ denotes free precession for a time period τ. Equation (19) and integration over the lineshape yields

$$\begin{aligned} r_1 &= r_3(o)\int_{-\infty}^{\infty} g(\omega_o-\bar{\omega}_o)\ \sin(\omega_o-\omega)\tau\ d\omega_o \\ r_2 &= r_3(o)\int_{-\infty}^{\infty} g(\omega_o-\bar{\omega}_o)\ \cos(\omega_o-\omega)\tau\ d\omega_o \end{aligned} \qquad (38)$$

and for a Lorentz lineshape function, the conventional experiment measures the signal

$$r_2 = r_3(o)\, e^{-\tau/T_2^*} \cos(\bar{\omega}_o-\omega)\tau \qquad (39)$$

where T_2^* is the inhomogeneous relaxation time associated with the Lorentz lineshape

$$g(\omega_o-\bar{\omega}_o) = \frac{T_2^*}{\pi(1+(\omega_o-\bar{\omega}_o)^2 T_2^{*2})} \qquad (40)$$

The probe pulse method uses an additional $\pi/2$ pulse giving $S = S(\omega_1 t = \pi/2)\ S_\tau S(\omega_1 t=\pi/2)$ and, after integration, yields an expression identical to Eq(39) for r_3.

E. Spin Echo

The conventional echo[40,41] has $S=S(\pi/2)S_\tau S(\pi)S_\tau{}'$ yielding

$$r_2 = r_3(o)e^{-\frac{\tau+\tau'}{T_2}}\ e^{-\frac{\tau-\tau'}{T_2^*}} \cos(\bar{\omega}_o-\omega)(\tau-\tau') \qquad (41)$$

and the probe pulse has $S = S(\pi/2)S_\tau S(\pi)S_{\tau'}S(\pi/2)$ giving rise to an identical expression for r_3. In a similar fashion, spin locking,[42,43] Carr-Purcell sequences,[41] and other experiments that have been designed to measure various forms of relaxation in magnetic resonance can be applied to a two level system and monitored not only by an observable related to r_1 and r_2, but also by an observable related to r_3 by use of the probe pulse method. The expressions are the same.

F. Fourier Transform Spectroscopy

The free induction decay, or equivalently, the echo shape is the cosine Fourier transform of the frequency distribution function, $g(\omega_o-\bar{\omega}_o)$, Eq(38). One would therefore expect that Fourier transform spectroscopy (FTS)[44] would be feasible with the probe pulse method. In conventional NMR, FTS has many advantages over the spectral sweep method and has developed into a powerful technique for obtaining spectra. However, there are several fundamental problems which prevent advantageous use of FTS with the probe pulse method. The first problem lies in the method itself. Since the loss of coherence must be monitored point-by-point in time, a single pulse no longer suffices to take the entire spectrum. The probe pulse effectively monitors only a single point in the time domain which corresponds to only a single point in the frequency domain. This implies that there is no theoretical advantage in FTS over the normal spectral sweep technique when the probe pulse is required. The "allowedness" of individual lines within a multiplet also becomes of critical importance in FTS, for, even under ideal conditions, a $\pi/2$ pulse for a f=1 transition will result in only a $\pi/4$ pulse for a f=.5 transition. For similar reasons, the relative spatial orientation considerations discussed earlier will effect the nutation angle for a given applied field strength $\overset{o}{\omega}_1$, and both these factors will lead to large intensity errors in the spectrum. These problems, coupled with the fact that many two-level systems have inhomogeneous broadening or multiplet splitting that is the same order of magnitude as the maximum size of ω_1 that can be generated experimentally, makes FTS a rather special kind of experiment and is limited to situations similar to that of NMR where multiplets are closely spaced relative to ω_1, f=1 for all transitions, and where there are no orientational effects present. Since double resonance experiments are usually much more sensitive than conventional detection, a spectral sweep while monitoring r_3 will be the most sensitive method for obtaining a spectrum except in those special cases in which FTS is particularly suitable.

IV. TWO LEVEL SYSTEM WITH FEEDING AND DECAY

The basic formalism described in Chapters II and III serves to adequately describe a ground-state system in which the total population in the two levels remains constant, or could be applied to an excited state situation in which the experiment takes place on a time scale that is much shorter than the lifetimes of the states themselves. However, if a general description for any two-level system is desired, the formalism must include the possibility that each state in the two-level system is capable of decay to a state outside the range of consideration and must also account for some mechanism that populates the states. By doing this, experiments that involve excited states, optical pumping, induced processes such as chemically induced nuclear and electron spin polarization,[45,46] and Stark shift optical coherence[47] may be treated for all time scales. By confining the problem to a reasonably simple form, exact solutions are possible that still reflect the important aspects of feeding and decay under the influence of a coherent driving field.

The theoretical development is broken into two parts, similar to the treatment of Chapters II and III. First a model system is established and easily manageable solutions are obtained in the absence of relaxation. Second, relaxation is added in a manner similar to that in Chapter III and complete exact expressions are obtained for both the transient and steady-state behavior. Although these expressions embody all the equations of previous chapters as special cases, the complete solutions are unwieldly enough to require a computer program, and it is the author's opinion that the simple vector picture discussed in Chapters II, III and the first part of IV will ultimately prove most useful in conceptualizing any new experiment and, for this reason, justifies their inclusion.

This particular problem has not been treated before. Perhaps the closest approach is that due to Icsevgi and Lamb,[48] but they considered a far more complex problem including the contribution of the ensemble to the total field and did not discuss the specific effects of feeding and decay on a coherently driven system. Similar approaches have been made by many other workers in laser physics,[49] but since they all include the effects of the ensemble field or a resonant cavity, their results are too complicated to apply to excited state coherence experiments, and no general closed form solutions exist. Early work in gas phase double resonance experiments also considered the problem of feeding and decay,[50] but no allowances were made to include separate decay channels from the excited state levels, and usually T_2 was set equal to T_1. It is hoped that the solutions presented here will help the reader to follow the elegant treatments of Refs. 48, 58, 61 and 62 in the context of the geometrical model.

A. Model System

In order to discuss the role that feeding and decay play in the excited state two-level coherent coupling problem, the following model system given in Fig. 6 is formulated. The entire experimental system is divided into two parts. The first part consists of the ensemble of "excited" two-level systems that are coupled by a driving field. The second part is taken to be an infinite reservoir that represents both a source and a sink for population to enter and leave the ensemble of two-level systems. At a given instant of time, the ensemble of two-level systems is evolving under the influence of the applied radiation field, and is

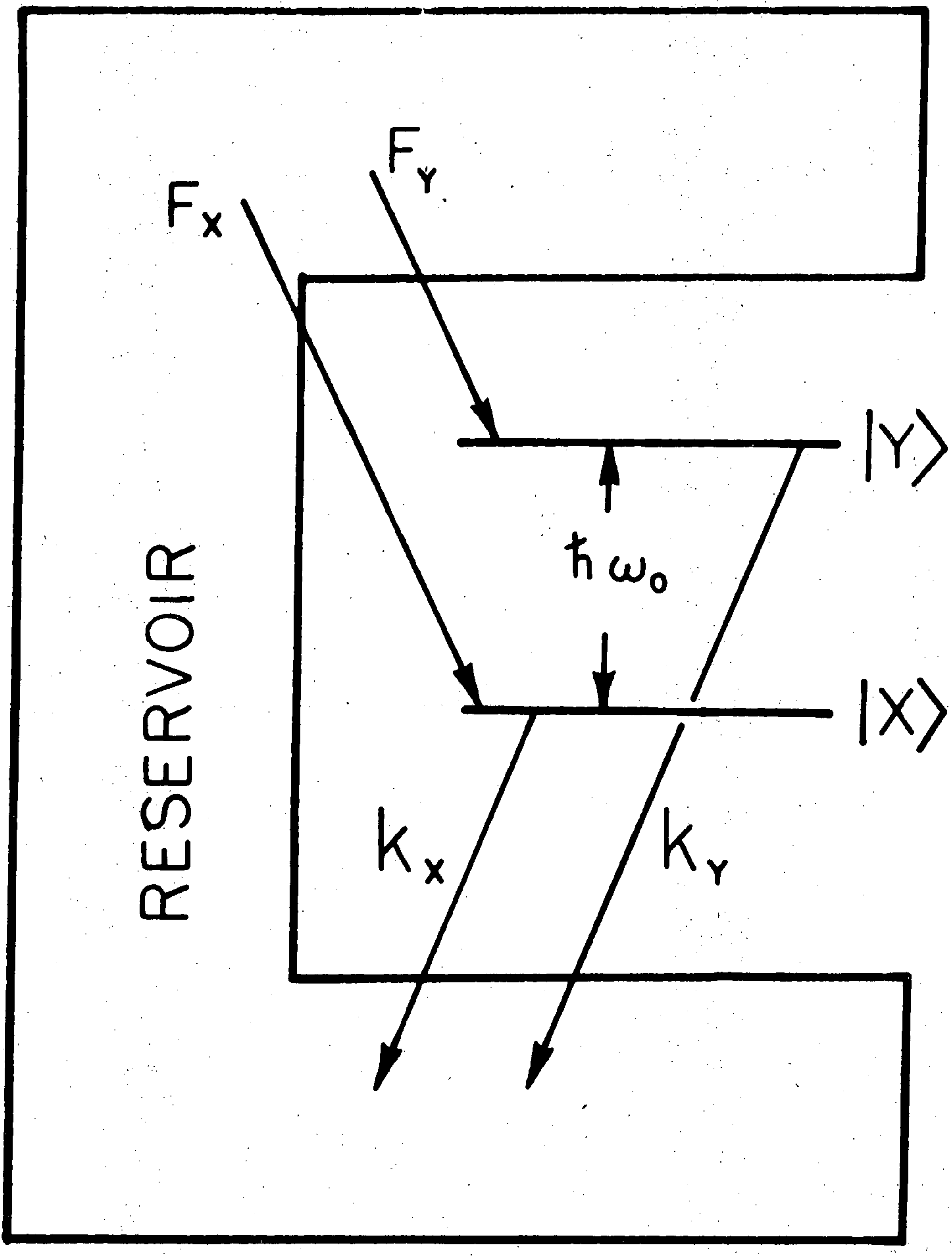

XBL 755-6294

Fig. 6. Model system used for the developments in Chapter IV.

also decaying into the reservoir at a rate which is characteristic of the decay rate constants k_x and k_y. Population is also constantly transferred incoherently from the reservoir into the ensemble at constant rates F_x and F_y. Only those states, $|y>$ and $|x>$ that are affected by the radiation field are included in the ensemble, implying that the reservoir is unaffected by the field. As a consequence, population which is transferred incoherently from the reservoir to the ensemble enters the ensemble in one of the eigenstates, and not in a coherent superposition state. However, once the population has entered the ensemble it may evolve into a coherent superposition state since it is now influenced by the radiation field. In terms of a density matrix description, this implies that feeding occurs only to the diagonal elements of the density matrix and off-diagonal elements occur only due to the effect of the radiation field on the population which is already in the ensemble. Decay, however, affects both the diagonal and off-diagonal elements.

From this model and the results of Chapter II it becomes quite simple to visualize qualitatively how the creation and destruction of the states affects the properties of the ensemble in the presence of a coherent driving field. At any given instant of time the ensemble may be described in terms of the torque equation, Eq(5), the r-vector representing the population that is present in the ensemble. During a small interval of time, new population is created as an additional vector that suddenly appears along r_3 and is immediately driven by the radiation field. At the same time the original vector is driven and decays according to k_x and k_y. The total time development is a sum over all the small time intervals. This picture will be used to describe the results of the expressions obtained for the transient nutation and spin locking in the presence of feeding and decay.

B. Solutions in Absence of Relaxation

By constructing a model system consisting of a reservoir, details of the feeding and decay processes are not considered explicitly and thus allow the many-body problem to become tractable. The simplest way to include decay of a state is to assume that the amplitude for being in the state decays exponentially.[51] For the two-level system this is expressed in terms of the rotating frame coefficients

$$\begin{aligned}\dot{y} &= -\frac{k_y}{2}\,y \\ \dot{x} &= -\frac{k_x}{2}\,x\end{aligned} \qquad (42)$$

k_y and k_x are physically observable rate constants associated with the decay of the states $|y>$ and $|x>$ respectively.

As discussed earlier, the populating process occurs only to the eigenstates $|y>$ and $|x>$ and cannot appear in a superposition state. This implies that the equations describing the feeding process must deal only with the probabilities yy* and xx* and cannot affect the terms which define the relative phase factor as given by xy* or yx*. For this reason a density matrix formulation is ideal (Note Eq(3)).

The decay terms in Eq(42) are incorporated into the density matrix by constructing the imaginary operator K given in the y-x basis by

$$K = \frac{i\hbar}{2}\begin{bmatrix} k_y & 0 \\ 0 & k_x \end{bmatrix} \qquad (43)$$

and the decay process is described by an anticommutator relation

$$i\hbar\dot{\rho} = -[K,\rho]_+ \tag{44}$$

The operator K must be imaginary in order to cause the density matrix to decay. In accordance with earlier discussions, feeding is allowed to only the diagonal terms of ρ, and may be expressed in terms of a feeding matrix F given by

$$F = i\hbar \begin{bmatrix} F_y & 0 \\ 0 & F_x \end{bmatrix} \tag{45}$$

The total equation of motion which includes feeding, decay, and a driving field is thus given by combining Eqs(17), (44), and (45)

$$i\hbar\dot{\rho}(t) = [\mathcal{H},\rho] - [K,\rho]_+ + F \tag{46}$$

A solution to Eq(46) is given by

$$\rho(t) = Q^\dagger\ [\rho(o) - \rho_s]Q + \rho_s \tag{47}$$

Where the matrix Q is

$$Q = \exp\left\{i\ \frac{(\mathcal{H} + K)}{\hbar}\ t\right\} \tag{48}$$

and ρ_s, the steady-state value of the density matrix, is obtained from Eq(46) by setting $\dot{\rho}(t) = 0$ and solving for ρ. Notice that since $\mathcal{H}$ is real and K imaginary the adjoint of Q is not the inverse

$$Q^\dagger = \exp\left\{-i\ \frac{(\mathcal{H}-K)}{\hbar}\ t\right\} \neq Q^{-1} \tag{49}$$

and thus Q is not unitary. The operations in Eq(47) do not result in a similarity transformation. This is to be expected, however, since the decay process must cause the trace of $\rho(t)$ to vanish - a result which is not possible with a similarity transformation. Owing to the fact that the constant trace condition has been relaxed, one will need four, rather than the usual three, independent variables to describe the density matrix completely. This can be done easily by defining the components of the density matrix as follows:

$$\rho(t) = \begin{bmatrix} r_y & \frac{r_1 - ir_2}{2} \\ \frac{r_1 + ir_2}{2} & r_x \end{bmatrix} \tag{50}$$

These components have a geometrical significance that is only slightly different from the FVH model. r_y is represented by a vector which points "up" in a three dimensional r-space whereas r_x points "down". They both share the same in-plane components r_1 and r_2. The FVH vector component r_3 is given by $r_y - r_x$. In terms of observables, r_y and r_x are proportional to the upper and lower level populations, respectively.

An explicit form for Q is obtained from Eq(48) using Putzer's method.[52]

$$Q = e^{\frac{-k_A t}{2}} \begin{bmatrix} \cos\frac{\Lambda t}{2} + \frac{k_D + i\Delta\omega}{\Lambda} \sin\frac{\Lambda t}{2} & \frac{if\omega_1}{\Lambda} \sin\frac{\Lambda t}{2} \\ \frac{if\omega_1}{\Lambda} \sin\frac{\Lambda t}{2} & \cos\frac{\Lambda t}{2} - \frac{k_D + i\Delta\omega}{\Lambda} \sin\frac{\Lambda t}{2} \end{bmatrix} \tag{51}$$

Eq(51) incorporates the following definitions

$$\begin{aligned} k_A &= \frac{k_x + k_y}{2} \\ k_D &= \frac{k_x - k_y}{2} \\ \Lambda &= [f^2\omega_1^2 + (\Delta\omega - ik_D)^2]^{1/2} \end{aligned} \tag{52}$$

As would be expected, Q becomes S, Eq(20), when there is no feeding or decay.

Before obtaining explicit expressions for the steady-state density matrix, ρ_s, it is worthwhile to expand Eq(46) in terms of the four r components.

$$\begin{aligned}
\dot{r}_1 &= -\Delta\omega r_2 - k_A r_1 \\
\dot{r}_2 &= \Delta\omega r_1 - f\omega_1(r_y - r_x) - k_A r_2 \\
\dot{r}_y &= f\omega_1 r_2/2 - k_y r_y + F_y \\
\dot{r}_x &= -f\omega_1 r_2/2 - k_x r_x + F_x
\end{aligned} \tag{53}$$

By comparing Eq(53) to the rotating frame Bloch equations, Eq(31), one can see immediately that the average of the decay rate constants k_A will have the same effect as a T_2 process and the combination of feeding and decay will appear to be a T_1 process. This is quite reasonable from a physical point of view since the in-plane components involve a superposition state that can be viewed as being "undecided" from which eigenstate it will eventually decay, thus giving rise to k_A. Also, an incoherent T_1 process will have a similar effect as decay from $|y>$ or $|x>$ into the reservoir with subsequent incoherent feeding into $|x>$ and $|y>$ respectively. The important difference between actual T_1 and feeding and decay, however, is that the final population difference in the levels is determined by a Boltzmann distribution in the T_1 case, as opposed to the feeding and decay process in which practically any population difference is possible, depending on the ratios of the feeding and decay constants and on the conditions of the experiment.

In view of the similarity between the rotating frame Bloch equations and Eq(53) the r components of ρ_s may be cast into a familiar form by defining the appropriate quantities. First, noting that the steady-state populations in the absence of a driving field are given by ($f\omega_1 = \Delta\omega = 0$)

$$\begin{aligned} \overset{\circ}{r}_y &= F_y/k_y \\ \overset{\circ}{r}_x &= F_x/k_x \\ \overset{\circ}{r}_3 &= \overset{\circ}{r}_y - \overset{\circ}{r}_x \end{aligned} \tag{54}$$

and by defining <u>effective</u> relaxation terms,

$$\begin{aligned} t_2 &= 1/k_A \\ t_1 &= k_A/k_x k_y \end{aligned} \tag{55}$$

ρ_s in terms of the r components is given by

$$\begin{aligned} r_1^s &= \overset{\circ}{r}_3 \, \Delta\omega f\omega_1 t_2^2 \;/\; D \\ r_2^s &= -\overset{\circ}{r}_3 f\omega_1 t_2 \;/\; D \\ r_y^s &= \left[\overset{\circ}{r}_y(1+\Delta\omega^2 t_2^2) + f^2\omega_1^2 t_1 t_2^2 \left(\frac{F_x+F_y}{2}\right)\right]/D \\ r_x^s &= \left[\overset{\circ}{r}_x(1+\Delta\omega^2 t_2^2) + f^2\omega_1^2 t_1 t_2^2 \left(\frac{F_x+F_y}{2}\right)\right]/D \\ r_3^s &= \overset{\circ}{r}_3(1+\Delta\omega^2 t_2^2) \;/D \end{aligned} \tag{56}$$

where the denominator D is defined as

$$D = 1 + \Delta\omega^2 t_2^2 + f^2\omega_1^2 t_1 t_2 \tag{57}$$

The mathematical forms for Eq(56) are identical to those encountered in magnetic resonance for slow passage spectral sweep. When the "power factor", $f^2\omega_1^2\, t_1 t_2$ in Eq(57), is small, the components reduce to Lorentzian lineshapes. It is interesting to note that the effective "transverse" relaxation, t_2, is determined by the average of the decay

<u>rate constants</u> whereas the effective spin-lattice relaxation, t_1, is determined by the average of the decay <u>lifetimes</u>.

The expression for F in Eq(45) could be generalized easily to situations in which the feeding occurs to a superposition state and also could be made time dependent. The solution for ρ_s follows a similar format.

If one wishes to monitor the effects of feeding and decay more explicitly, Eq(47) may be broken up into three parts.

$$\rho(t) = \underbrace{Q^\dagger \rho(o) Q}_{1} - \underbrace{Q^\dagger \rho_s^y Q + \rho_s^y}_{2} - \underbrace{Q^\dagger \rho_s^x Q + \rho_s^x}_{3} \qquad (58)$$

Part 1 is the time evolution of the population that is in the ensemble at t=0. Part 2 is found by solving for ρ_s, setting $F_x=0$, and similarly Part 3 is found by setting $F_y=0$. Parts 2 and 3 describe the time evolution of the population that subsequently feeds into $|y\rangle$ and $|x\rangle$, respectively.

C. <u>Special Cases of Eq(47)</u>

1. <u>No Driving Field</u>

Consider first the trivial case in which there is no driving field. From the model system pictured in Fig. 5 one can write simple rate equations for the r components by inspection. These expressions agree with those obtained from Eq(47) after setting $\omega_1 = \Delta\omega = 0$. Q has a very simple form

$$Q = e^{\frac{-Kt}{i\hbar}} = Q^\dagger$$

and the solutions are

$$\begin{aligned} r_1 &= r_1(o)\,e^{-k_A t} \\ r_2 &= r_2(o)\,e^{-k_A t} \\ r_y &= (r_y(o)-F_y/k_y)\,e^{-k_y t} + F_y/k_y \\ r_x &= (r_x(o)-F_x/k_x)\,e^{-k_x t} + F_x/k_x \end{aligned} \tag{59}$$

Notice that r_1 and r_2 are not fed, but merely decay from whatever initial values they had at t=0.

2. On Resonance Transient Nutation

In this case, $r_1(o)=r_2(o)=\Delta\omega=0$, $r_y(o)=r_y^{\circ}$, $r_x(o)=r_x^{\circ}$ and Eq(47) yields expressions as complicated as Eq(32).

$$\begin{aligned} r_1(t) &= 0 \\ r_2(t) &= \frac{e^{-k_A t}}{\alpha^2}\left[r_2^s(k_D^2-f^2\omega_1^2\cos\alpha t) - (r_3^{\circ}-r_3^s)\alpha f\omega_1\sin\alpha t \right.\\ &\qquad \left. -(r_y^{\circ}-r_y^s+r_x^{\circ}-r_x^s)f\omega_1 k_D(1-\cos\alpha t)\right] + r_2^s \\ r_y(t) &= \frac{e^{-k_A t}}{\alpha^2}\left[(r_y^{\circ}-r_y^s)\left(\alpha\cos\frac{\alpha t}{2} + k_D\sin\frac{\alpha t}{2}\right)^2 + (r_x^{\circ}-r_x^s)f^2\omega_1^2\sin^2\left(\frac{\alpha t}{2}\right)\right.\\ &\qquad \left. -r_2^s f\omega_1\sin\frac{\alpha t}{2}\left(\alpha\cos\frac{\alpha t}{2} + k_D\sin\frac{\alpha t}{2}\right)\right] + r_y^s \\ r_x(t) &= \frac{e^{-k_A t}}{\alpha^2}\left[(r_x^{\circ}-r_x^s)\left(\alpha\cos\frac{\alpha t}{2} - k_D\sin\frac{\alpha t}{2}\right)^2 + (r_y^{\circ}-r_y^s)f^2\omega_1^2\sin^2\left(\frac{\alpha t}{2}\right)\right.\\ &\qquad \left. +r_2^s f\omega_1\sin\frac{\alpha t}{2}\left(\alpha\cos\frac{\alpha t}{2} - k_D\sin\frac{\alpha t}{2}\right)\right] + r_x^s \end{aligned} \tag{60}$$

where $\alpha = (f^2\omega_1^2 - k_D^2)^{1/2}$

Equation (60) has the basic form of a damped harmonic oscillator. The qualitative appearance of the curves is quite simple, since for small values of ω_1 the exponential terms dominate and mask the phase shifts introduced by k_D. However, as soon as $f\omega_1$ becomes large enough to cause an appreciable number of oscillations, $f\omega_1 >> k_A$, it also follows that $f\omega_1 >> k_D$ and the waveforms approach simple expressions similar to those of Eq(34)

$$\begin{aligned}
r_1(t) &= 0 \\
r_2(t) &= -r_3^o e^{-k_A t} \sin f\omega_1 t - \frac{r_3^o k_x k_y}{\omega_1 k_A} \\
r_y(t) &= \frac{e^{-k_A t}}{2} [(N^o - N^s) + r_3^o \cos f\omega_1 t] + \frac{N^s}{2} \\
r_x(t) &= \frac{e^{-k_A t}}{2} [(N^o - N^s) - r_3^o \cos f\omega_1 t] + \frac{N^s}{2}
\end{aligned} \tag{61}$$

where

$$N^o = r_y^o + r_x^o$$

$$N^s = r_y^s + r_x^s = (F_x + F_y)/k_A$$

r_y and r_x may be combined in two ways. First, the r_3 component may be computed.

$$r_y - r_x = r_3(t) = r_3^o \, e^{-k_A t} \cos f\omega_1 t \tag{62}$$

The motion corresponds to what the geometrical picture would predict: oscillations with frequency $f\omega_1$ damped by the average of the decay rate constants, reaching a steady-state vector sum of zero since a uniform "disc" of vectors will be formed in the r_2-r_3 plane. Notice that the decay constant is $k_A = 1/t_2$ as opposed to $1/2T_2$ in Eq. (34). This factor of two arises from the fact that T_2 is responsible for decay of the <u>inplane</u> components only, and a high power field that drives the vector around amounts to the vector being in the plane only half the time t, on the average. Decay from the states occurs for all components, however, and the high field will only serve to average the decay rate constants as evidenced by k_A.

The second combination of r_y and r_x results in a term that reflects how the total population in the two-level ensemble develops in time as a result of feeding, decay, and a high intensity driving field.

$$r_y + r_x = N(t) = (N^o - N^s)e^{-k_A t} + N^s \tag{63}$$

Equation (63) may be obtained from intuitive arguments as its simple form would suggest. Figure (5) implies the following rate equations for r_y and r_x in the absence of a driving field.

$$\begin{aligned} \dot{r}_y &= -k_y r_y + F_y \\ \dot{r}_x &= -k_x r_x + F_x \end{aligned} \tag{64}$$

These equations result in the last two solutions in Eq. (59). Equation (64) may be written in terms of the total population as

$$\dot{N} = -k_y r_y - k_x r_x + F_x + F_y \quad . \tag{65}$$

Now if a very strong field is applied, it may be assumed that the populations in the two levels remain equal throughout the time development of N. This is tantamount to the condition $f\omega_1 \gg k_A$ which implies that many nutations are made before appreciable feeding or decay can take place. Under this condition $r_y = r_x = N/2$ and Eq. (65) becomes

$$\dot{N} = -k_A N + F_x + F_y \tag{66}$$

which has the same solution as Eq. (63). Note that this simple argument does not predict the correct behavior for $\dot{r}_y$ or $\dot{r}_x = N/2$, Eq. (66) again, since there is no condition built into the mathematics that gives nutation, and as a result the $r_3^o \cos f\omega_1 t$ term is missing.

D. Coherence Experiments

As is the case in magnetic resonance, the ability to do well-defined pulse rotations of the r-vector depends upon the relationship between the applied field strength and the effective relaxation, $t_2=1/k_A$. The similarity between Eq. (53) and the rotating frame Bloch equations makes it unnecessary to go through the same arguments as in Chapter III for the free induction decay and spin echo. In fact, for most systems of interest, the homogeneous relaxation time, T_2, will be orders of magnitude shorter than the lifetimes of the two levels, and as long as the experiment is sufficiently short the arguments in Chapter III may be used directly, ignoring feeding and decay.

There is one coherence experiment, not mentioned in Chapter III, that is worthwhile discussing in terms of the preceeding development. If the modified form of the Bloch equations is applicable to a particular system, a spin-locking[42,43] experiment can be performed, and the coherent component can be made to last a time that greatly exceeds the homogeneous relaxation time. It would therefore be of interest to investigate the effects of feeding and decay on such an experiment. First a $\pi/2$ pulse is applied, yielding from Eq. (61), $k_A t \cong 0$,

$$\begin{aligned} r_1(\pi/2) &= 0 \\ r_2(\pi/2) &= -r_3^o \\ r_y(\pi/2) &= N^o/2 \\ r_x(\pi/2) &= N^o/2 \end{aligned} \tag{67}$$

and the populations appear "saturated". Shifting the phase of the driving field is tantamount to redefining the initial conditions $r_1(0) = -r_3^o$, $r_2(0) = 0$, and from Eqs. (53) and (61) the spin-lock signal is given by

$$\begin{aligned} r_1(t) &= -r_3^o\, e^{-k_A t} \\ r_2(t) &= 0 \\ r_y(t) &= \frac{e^{-k_A t}}{2}\left(\frac{N^o}{2} - N^s\right) + \frac{N^s}{2} \\ r_x(t) &= \frac{e^{-k_A t}}{2}\left(\frac{N^o}{2} - N^s\right) + \frac{N^s}{2} \end{aligned} \tag{68}$$

An additional phase-shifted $\pi/2$ probe pulse would be required to monitor $r_1(t)$ if an observable associated with r_y or r_x is used to measure the spin-lock signal. It is interesting to note that the act of phase shifting effectively isolates the spin-lock component from the feeding process. In terms of the vector model, population that enters the ensemble subsequent to the establishment of the spin lock component forms a uniform disc in the r_2-r_3 plane and does not affect the spin-lock signal. This situation is not true, however, is the field is applied off-resonance, for then the disc becomes a "cone" about the effective field direction resulting in a component along the direction of the spin-lock signal. As will be demonstrated in the next section, this component results from a steady-state solution, and can thus cause anomolous decay times for the spin-lock signal.

E. Feeding, Decay, and Relaxation-General Solution

In order to obtain a complete description for the system pictured in Fig. 5, the modified Bloch equations, Eq. (31), will be combined with Eq. (53). This procedure is done mainly for the sake of completeness since the analytical expressions for the general solution mask all the physics that is contained within them. It is fortunate that for most experimental situations the simple approaches presented earlier do not vary qualitatively from the solutions to be presented in this section, for then meaningful experiments may be constructed by use of the vector model and Eq. (47).

In terms of the r-vector components, the complete equations of motion that include driving field, feeding and decay and relaxation are given by

$$\begin{aligned}
\dot{r}_1 &= -\Delta\omega r_2 - (k_A + 1/T_{2e})r_1 \\
\dot{r}_2 &= \Delta\omega r_1 - f\omega_1(r_y - r_x) - (k_A + 1/T_2)r_2 \\
\dot{r}_y &= f\omega_1 r_2/2 - (k_y + 1/T_y)r_y + r_x/T_x + F_y \\
\dot{r}_x &= -f\omega_1 r_2/2 - (k_x + 1/T_x)r_x + r_y/T_y + F_x
\end{aligned} \tag{69}$$

The new parameters $1/T_x$ and $1/T_y$ are related to the probability per unit time for a transition from $|x\rangle$ to $|y\rangle$ and from $|y\rangle$ to $|x\rangle$, respectively. This form allows for spontaneous emission from $|y\rangle$ to $|x\rangle$, in addition to "spin-lattice relaxation" terms. Specifically,

T_y may be separated into two terms

$$\frac{1}{T_y} = \frac{1}{T_y^{spon}} + \frac{1}{T_{1y}} \qquad (70)$$

in which T_y^{spon} is the spontaneous emission lifetime, and T_{1y} is related to the normal thermal probability for a transition from $|y\rangle$ to $|x\rangle$. If spontaneous emission is negligible, as is the case in a rf region of the applied field, T_1, as given in Eq. (31), is related by

$$\frac{1}{T_1} = \frac{1}{T_x} + \frac{1}{T_{1y}} \quad . \qquad (71)$$

T_x and T_{1y} are related by a Boltzman factor

$$\frac{T_{1y}}{T_x} = e^{-\hbar\omega_o/kT} \quad . \qquad (72)$$

1. Steady-State Solutions

The t=∞ values for the r-vector components are easily obtained by setting the time derivatives in Eq. (69) to zero. As before, these solutions may be cast into a form that is easy to interpret by virtue of their similarity to magnetic resonance counterparts.

$$\begin{aligned}
r_1^s &= r_3^o\, f\omega_1 \Delta\omega T T_e / D \\
r_2^s &= -r_3^o\, f\omega_1 T / D \\
r_y^s &= \left[r_y^o (1 + \Delta\omega^2 T T_e) + \frac{f^2\omega_1^2 T\tau}{k_A} \left(\frac{F_x + F_y}{2} \right) \right] / D \\
r_x^s &= \left[r_x^o (1 + \Delta\omega^2 T T_e) + \frac{f^2\omega_1^2 T\tau}{k_A} \left(\frac{F_x + F_y}{2} \right) \right] / D
\end{aligned} \tag{73}$$

where

$$\begin{aligned}
D &= 1 + \Delta\omega^2 T T_e + f^2\omega_1^2 T\tau \\
\frac{1}{T} &= k_A + \frac{1}{T_2} \\
\frac{1}{T_e} &= k_A + \frac{1}{T_{2e}} \\
\tau &= k_A / (k_x k_y + k_y / T_x + k_x / T_y) \\
r_y^o &= \frac{\tau}{k_A} \left(F_y k_x + \frac{F_x + F_y}{T_x} \right) \\
r_x^o &= \frac{\tau}{k_A} \left(F_x k_y + \frac{F_x + F_y}{T_y} \right) \\
r_3^o &= r_y^o - r_x^o \quad .
\end{aligned}$$

These components may then be used to construct a steady-state density matrix, ρ_s, according to Eq. (50).

2. Transient Solutions

Equation (69) is difficult to express in a form such as Eq. (46), in which the density matrix equation of motion is described in terms of 2×2 commutators. A more general approach is to use the "superoperator" or "Liouville operator"[53] trick. In this case the four elements of the density matrix are treated as components of a four-vector operated on by a 4×4 matrix that not only implicitly contains the commutators indicated in Eq. (46), but in addition the method allows one to add phenomenological relaxation terms as easily as was done in Eq. (69). Thus Eq. (69) may also be represented as

$$i\hbar\dot{\rho} = \hbar L\rho + i\hbar F \tag{74}$$

The elements arising from $\mathcal{H}$ are given by

$$\hbar L_{mn,m'n'} = \mathcal{H}_{mm'}\delta_{nn'} - \delta_{mm'}\mathcal{H}_{n'n} \tag{75}$$

and the explicit form for L is

$$L = \begin{bmatrix} -iK_y & -\frac{f\omega_1}{2} & \frac{f\omega_1}{2} & \frac{i}{T_x} \\ -\frac{f\omega_1}{2} & \Delta\omega-iK_A & -iK_D & \frac{f\omega_1}{2} \\ \frac{f\omega_1}{2} & -iK_D & -\Delta\omega-iK_A & -\frac{f\omega_1}{2} \\ \frac{i}{T_y} & \frac{f\omega_1}{2} & -\frac{f\omega_1}{2} & -iK_x \end{bmatrix} \tag{76}$$

whereas ρ and F are given by the column vectors

$$\rho = \begin{bmatrix} \rho_{yy} \\ \rho_{yx} \\ \rho_{xy} \\ \rho_{xx} \end{bmatrix} = \begin{bmatrix} r_y \\ r_1 - ir_2 \\ r_1 + ir_2 \\ r_x \end{bmatrix} \qquad F = \begin{bmatrix} F_y \\ 0 \\ 0 \\ F_x \end{bmatrix} \tag{77}$$

The following definitions have been employed

$$\begin{aligned} K_y &= k_y + 1/T_y \\ K_x &= k_x + 1/T_x \\ K_A &= k_A + 1/2(1/T_{2e} + 1/T_2) \\ K_D &= 1/2(1/T_{2e} - 1/T_2) \quad . \end{aligned} \tag{78}$$

The solution to Eq. (74) is deceptively simple

$$\rho(t) = e^{-iLt} (\rho(0) - \rho_s) + \rho_s \tag{79}$$

The entire problem of calculating the time dependence of $\rho(t)$ now lies in the evaluation of the exponential operator which contains a 4×4 non-hermitian matrix. The evaluation of such an exponential operator for <u>any</u> n×n matrix has been given by Putzer,[52] and application of this theorem to the problem at hand is given in Appendix A. An important point to note is that since the evaluation involves an eigenvalue problem, the 4×4 matrix implies a quartic equation that may be solved exactly, and since this is the highest order polynomial that may be solved exactly, the 2×2 density matrix is the maximum size that may be evaluated in closed form. This feature has little practical significance, however, since many iterative methods exist for finding the roots of an nth degree polynomial to any degree of accuracy. Another point worth mentioning is that despite the attractively simple form for Eq. (79), it is highly impractical even for simple special cases, and equations such as Eq. (47) or Eq. (19) are far easier to work with. Equation (79) is therefore best left to the computer for evaluation.

3. General Transient Solutions Including Inhomogeneous Broadening

Equation (79) may be programmed on a computer and a sum of solutions weighted by an empirical or analytical lineshape function may be taken to include the effects of inhomogeneous broadening. Figure 7 compares the waveforms produced by successive additions of relaxation parameters to the transient nutation. Note that for sufficiently high driving fields the inhomogeneous broadening has little effect on the transient nutation, (a) and (b). Curves (c) and (d) have been arranged so that $k_A = T_2$ of curves (a) and (b) in order to demonstrate the faster decay expected from k_A as discussed in Sec. IV-B. Note that the difference in k_D, (c) vs. (d), has little effect on the waveform.

Therefore, for high power fields, the equations developed in Chapter III will be sufficient in most cases for short times, and simple "rate equations" will be applicible for long times (see Sec. V-C).

4. Inhomogeneous Broadening and Slow Passage Lineshapes

By integrating Eq. (73) over the inhomogeneous distribution $g(\omega_o - \bar{\omega}_o)$, Eq. (40), one obtains the expected lineshape that would be observed in a slow passage spectral sweep. These averages, denoted by $\langle r_i \rangle_{\omega_o}$, are

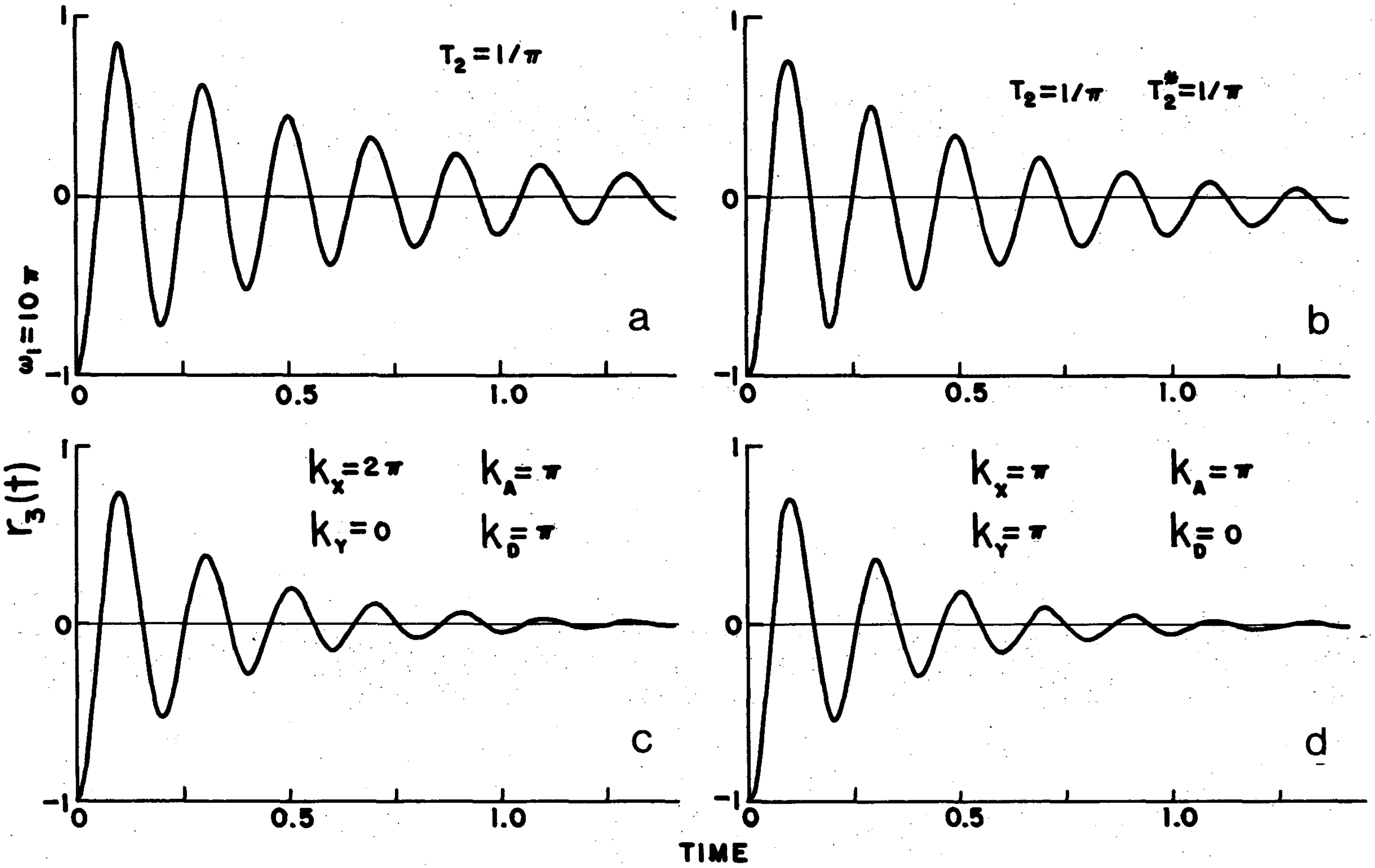

XBL 755-6283

Fig. 7. Comparison of exact transient solutions for various parameters in the high driving field range.

$$
\begin{aligned}
\langle r_1^s \rangle_{\omega_o} &= r_3^o f\omega_1 \overline{\Delta\omega}/D^* \\
\langle r_2^s \rangle_{\omega_o} &= -r_3^o\ f\omega_1 \left[\frac{1}{T_e} + \frac{1}{T_2^*}\left(\frac{\sqrt{T/T_e}}{\sqrt{1 + f^2\omega_1^2 T\tau}}\right)\right] \Big/ D^* \\
\langle r_y^s \rangle_{\omega_o} &= \left\{ r_y^o \left[\frac{1}{TT_e} + \frac{1}{T_2^{*2}} + \frac{1}{T_2^*\sqrt{TT_e}}\left(\sqrt{1+f^2\omega_1^2 T\tau} + \frac{1}{\sqrt{1+f^2\omega_1^2 T\tau}}\right) + \overline{\Delta\omega}^2\right] \right. \\
&\quad \left. + \frac{f^2\omega_1^2 T\tau}{k_A}\left(\frac{F_x+F_y}{2}\right)\left(\frac{1}{TT_e} + \frac{1}{T_2^*\ \sqrt{TT_e}\ \sqrt{1 + f^2\omega_1^2 T\tau}}\right)\right\} \Big/ D^*
\end{aligned}
\tag{80}
$$

$$\langle r_x^s \rangle_{\omega_o} = \{r_x^o\ [\text{ same as } r_y^s\ .\ .\ .] + .\ .\ .\}$$

where T_2^* is the inhomogeneous relaxation time and

$$\overline{\Delta\omega} = \overline{\omega}_o - \omega$$

$$D^* = \overline{\Delta\omega}^2 + \left(\frac{1}{T_2^*} + \frac{1}{\sqrt{TT_e}}\ \sqrt{1 + f^2\omega_1^2 T\tau}\right)^2 \quad .$$

For low driving field powers Eq. (80) reduces to the more familiar Lorentzian forms

$$
\begin{aligned}
\langle r_1^s \rangle_{\omega_o} &\cong \frac{r_3^o f\omega_1 \overline{\Delta\omega}\ \Gamma^2}{1 + \overline{\Delta\omega}^2\Gamma^2} \\
\langle r_2^s \rangle_{\omega_o} &\cong \frac{-r_3^o f\omega_1\ \Gamma}{1 + \overline{\Delta\omega}^2\ \Gamma^2} \\
\langle r_y^s \rangle_{\omega_o} &\cong r_y^o + \frac{f^2\omega_1^2\ \Gamma\tau\left(\dfrac{F_x + F_y}{k_x + k_y}\right)}{1 + \overline{\Delta\omega}^2\ \Gamma^2} \\
\langle r_x^s \rangle_{\omega_o} &\cong r_x^o + \text{same as } r_y^s
\end{aligned}
\tag{81}
$$

$$\langle r_3^s \rangle_{\omega_o} \cong r_3^o \left(1 - \frac{f^2\omega_1^2\Gamma\tau}{1 + \overline{\Delta\omega}^2\Gamma^2}\right)$$

$$1/\Gamma = 1/T + 1/T_2^* \quad \text{and} \quad T \cong T_e$$

Equation (81) represents the expected lineshape from a low power cw spectrum of a single inhomogeneously broadened line. Note that the inplane components r_1 and r_2 represent the dispersion and absorption lineshapes commonly encountered in magnetic resonance. The signals are related by the Kramers-Kronig conditions and are also proportional to the amplitude of the applied radiation field and the transition amplitude. r_y and r_x represent the energy absorbed or emitted by the system and the signal is proportional to the intensity of the applied field and the transition probability, as would be expected.

The "saturation" characteristics of Eq. (80) may be investigated by looking at the high power driving field case.

$$\begin{aligned}
\langle r_1^s \rangle_{\omega_o} &\cong \frac{r_3^o\, f\omega_1\, \overline{\Delta\omega}}{\overline{\Delta\omega}^2 + \dfrac{f^2\omega_1^2 T\tau}{TT_e}} \qquad (82)\\
\langle r_2^s \rangle_{\omega_o} &\cong 0\\
\langle r_y^s \rangle_{\omega_o} &\cong \frac{r_y^o\left(\dfrac{f\omega_1}{T_2^*}\sqrt{\dfrac{\tau}{T_e}} + \overline{\Delta\omega}^2\right) + \dfrac{N^s}{2}\,\dfrac{f^2\omega_1^2 T\tau}{TT_e}}{\overline{\Delta\omega}^2 + \dfrac{f^2\omega_1^2 T\tau}{TT_e}}
\end{aligned}$$

The dispersion signal is a maximum off resonance; the absorption signal approaches zero for all values of $\overline{\Delta\omega}$; and the population components approach equal values and are a maximum on resonance.

All the steady-state behavior is quite simple to picture in the vector model as demonstrated in the diagram of Fig. 8. The steady-state condition implies that a uniformly distributed cone of vectors about the effective field direction will result in the presence of high-power radiation. The vector sum results in a resultant that lies directly along the applied field direction and is thus effectively "spin-locked" without introducing any phase shifts. A simple geometrical argument shows that the resultant shrinks to zero either as one goes very far from resonance, or as exact resonance is approaced, and becomes a maximum when $f\omega_1=\overline{\Delta\omega}$. Since the effective field lies in the r_1-r_3 plane, $\langle r_2^s \rangle_{\omega_0}$ will always be zero for high power driving fields. Non-zero values for $\langle r_2^s \rangle_{\omega_0}$ come about when the relaxation mechanisms compete strongly enough with the driving field such that each individual vector decays before a complete revolution about the effective field can occur. In this fashion a "lopsided' cone or disc is formed that has a resultant component in the r_2 direction.

F. Steady-State Coherence

Equation (80) implies that a coherent component can be made to last an infinite amount of time. This may at first seem surprising since one might think that the lifetime of the states involved would obviously be the limiting time that a coherent component could be maintained. However the suggestive forms of Eqs. (69) and (73) indicate that the mathematical formalism is no different than the Bloch equations, and that the steady-state solutions correspond to "nuclear induction"[38]

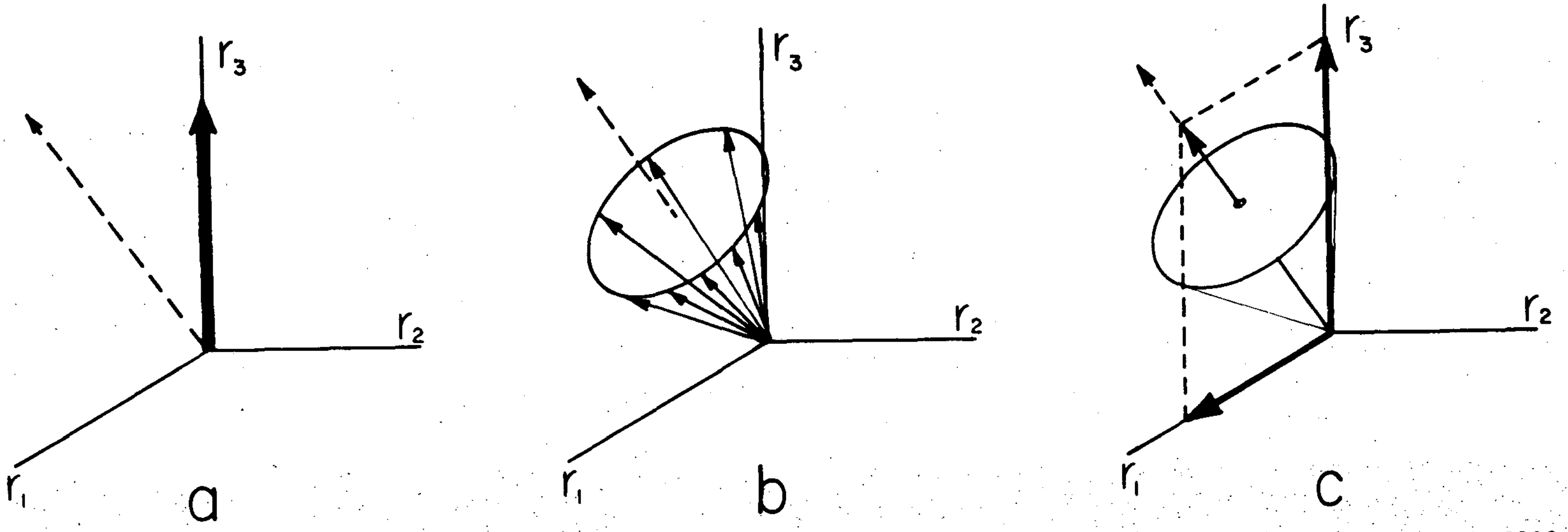

XBL 755-6292

Fig. 8. Development of steady-state components viewed in terms of the vector model. (a) initial value of the vector along r_3 and the direction of the "effective field", dashed line whose r_1 component is $f\omega_1$ and r_3 component is $\Delta\omega$. (b) through a combination of relaxation and strong driving field a uniform cone is established about the effective field. (c) The vector sum of the cone yields an r_1 and r_3 component that is stationary in time.

signals, u and v. In terms of the feeding and decay picture, it is easy to see that although individual members in the ensemble are constantly being fed, driven, and eventually decay, the coherent driving field serves to maintain the coherence indefinitely.

It is worthwhile to find and compare the maximum values of the coherent components. The maximum of $\langle r_1^s \rangle_{\omega_o}$ occurs off-resonance at a value given by

$$\overline{\Delta\omega}_{max} = \frac{1}{T_2^*} + \frac{1}{\sqrt{TT_e}} \sqrt{1 + f^2\omega_1^2 T\tau} \qquad (83)$$

yielding for the component

$$\langle r_1^s \rangle_{\omega_o} = \frac{r_3^o f\omega_1}{2\left(\frac{1}{T_2^*} + \frac{1}{\sqrt{TT_e}} \sqrt{1 + f^2\omega_1^2 T\tau}\right)} \ . \qquad (84)$$

This component attains its largest value for very high fields

$$\overline{\Delta\omega}_{max} \cong f\omega_1 \sqrt{\frac{\tau}{T_e}} \qquad (85)$$

and

$$\langle r_1^s \rangle_{\omega_o} \text{ (max)} \cong \frac{r_3^o}{2} \sqrt{\frac{T_e}{\tau}} \ .$$

In the absence of appreciable spin-lattice relaxation, and if $T_{2e} \to \infty$ as $\omega_1 \to \infty$, $T_e = k_A$, and if $k_x = k_y$, the component becomes what the vector model would predict, $\langle r_1^s \rangle_{\omega_o} = r_3^o/2 = \langle r_3^s \rangle_{\omega_o}$, and $\overline{\Delta\omega} = f\omega_1$. The maximum value of $\langle r_2^s \rangle_{\omega_o}$ is obtained for an intermediate value of $f\omega_1$ on resonance and is therefore a more complicated function of the two relaxation times T_2 and T_2^*. In the absence of inhomogeneous broadening it is easy to show that

$$\langle r_2^s \rangle_{\omega_o} (\max) = \frac{r_3^o}{2} \sqrt{\frac{T}{\tau}} \tag{86}$$

The important difference between Eq. (86) and Eq. (85) lies in the fact that T_e can be very much larger than T since Eq. (85) is obtained under high driving field conditions. If T_e is not dependent on ω_1, the maximum values of the components would be the same in the absence of inhomogeneous broadening. Including the effects of T_2^* again favors the r_1 component, for the high field conditions make $\langle r_1^s \rangle_{\omega_o}$ (max) insensitive to inhomogeneous broadening. It therefore becomes convenient to use the r_1 component as a normalizing factor and plot the ratio of $\langle r_2 \rangle_{\omega_o}$ (max) to $\langle r_1 \rangle_{\omega_o}$ (max) as a function of the unitless parameter T/T_2^*. This is given in Fig. 9, where it has been assumed that $T=T_e$ for the sake of comparison. Thus, through a combination of $T_e(\omega_1)$ and T_2^*, the largest possible value for a coherent component is obtained in the off resonance "dispersion" signal, and could be orders of magnitude larger than the on-resonance "absorption signal".

This feature of coherence is not particularly important for the rf region of resonance frequencies, except perhaps for sensitivity considerations, but gains considerable importance in the microwave and optical regions owing to the fact that the coherent component represents a macroscopic oscillating dipole and is responsible for maser action in an inverted medium within a resonant cavity.

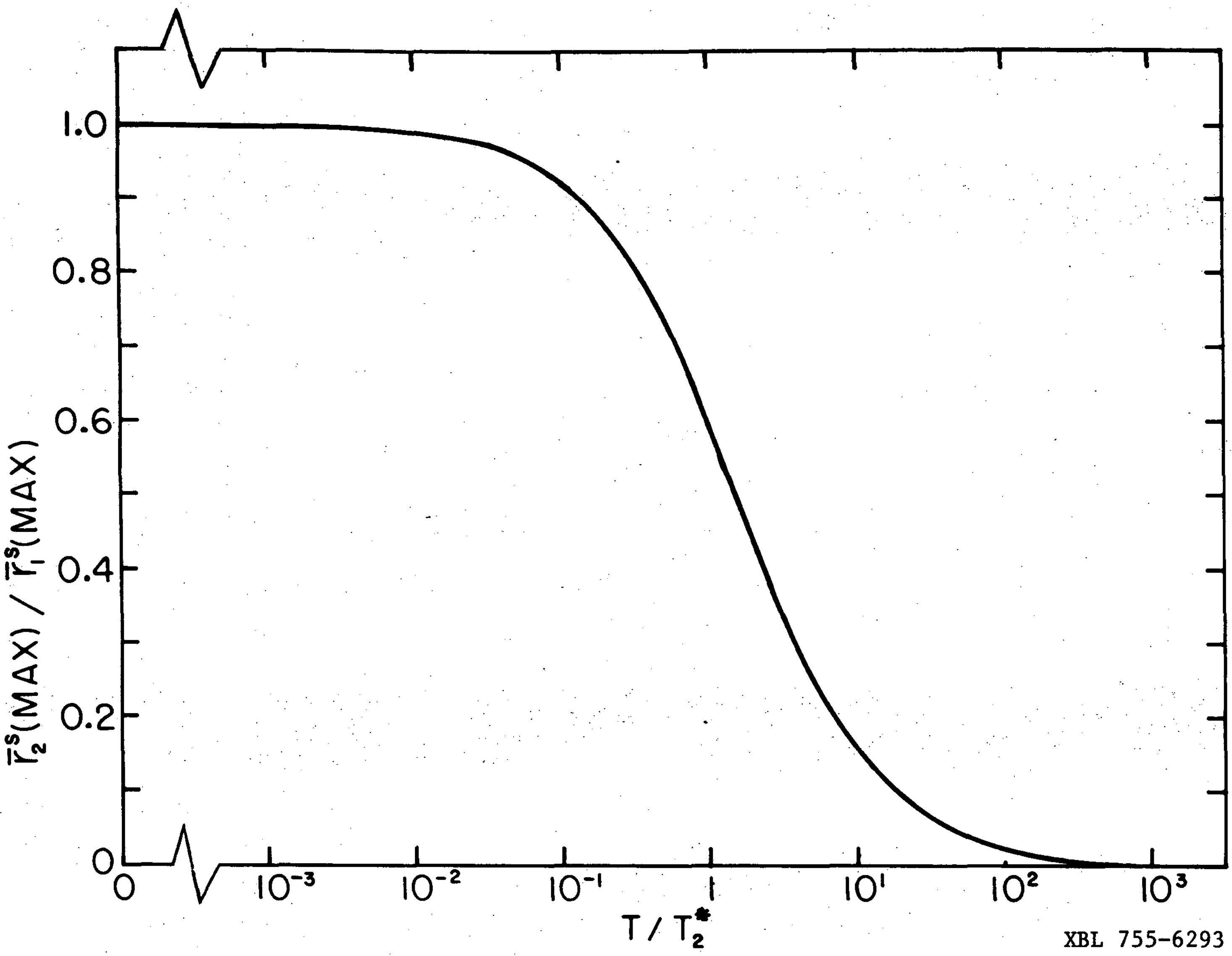

XBL 755-6293

Fig. 9. Maximum value of r_2^s, normalized by the invariant r_1^s, as a function of the unitless parameter T/T_2^*. Appreciable inhomogeneous broadening ($T/T_2^* > 1$) causes a significant decrease in the r_2^s component.

Since the amplitude of the maser radiation is proportional to the size of the inplane component in a conventional on-resonance amplifying system, it is tempting to consider the previous arguments comparing r_1 and r_2 components with respect to the maximum intensity of coherent radiation that could be obtained from a given system. These arguments predict that a properly chosen system that possesses a ω_1 dependent T_{2e} and has appreciable inhomogeneous broadening could conceivably produce coherent radiation fields that are orders of magnitude larger that the fields that could be produced by on-resonance excitation. In the same sense that on-resonance coherence is self-regulating at saturation, the off-resonance experiment self-regulates about the value given in Eq. (85). Unfortunately the application of these results to optical systems that possess appreciable gain is not straightforward since the driving field must be modified to include spatial effects and the contribution of the coherent component to the driving field itself, and it is not clear whether this property could be exploited to increase the power output of a given system.

One aspect of steady-state coherence may possibly be exploited, however, in the study of superradiance.[54] Dicke first presented the idea in 1954, but it was not widely discussed until recently. The topic has been obscured by semantics and experimental misinterpretation and is presently the subject of considerable debate.[55] The steady-state component provides a novel method for maintaining and controlling a superradiant state by use of a coherent driving field and incoherent feeding. By choosing an appropriate system consisting of a thin sample with long relaxation times, a large steady-state vector may be maintained by an intense off-resonance coherent driving field, and the system may effectively be prepared in a state of any "cooperation number". The field may then be turned off and the system studied as it evolves in time, and in this way the various properties of the superradiant state could be "mapped out".

G. Extension to the Optical Frequency Region

The previous treatments all utilized the following assumptions:

(1) semiclassical, monochromatic, coherent driving field

(2) wavelength of driving field is large compared to the size of the entire ensemble.

(3) fields produced by ensemble are negligible.

Assumption (1) may be modified in the semiclassical limit to include spatial effects and deviations from temporal and spatial coherence by considering a more general form for V(t) (Eq. (10)).

$$V(z,t) = \hbar\sigma_1 f\omega_1(z,t)\cos(\omega t - kz + \phi(z,t)) \tag{87}$$

and Eq. (10) may be considered to have been derived from Eq. (87) with the approximations

$$\frac{\partial\omega_1}{\partial z} \ll k\omega_1\,, \quad \frac{\partial\omega_1}{\partial t} \ll \omega\omega_1, \quad \frac{\partial\phi}{\partial z} \ll k\phi\,, \quad \frac{\partial\phi}{\partial t} \ll \omega\phi\,. \tag{88}$$

Assumption (2) may be expressed in terms of the sample length, Z,

$$kZ \ll 1 \tag{89}$$

and Eq. (10) then follows.

1. Spatial Considerations

Assumption (2) may be eliminated quite easily provided that (1) and (3) are retained. In this case the strength of the applied field does indeed vary spatially across the sample, but the relationship between any two points within the sample is trivially related by the speed of light in the sample medium. As long as (1) and (3) hold, there is no dispersion, and the ensemble may be considered to be coherently coupled, for although different parts of the sample do not "simultaneously" experience the same field, each point z will experience the same field at the "retarded" time t-z/c. A novel way to include this consideration in the formalism of chapter II is the following. Including the spatial dependence explicitly, Eq. (12) becomes

$$\mathcal{H}'_j = \frac{\hbar\omega_o}{2}\sigma_3 + \frac{\hbar f\omega_1}{2} e^{-i\sigma_3 \frac{\omega t - kz_j}{2}} \sigma_1 e^{i\sigma_3 \frac{\omega t - kz_j}{2}} \tag{90}$$

where $\mathcal{H}'_j$ is now a different Hamiltonian for each molecule in the ensemble with position z_j. Utilizing the same reasons that prompted a rotating frame transformation, both the temporal and spatial dependence may be removed from the effective Hamiltonian, $\mathcal{H}$. Defining a unitary operator similar to Eq. (15)

$$U_{k,j} = e^{-i\sigma_3 \frac{\omega t - kz_j}{2}} \quad . \tag{91}$$

Each density matrix for the jth molecule may be transformed as in Eq. (16), and each transformed density matrix now obeys the same equation of motion which is identical to Eq. (17), and the entire development, from Eq. (17) on, may be applied. Of course the spatial dependence has not actually been "removed" by these manipulations, but since it is of a trivial nature, the dependence may be incorporated in the unitary operator where it does not interfere with the equation of motion, just as in the case of the rotating frame transformation. Notice that Eq. (91) is tantamount to transforming to a rotating frame in which the substitution for the retarded time $t-z_j/c$ has been made in Eq. (15). Since (1) and (3) insure no dispersion, the group and phase velocities are equal, $c=\omega/k$, and Eq. (91) follows.

At this point one might speculate on a "decay frame" transformation that would take the well-defined decay of the states and place it in a unitary transformation in the same fashion as the rotating frame and spatial transformation. If this could be done, the equations would reduce to very simple forms again. Unfortunately this is not possible, for even though it is well defined, the overall decay rate at any given time is strictly dependent on the position of the r-vector, and therefore the decay terms must necessarily be a part of the equation of motion. However, under the special condition $k_x=k_y$, the decay may indeed be removed from the equation of motion and incorporated in the unitary operator, for in this case the vector has the same probability for decay, independent of its position in r space.

2. Photon Echo

The spatial transformation is not as trivial as the rotating frame transformation and will depend strongly on the shape of the sample, how it is driven by the applied field, and how it is observed. One special case worth considering is that of a small sample observed at a large distance. In this situation the observed behavior of the system will be the sum of each density matrix ρ_j resulting from the Hamiltonian $\mathcal{H}_j$. The spatial dependence may be left in as an effective phase with $-\vec{k}\cdot\vec{r}_j$ replacing ϕ in Eq. (10) and Eq. (20). For the sake of example an echo sequence is taken in which the first $\pi/2$ pulse enters the sample with wavevector $\vec{k}_1$ and the π pulse enters at a different angle, but with the same frequency, $\vec{k}_2$, $\vec{k}_1 \neq \vec{k}_2$, $|\vec{k}_1| = |\vec{k}_2|$. Repeated application of Eq. (19) yields a final density matrix for each member in the ensemble assuming that everything starts in the ground state $r_x=1$, $r_y=0=r_1=r_2$

$$\rho_j = \begin{bmatrix} \frac{1}{2} & ie^{i\Delta\omega(t-t')}\, e^{i\frac{(2\vec{k}_2-\vec{k}_1)}{2}\cdot\vec{r}_j} \\ -ie^{-i\Delta\omega(t-t')}\, e^{-i\frac{(2\vec{k}_2-\vec{k}_1)}{2}\cdot\vec{r}_j} & \frac{1}{2} \end{bmatrix} . \qquad (92)$$

For a large number of closely spaced members in the ensemble, the sum over j becomes an integral over the function $G(\vec{r})$ that describes the shape of the sample. The form of Eq. (92) demonstrates that this will result in the spatial Fourier transform of $G(\vec{r})$. If $G(\vec{r})$ is spherical with sufficiently large radius, the off-diagonal elements are reduced to δ functions with argument $2\vec{k}_2-\vec{k}_1$. A simple geometrical argument demonstrates that if the π pulse is applied at an angle α

with respect to the initial $\pi/2$ pulse, a burst of coherent radiation associated with the formation of a photon echo will be emitted at an angle 2α with magnitude $\sim|k_1|$ provided that α is small enough, in accordance with the predictions and results of Ref. 31. Note that there would be no directional dependence associated with the normal spontaneous emission from r_y.

3. Photon Echo with Probe Pulse

Several problems are present with the photon echo experiment, most of them associated with detector overload and sensitivity. In this situation the probe pulse method might prove to be more useful since the spontaneous emission may be monitored at any angle. Specifically, if an additional $\pi/2$ probe pulse is applied to ρ_j in Eq. (92), r_{yj} is given by

$$r_{yj} = \frac{1}{2}\left[1 - \frac{1}{2}\left(e^{i\Delta\omega(t-t')}e^{i(\vec{k}_2-\vec{k}_1)\cdot r_j} - e^{-i\Delta\omega(t-t')}e^{-i(\vec{k}_2-\vec{k}_1)\cdot r_j}\right)\right] \tag{93}$$

and $\vec{k}_1$ may be set equal to $\vec{k}_2$ since the detector is not montoring the coherent radiation, again rendering the r_y component spatially independent. Assuming an on resonance echo and a Lorentz line shape, the photon echo would then be given by

$$r_y = \frac{1}{2}\left(1 - e^{-\frac{t-t'}{T_2^*}}\right) \tag{94}$$

which corresponds to no spontaneous emission at echo maximum and emission corresponding to saturation at values of t-t' far from echo maximum.

In order to accurately map out the actual echo shape the probe pulse must be sufficiently short compared to T_2^*, but, since the echo shape is not particularly interesting anyway, this requirement is not essential. However, the echo maximum decay may be accurately monitored with pulses that do not meet this condition. An additional point must be made with respect to the method used to monitor Eq. (94). An optical system often cannot maintain temporal coherence for the time required to perform the entire echo sequence and may result in the condition in which each successive pulse has a random phase relationship with respect to the pulse preceeding it. It is easy to see that this fact has no particular significance in terms of the actual echo formation since the random phase merely causes the echo to form in different parts of the r_1-r_2 plane which implies that the burst of coherent radiation has a different phase each time the experiment is performed. This feature is much more important for the probe pulse, however, since a random phase will result in the vector being rotated "up" just as many times as it is turned "down" and a time average of many experiments will yield no signal unless a method that measures the "rms" excursions of the vector is used. Of course this problem is also present when microwave transition frequencies are being used, and one must therefore insure that a time-averaged probe sequence measures the decay due to molecular relaxation and not the residual FM of the microwave sweeper.

V. SPECIFIC APPLICATIONS TO PHOSPHORESCENT TRIPLET STATES IN ZERO FIELD

In this chapter, the formalism developed in chapters II, III, and IV is applied specifically to the problem of zero field phosphorescent triplet states. The alterations and additional assumptions are first outlined and then illustrated with a few exemplary experimental results.

The second part of the chapter gives a detailed account of the actual experimental techniques and equipment required to perform optically detected coherence experiments in zero field.

A. Relationship between the Geometrical Picture and Phosphorescence

The triplet state of many molecular solids is nondegenerate in zero field, owing to the electron dipole-dipole interaction and is commonly expressed in terms of the Hamiltonian[13]

$$\mathcal{H}_o = -XS_x^2 - YS_y^2 - ZS_z^2 \, . \tag{95}$$

The three spin sublevel eigenfunctions, τ_x, τ_y, τ_z, are often quantized along the symmetry axes of the molecule, and can be mixed by the spin operators S_x, S_y, S_z. The matrix elements are given by

$$\langle \tau_i | S_j | \tau_k \rangle = i\hbar \qquad i,j,k = x,y,z \text{ cyclic permutation} \, . \tag{96}$$

Since $\mathcal{H}_o$ is traceless, it is also expressed in terms of the two parameters D and E.

The triplet spin sublevels may be populated by excitation of a number of singlet states with broadband emission from a mercury arc lamp, and the weak interactions resulting from spin-orbit coupling allow intersystem crossing to triplet states of the proper symmetry. Rapid internal conversion populates the lowest triplet state, and, owing to symmetry restrictions, significantly large nonboltzman population distributions between the various spin sublevels may result at sufficiently low temperatures, usually around that of liquid helium.[19] A microwave field may be applied to such a system, and if there is any population difference between two of the three levels, the resonance spectrum may be recorded by monitoring the change in phosphorescence that results when the applied field alters the populations between the levels. The form of the perturbation given in Eq. (10) is explicitly for the triplet state

$$\omega_1\hat{\mu} = \gamma H_1\langle \tau_i|S_j|\tau_k\rangle \tag{97}$$

where H_1 is the amplitude of the magnetic component of the EM field and γ is the gyromagnetic ratio of the electron. The imaginary form for the matrix elements implies that $\mathcal{H}'$ in Eq. (12) should be expressed in terms of σ_2, but, as Eq. (6) demonstrates, this amounts to only a 90° phase shift in the applied field direction, and the results of the preceeding chapters apply with trivial modifications that do not warrant further consideration.

In general, the observable that is associated with the triplet state phosphorescence arises from the coupling of the singlet and triplet states by a weak spin-orbit perturbation.[56,57] The triplet state is thus an admixture of triplet and singlet vibronic levels,

$$|\tau_i\rangle \cong |\tau_i\rangle + \sum_n C_n^i |S_n\rangle + \text{triplet terms} \tag{98}$$

and emission to the ground state manifold, S_o, is made possible through an electric dipole transition that couples with the singlet admixture.

$$\langle\tau_i|\mu_J|S_o\rangle \cong \sum_n C_n^i \langle S_n|\mu_J|S_o\rangle \equiv C_J^i \tag{99}$$

The expressions in Eq. (98) and (99) are grossly oversimplified but are quite adequate to describe the problem. The subscript J denotes the polarization of the electric field, determined by symmetry considerations.

The observed phosphorescence may now be obtained from the density matrix by constructing a "phosphorescence operator"[58]

$$P_J \equiv |\mu_J|S_o\rangle\langle S_o|\mu_J| \tag{100}$$

and determining its expectation value

$$\langle P_J\rangle = \mathrm{Tr}[\rho P_J] \tag{101}$$

this may be expressed in terms of the r-vector components from Eq. (7)

$$\langle P_J\rangle = \frac{1}{2}|C_J^y|^2(1+r_3) + \frac{1}{2}|C_J^x|^2(1-r_3) + \mathrm{Re}(C_J^{y*}C_J^x)(r_1-ir_2)$$

or (102)

$$\langle P_J\rangle = |C_J^y|^2 r_y + |C_J^x|^2 r_x + \mathrm{Re}(C_J^{y*}C_J^x)(r_1-ir_2)$$

$|C_J^y|^2$ and $|C_J^x|^2$ may be identified with the radiative rate constants k_y^r and k_x^r, respectively, where the r superscripts have been included to allow for nonradiative processes that could also contribute to the total rate constant k. In general, the symmetry properties associated with many molecules place fairly strict limitations on the various allowed polarizations and usually one of the two coefficients C_J^y or C_J^x is zero for a given polarization, J. Under this condition it can be seen that

$$\langle P_J \rangle \propto r_3 + \text{constant} . \tag{103}$$

Equation (103) implies that any change in the observed phosphorescence is manifested as a proportional change in r_3, as would be expected.

The special case in which C_J^y and C_J^x are both nonzero merits further attention. Under this condition, the coherent components are actually manifested in the phosphorescence as a modulation at the larmor frequency. Furthermore, if $C_J^y = C_J^x$, Eq. (102) reduces to

$$\langle P_J \rangle = k^r(1 + r_1\cos\omega t + r_2\sin\omega t) \tag{104}$$

where the off-diagonal element of the density matrix has been converted back to laboratory coordinates. A 100% modulation of the phosphorescence occurs at the larmor frequency if a coherent state is created in the absence of relaxation. This phenomenon was first discussed in relationship to zero field phosphorescence by Harris[21] and is quite similar to analagous results obtained in gases[59] and solids[60] in other double resonance studies. The effect has had considerable theoretical attention as well.[58,61,62] Notice, however, that for the general situation a probe pulse would be required to monitor the coherence if phosphorescence is used as the observable.

The model system depicted in Fig. 5 will be quite well suited to describe triplet state coherence experiments provided that the constant feeding parameters F_x and F_y may be justified, and also there must be no interference from the third level through spin-lattice relaxation. The second requirement may be met by cooling the sample to a sufficiently low temperature, and the first condition is valid provided that the singlet states are optically pumped at a constant rate and that the ground state is not significantly depleted. All these conditions are experimentally attainable.

In zero field, intersystem crossing occurs incoherently to the eigenstates, satisfying the form for F in Eq. (45). Thus, the mathematical formalism is quite easily applied to zero field triplet states.

B. Experimental Examples

Figure 10 depicts an optically detected transient nutation for high power on and off resonance pulses. Since oscillitory behavior is observed, it is possible to coherently couple two levels in the triplet state. Note that a rough determination of the nutation frequency corresponds reasonably well to $\bar{\omega}$ of Eq. (21) despite the strong damping present. The damping is caused primarily by applied field inhomogeneities as can be verified by lowering the power and observing that the same number of oscillations occur. This inhomogeneity is to be expected since the coupling to the sample is done through a slow wave helix.[63]

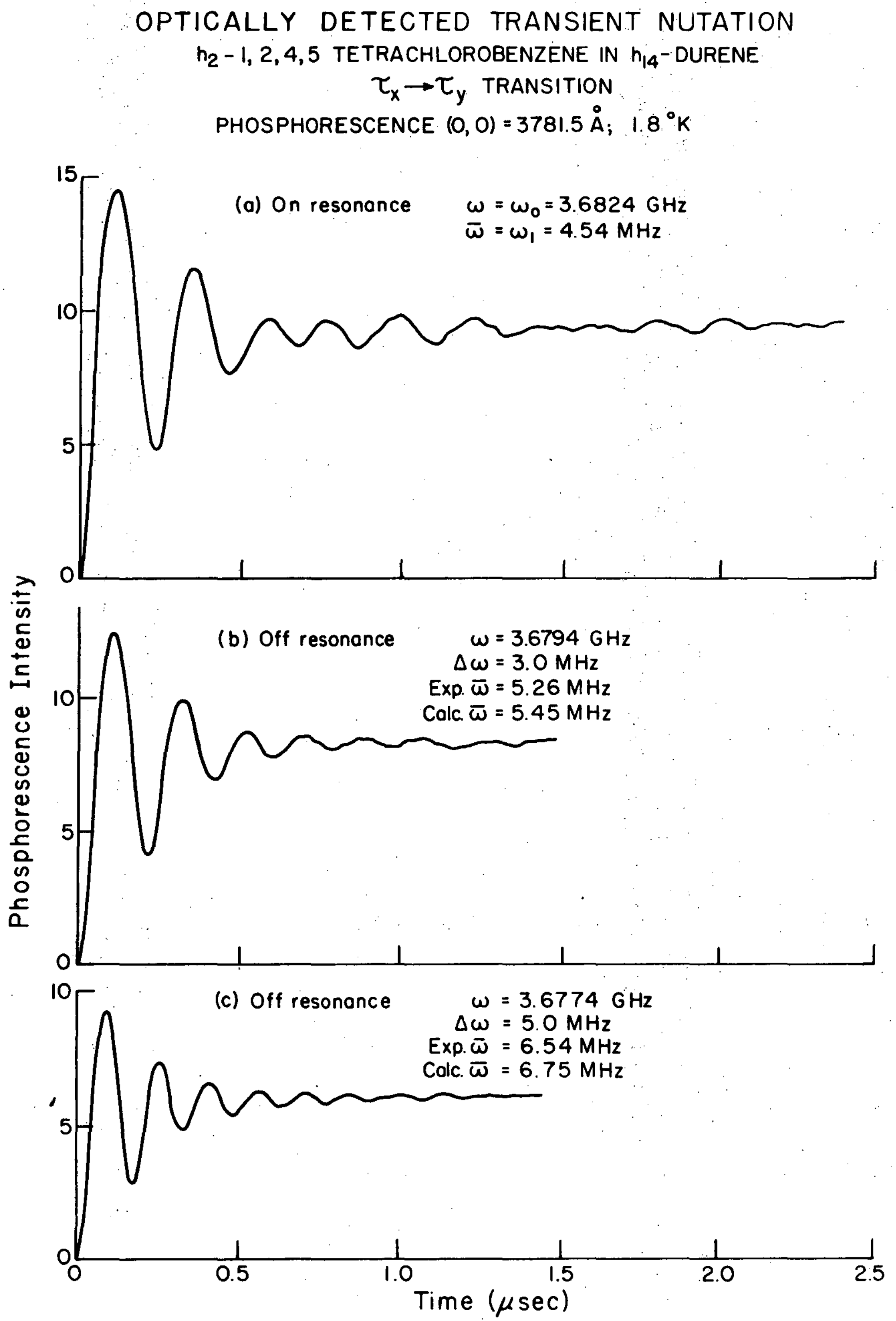

XBL 7310-5453

Fig. 10. Optically detected transient nutation. The change in phosphorescence intensity ($\propto r_3$) is plotted as a function of the duration of the microwave pulse.

Figure 11 illustrates the frequency response to a high power pulse for a π and a 2π pulse whose theoretical forms are given by (b) and (d) in Fig. 3. Although inhomogeneities and unleveled power distort the waveforms considerably, the characteristic 2π "hole" can be seen, and the waveforms clearly demonstrate that the response is not merely the Fourier transform of a short pulse. Reference 36 gives a particularly convincing set of waveforms of this type for hypersonic molecular beams.

Examples of optically detected electron spin echoes are given in Figs. 12 and 13. Notice that the probe pulse is required and is applied point-by-point in time in order to map out the echo shape. A transient nutation determines the length of time required to produce the pulses used in the sequence. Both the on and off resonance echo shapes are described by Eq. (41).

The decay of the echo maximum peak as a function of the total waiting period, $\tau+\tau'$ in Eq. (41), will give the homogeneous relaxation time, T_2, as illustrated in Fig. 14. The decay is a single exponential for this particular system.

The problems inherent with optically detected Fourier transform spectroscopy are demonstrated in Fig. 15. As expected, there are large intensity errors present. The echo was obtained by utilizing pulses where ω_1=5 MHz. Since the multiplet structure is 5 MHz wide, this would also contribute to intensity errors because the proper condition for FTS is that $\omega_1 \gg \Delta\omega$.

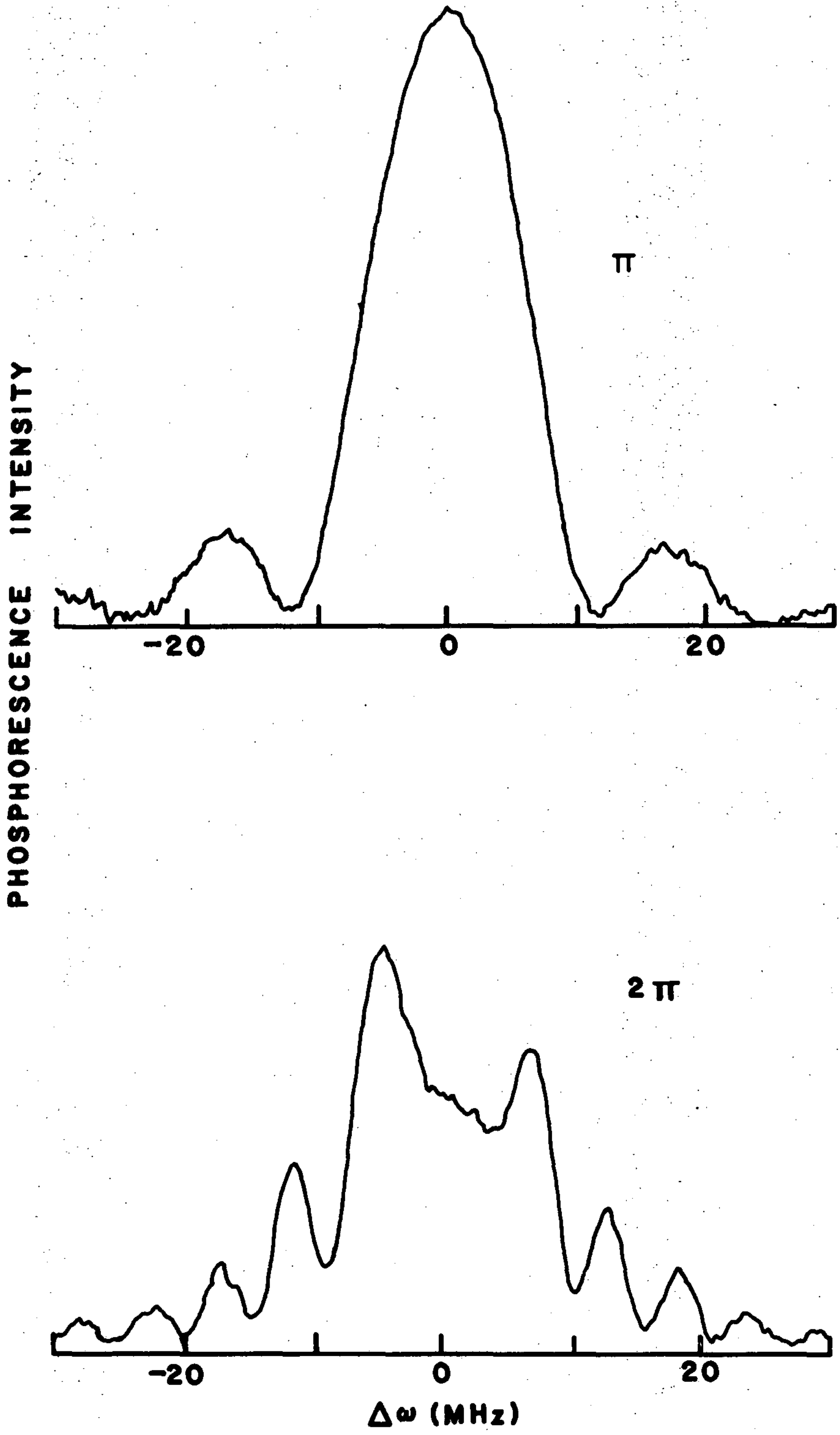

XBL 755-6289

Fig. 11. Experimentally determined response of the triplet state phosphorescence to a high power microwave pulse. These are to be compared to the predicted forms in Fig. 3.

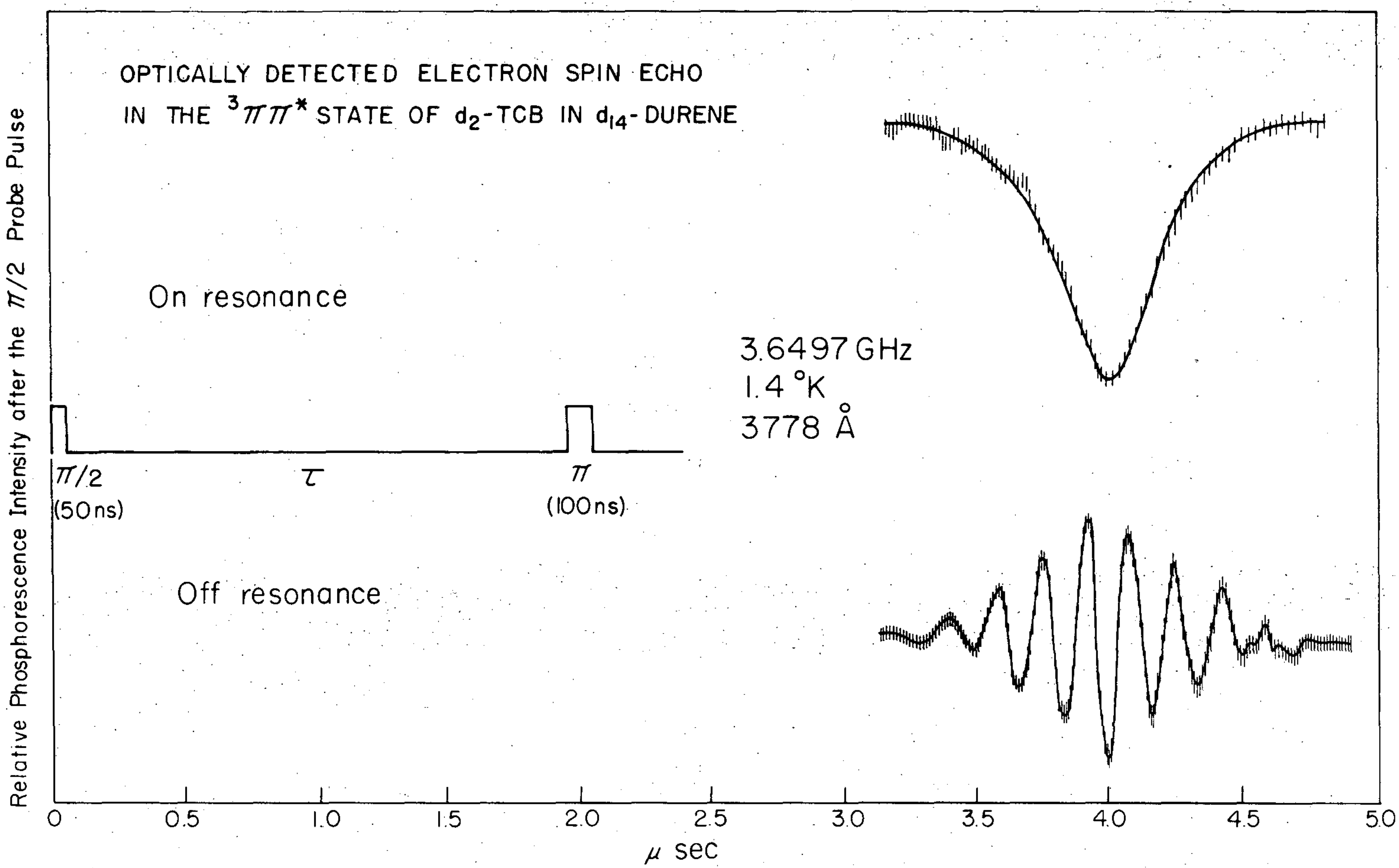

XBL731-5689

Fig. 12. Optically detected zero-field electron spin echo. The π refocussing pulse is applied 2 μsec after the initial $\pi/2$ pulse and the final $\pi/2$ probe pulse is swept in time. The echoes at the right are traced out point by point as the probe pulse is applied at the time given on the abscissa. The vertical lines are noise at each point in time.

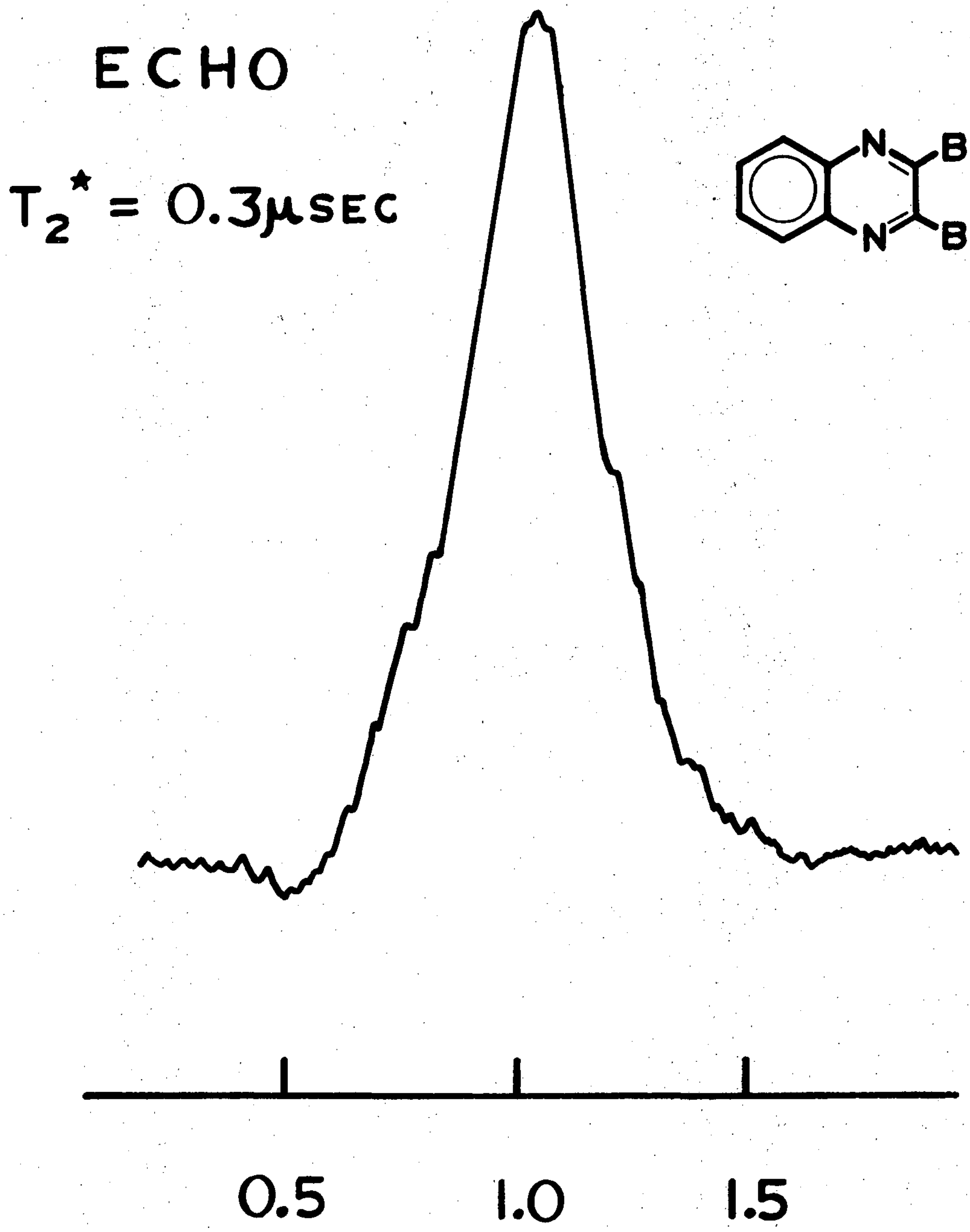

XBL 755-6291

Fig. 13. Echo traced out by the device shown in Fig. 23.

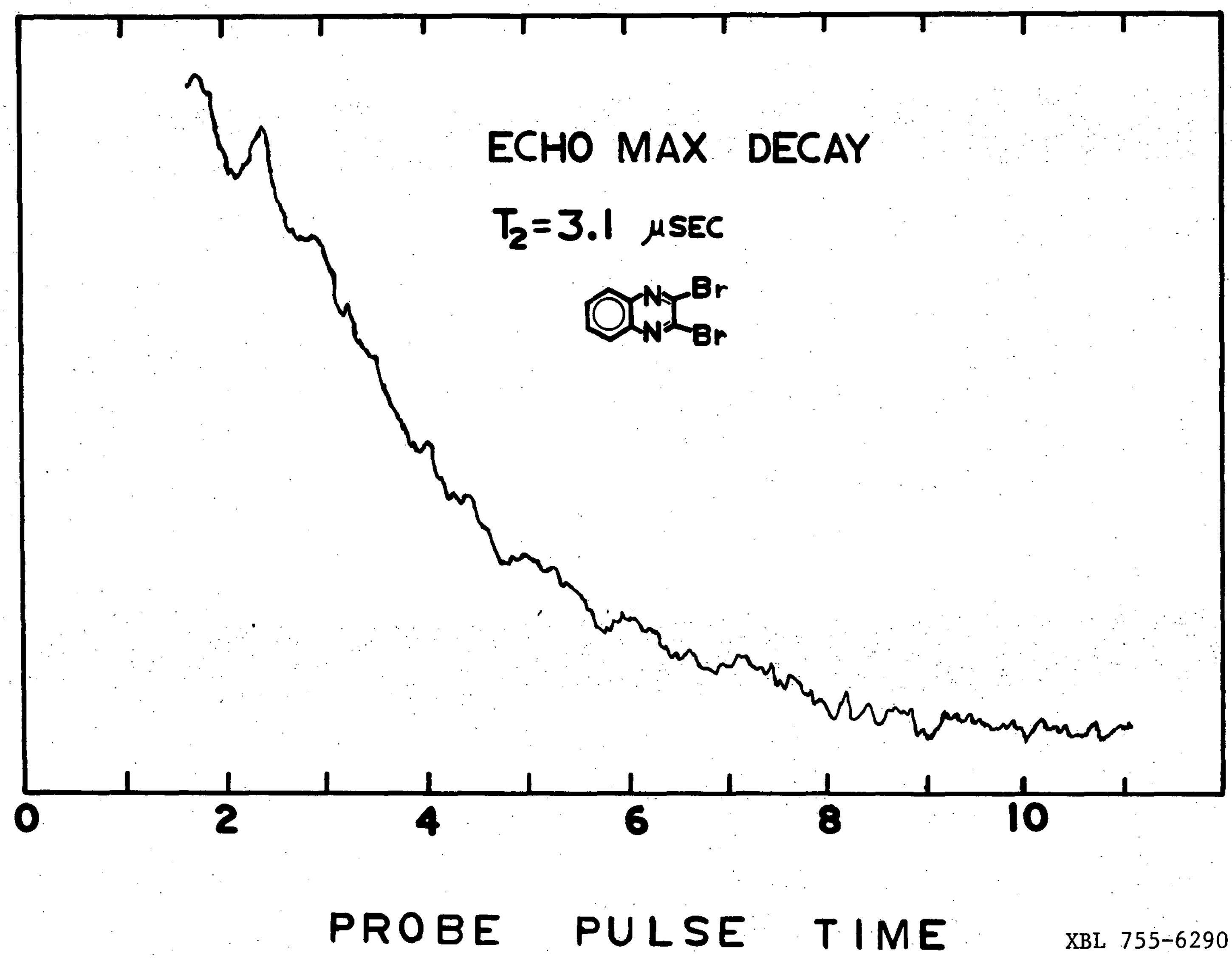

XBL 755-6290

Fig. 14. Trace of the echo/maximum decay from the device shown in Fig. 24.

C. Comparison of Solutions to Previous Zero Field Experiments

The optically detected cw spectrum given by Eq. (80) and (81) has of course been well established from the beginnings of zero-field phosphorescence microwave double resonance. However, the actual analytical form has never been derived but merely assumed to have the same form as in magnetic resonance. One advantage present in cw optical detection that is lacking in conventional EPR detection results from the different saturation characteristics, given by Eq. (82), allowing one to obtain a maximum signal with maximum power, and therefore there is no danger in making a sought after transition dissappear by applying the incorrect magnitude of driving field, as is often encountered with conventional magnetic resonance. For low powers, the optically detected EPR signal is linear in the power of the applied field, Eq. (81), and this behavior has been observed.[64]

At this point it is worthwhile to take the results of chapters II, III, and IV as they apply to phosphorescent triplet states and compare them to previous work by other authors. With two exceptions [21,22] a "rate equation" approach has been taken to describe the transient behavior of the triplet state under the influence of a perturbing microwave field, and all this previous work may be shown to be special cases of Eq. (53) or Eq. (69). The earliest treatments[65,66] assumed the same arguments that led to Eq. (63), namely that $r_y(t)=r_x(t)$ during the entire time development of the populations. If steady-state conditions are achieved under a strong rf field, the total population is N^s of Eq. (63), and by turning off just the optical pump, $F_x=F_y=0$, but leaving the microwaves on, Eq. (10) of Ref. 66 follows.

$$N = N^s e^{-k_A t} \tag{105}$$

Shain and Sharnoff[67] proposed a set of differential rate equations to describe a new method for measuring the various feeding and decay parameters associated with zero field triplet states. Their equations may be obtained as a special case of Eq. (69) if one considers the conditions on-resonance, $\Delta\omega=0$, negligible spin-lattice relaxation, $1/T_x=1/T_y=0$, and considering times after the coherent component transients have decayed away, $\dot{r}_1=\dot{r}_2=0$. Equation (69) then becomes

$$\begin{aligned} r_1 &= 0 \\ r_2 &= -f\omega_1 T(r_y-r_x) \\ \dot{r}_y &= f\omega_1 r_2/2 - k_y r_y + F_y \\ \dot{r}_x &= -f\omega_1 r_2/2 - k_x r_x + F_x \end{aligned} \tag{106}$$

and Eq. (1) of Ref. 67 follows provided that one identifies the "induced transition rate", W, with the term

$$W \equiv \frac{f^2\omega_1^2 T}{2} \tag{107}$$

The expressions in Eq. (2) of Ref. 67 follow if this definition is incorporated into the steady-state terms given in Eq. (73).

The explicit form for W and the conditions under which it is derived clarify the rather nebulous statements made by Shain and Sharnoff relating to the applicability of their Eq. (1). Since $T \cong T_2$ for triplet state systems, Eq. (106) will not be applicable until

$t \cong 10T_2$, which is the time that it would take the transient nutation to stop oscillating. The simpler arguments of El-Sayed, et al.[65,66] are a special case of Eq. (106) for $W=\infty$, for then N^s results in the steady-state solutions.

In addition to the minor semantic difficulties associated with Ref. 67, a more serious error is made by assuming, without stating so, that the line is homogeneously broadened, hence effectively equating $(2\pi\Delta\nu)^{-1}$ with T_2. The shortest T_2 that has been measured is 3μ sec, implying that the homogeneous linewidth, should be 0.1 MHz, which is narrower by a factor of ten than the observed low power linewidths. This, coupled with the fact that the echo is observed, rules out homogeneous broadening, and an expression such as Eq. (80) must therefore be used. If an intermediate value of $f\omega_1$ is used as Ref. 67 suggests, "$\gamma H_{rf} \ll 2\pi\Delta\nu$", implying that $f\omega_1 T_2^* \ll 1$, the true value of $B_{ij}(\omega)$ is not as simple as their Eq. (3), and care must be used when one attempts to obtain relative populations and feeding rates by their method. Further, prolonged application of a high power microwave field can physically heat the sample and alter the populations through spin-lattice relaxation. These, and other problems related to the measurement of kinetic parameters associated with the triplet state are amply discussed in Refs. 68 and 69.

If the equations in (106) are further simplified by assuming steady-state conditions for r_y and r_x as well, Eqs. (1) and (2) of Ref. 70 follow, provided that the "cross section" and "power" are defined as $\sigma P=W$, Eq. (107).

1. Extension to Three Levels

An extensive search through the literature has not revealed any equations dealing with zero field ODMR that are not a special case of Eq. (69), save those treatments that consider spin lattice relaxation between all three triplet spin sublevels, in which case Eq. (69) does not apply. The extension to a three level system is straightforward since only relaxation terms and a third population component, r_z, need to be added to Eq. (69). A 9×9 Liouville matrix, many of whose elements are zero, may be constructed and a solution analagous to Eq. (79) follows immediately. The evaluation of the exponential matrix would prove to be a formidable but soluble problem.

2. Comparison to the Work of Icsevgi and Lamb

Equation (69) can be seen to be a special case of Eq. (52) from Ref. 48, if the following assumptions are made. Set $T_{2e}=T_2$ and ignore spin-lattice relaxation and spontaneous emission in Eq. (69). Convert the r-vector components to the laboratory frame, and relate the rotating frame components r_1 and r_2 to the in-phase and out-of-phase components of the polarization. This may be done by considering Eqs. (13), (19), and (43) of Ref. 48, resulting in the relations $C(v,z,t)=fr_1$, $S(v,z,t)=-fr_2$. Assuming that $v=0$ and ignoring the spatial dependence, Eq. (52) of Ref. 48 reduces to Eq. (69) with the substitutions

$$\begin{aligned}
(\omega-\nu) &= \Delta\omega \\
C &= fr_1 \\
S &= -fr_2 \\
\gamma_{ab} &= 1/T \\
\Lambda_a &= F_y \\
\Lambda_b &= F_x \\
P &= f \\
\varepsilon &= -\hbar\omega_1 \\
\gamma_a &= k_y \\
\gamma_b &= k_x
\end{aligned}$$

The steady-state solutions, Eq. (73), are also obtained in Sec. III of Ref. 48, the "monochromatic wave" case. Similarly, the solutions for "long pulses" and "ultrashort pulses" compare with Eq. (106) and Eq. (22). Note however that, owing to the complexity of the problem in Ref. 48, numerical integration is required for the intermediate cases whereas Eq. (69) may be solved exactly.

D. Steady-State Coherence

Owing to the possible ramifications of off-resonance steady-state coherence discussed earlier, it would be worthwhile to determine whether coherence may indeed be made to last times far exceeding the lifetimes of the states involved. To this purpose two experiments were performed.

The first experimental pulse sequence utilizes a spin echo to detect the coherent component. First an off-resonance microwave field of long duration is applied to the sample, "long" implying sufficient time to establish the steady-state values of the density matrix. This pulse establishes the coherent component given by Eq. (82). At the end of the long pulse an optically detected echo sequence is performed on the coherent component produced by the long pulse. It should be noted here that since the coherent component is produced along r_1 the echo corresponds to the first echo in an off-resonance Meiboom-Gill[71] sequence.

A second method that utilizes the probe pulse was also used to monitor the coherent component. Since the steady-state vector lies along the effective field direction, a phase shifted pulse is required to rotate the coherent component. The situation is complicated by the fact that both r_1 and r_3 components are produced by the long pulse. Therefore a probe pulse causes a change in the total phosphorescence that is proportional to the contributions from both these components. This problem may be solved by performing another sequence in which the probe pulse is applied at a time $t \gg 5T_2^*$. In this case the r_1 component has completely dephased and the resulting contribution from the r_3 component may be subtracted from the first sequence leaving only the contribution due to the steady-state coherent component.

Eq. (85) gives the maximum value of the steady-state coherent component under high power conditions. If $T_e \rightarrow 1/k_A$ as $\omega_1 \rightarrow \infty$, and if spin-lattice relaxation is negligible, then the component is given by

$$\langle r_1^s \rangle_{\omega_o} (\max) \cong \frac{r_3^o}{2} \sqrt{\frac{k_x k_y}{k_A^2}} \tag{108}$$

The radical term is maximum when $k_x=k_y$, and thus it is best to choose a system in which two of the three levels have similar lifetimes, yet are fed differently enough to produce a significant r_3^o component. For these reasons, 1,2,4,5-tetrachlorobenzene as a 1% guest in a durene host was chosen. For this system the τ_z and τ_y sublevels have similar lifetimes of 36 and 38 msec, respectively, yet the steady-state population difference is four times higher in τ_z than it is in τ_y, at 1.8°K.

Figure 16 outlines the echo method for steady-state coherence detection and also gives an experimental trace of such an optically detected echo. The long pulse was applied 5 MHz off-resonance for 100 msec, and a suitable waiting time of 1 μsec was used to allow the coherent component to fan out yet not so long as to allow homogeneous relaxation to eliminate the echo signal.

The observation of an echo graphically demonstrates the existence of the coherent component but unfortunately cannot be used as a quantitative measure of the size of the component owing to the method used to record it. After a pulse sequence is completed, it is desirable to wait at least five phosphorescence lifetimes before the next sequence is initiated in order to insure that the system has returned to equilibrium. For this system 175 msec is required. For a 100 msec "long" pulse, a reference frequency of 1.8 Hz must be used, when a lock-in amplifier is employed and for longer pulses of course even lower frequencies must be used. These low frequencies contain a great deal of noise. In addition, the change in phosphorescence due just to the long pulse becomes a much larger signal than the echo signal. These conditions require an unusually high Q factor and frequency independent

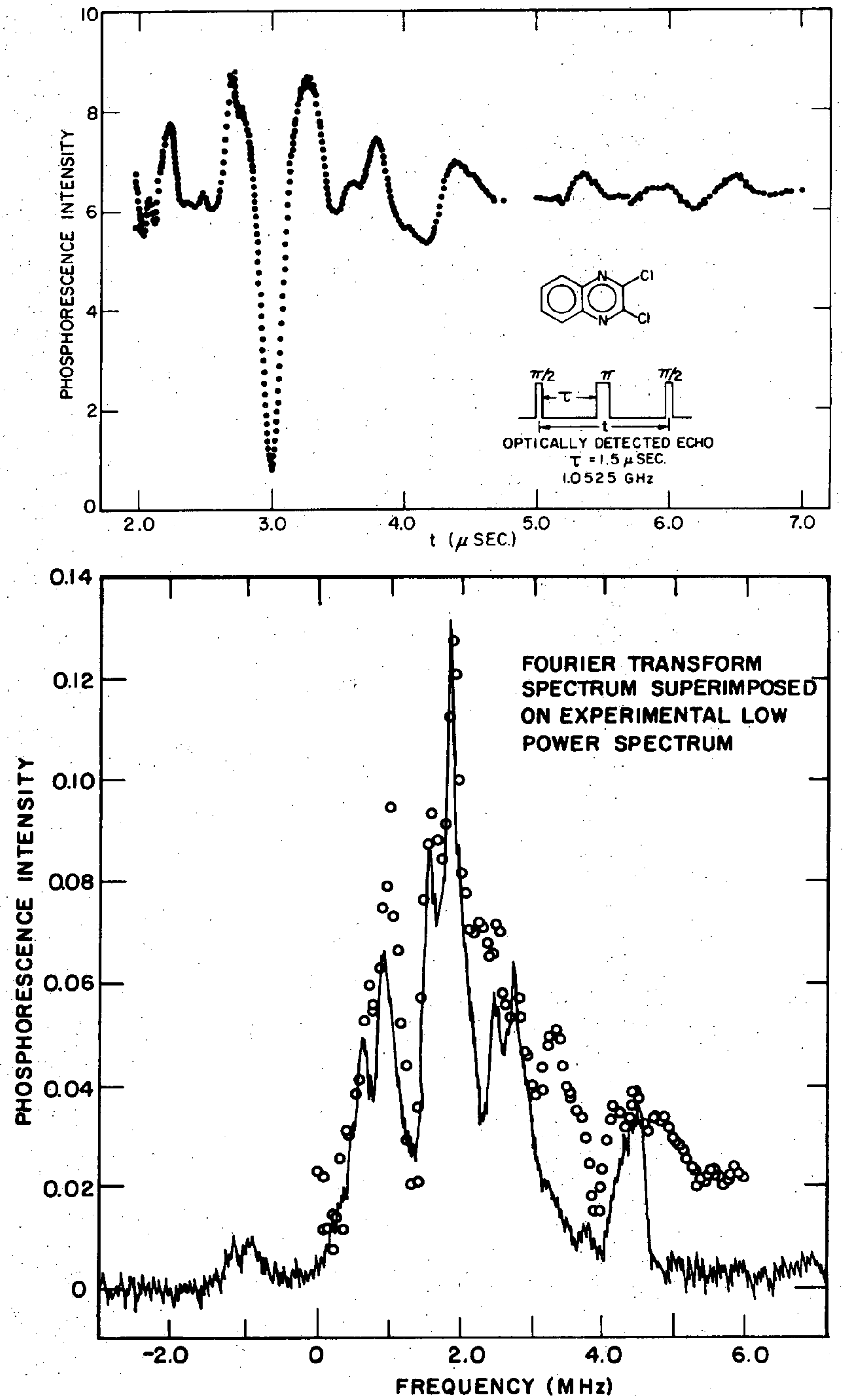

XBL 743-5728A

Fig. 15. Top: Optically detected spin echo of the 1.0552 GHz transition of 2,3-dichloroquinoxaline in 1,2,4,5-tetrachlorobenzene. The interval τ between the initial π/2 pulse and the π pulse is 1.5 μsec. The probe pulse is applied at time t after the initial π/2 pulse and is swept in time. Bottom: Fourier transform of the echo superimposed on the low power conventional ODMR spectrum.

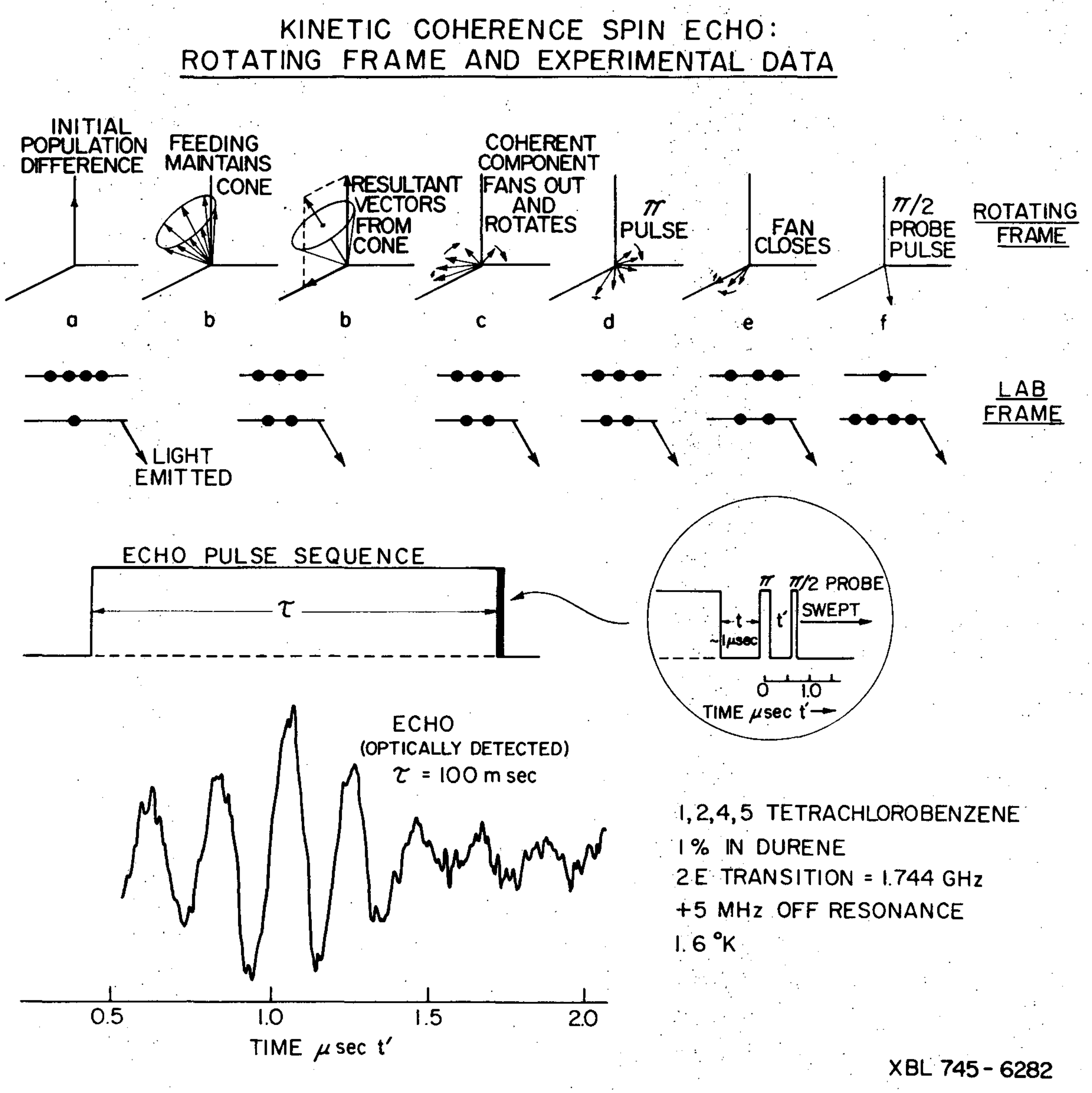

Fig. 16. Echo sequence desgined to detect the steady-state coherent component.

gain for regions in which a lock-in amplifier is not particularly well suited. Therefore, to avoid these difficulties, the second method involving two probe pulse sequences was employed to detect any decay of the coherent component that may not have been accounted for.

Figure 17 outlines the pulse sequence and experimental waveforms that resulted from averaging the signal with a digital CAT. The lower part of the figure gives a plot of the difference between the two sequences. It can be seen from this figure that the amplitude of the coherent component remains constant for times as long as two seconds, corresponding to 57 triplet lifetimes and shows no tendency to decrease.

E. Coherence Lifetimes

The experimental results presented here demonstrate that the length of time that the coherent component can be made to last varies over a very wide range. As an example consider the tetrachlorobenzene-durene system. A free induction decay reflects the lineshape, and the coherence lasts only 100 nsec. The echo sequence can refocus the fan but the homogeneous lifetime restricts the coherence time to 4 μsec. Reference 72 obtained coherence times of 24 msec for this system by utilizing a spin locking sequence. Finally, the last experiment presented in this work demonstrated that it is possible to produce an infinite coherence time. Each of these experiments may deal with different sources of relaxation phenomena, including trapping and detrapping of excitation in relation to coherent energy migration in solids. The results presented here serve only to demonstrate the

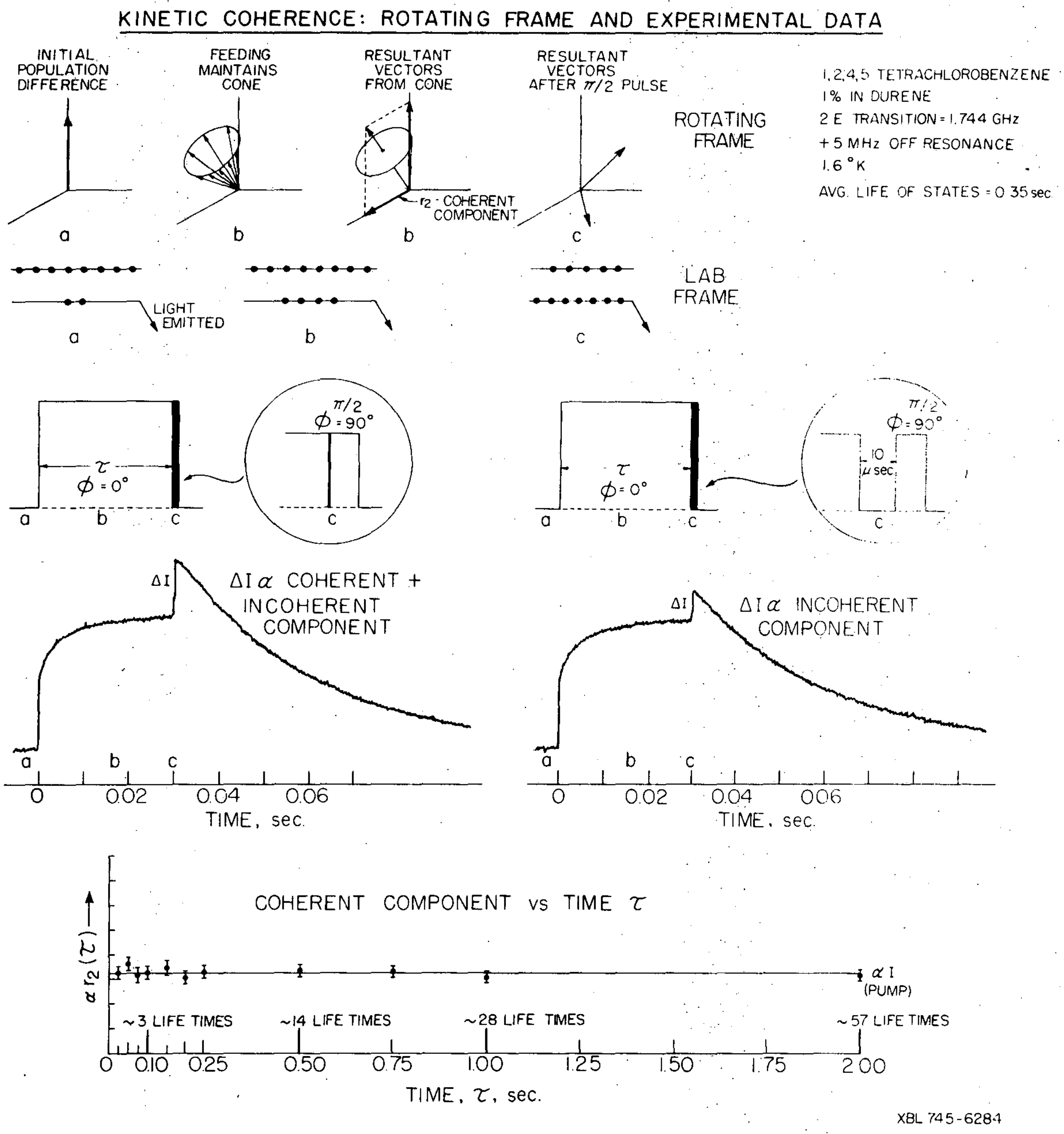

Fig. 17. Probe pulse sequence designed to measure the coherent component for extended periods of tieme.

formalism of chapters II, III and IV, and to establish the feasibility of optically detected coherence experiments in zero field phosphorescence microwave double resonance.

F. Further Considerations Associated with ODMR Coherence Measurements

As was discussed earlier, inhomogeneous driving fields, allowedness considerations and orientational effects can all contribute to difficulties with the transient nutation. Since the transient nutation serves as the keystone in practically all coherence experiments, it is desirable to minimize any problems that may interfere with this experiment. These factors will now be discussed.

1. Allowedness

This problem has already been discussed in reference to Fourier transform spectroscopy. Very little can be done about this since it is an intrinsic property of the system. In some situations it might be useful to produce an effective $\pi/2$ pulse by starting at some value $\Delta\omega$ from the center of a multiplet and then turning on a very intense field slowly enough that the adiabatic theorem holds for all lines in the multiplet. This assumes that there are no lines that are orders of magnitude different in f value, for in this case the adiabatic theorem may not be satisfied for all lines simultaneously. However if the f values lie within the same order of magnitude, the r vectors can be made to follow the effective field as it rotates down toward the plane, and in this fashion a more "accurate" $\pi/2$ pulse may be achieved.

Unfortunately, the field strengths that are experimentally attainable could hardly be classified as "very intense" compared to normal EPR linewidths encountered in ODMR, and some compromising must still be done.

2. Driving Field Inhomogeneities

This problem arises entirely from the traditional method for coupling microwaves to the sample through a slow wave helix. If one molecular system is to be studied extensively, it would be well to sacrifice the broadband characteristics of a slow wave helix for a cavity that would be homogeneous, but unfortunately, a cavity does not have as high H_1 field strengths as a helix. In some cases the "fan" caused by inhomogeneous broadening may be "folded back" by phase shifting 180° in different parts of the pulse sequence. This is the basis for the "rotary echo"[73] which is simply a periodically phase shifted transient nutation. The probe pulse echo could also utilize this feature, eg $(\pi/2, 0°)$, $(\pi, 180°)$, $(\pi/2, 0°)$.

3. Orientational Effects

Much of EPR is done in rigid glass matricies, but, as was demonstrated earlier, a random array of "polarized transitions" in zero field will not yield a particularly useful transient nutation in zero field. Coherence experiments must therefore be done in single crystal systems, in which there is a regular array of "oriented" molecules. Even in single crystal systems, however, orientational effects will still occur from the translationally inequivalent molecules within the unit cell. This problem may be exemplified by considering a single crystal of durene, in which a small percentage of 1,2,4,5-tetrachlorobenzene (TCB) has been introduced. Since the relative sizes of the two molecules are the same, TCB molecules are arranged within the lattice by substituting for durene molecules, and one must therefore consider the durene crystal structure in order to determine the orientational effects on the TCB transient nutation.

Durene is monoclinic with two molecules per unit cell, and belongs to the space group $P2_1/a$.[74] The unit cell dimensions are

$$a_o = 11.57\ \text{Å}$$
$$b_o = 5.77\ \text{Å}$$
$$c_o = 7.03\ \text{Å}$$
$$\beta = 113^\circ\ 18'$$

The general atom positions are listed in Table I. This table also lists the direction cosines of each molecule in the unit cell with the orthogonal crystal axis system a,b,c' and also the direction cosines and associated angles of the molecules with respect to each other.

Table I reveals that a transition associated with the x axis of TCB doped substitutionally in durene could have strong orientational effects since the transition moment directions are nearly orthogonal. Figure 18 illustrates the frequency spectrum of effective nutation frequencies that would result from a linearly polarized driving field that is initially applied (0°) along the x axis of one of the molecules of the unit cell with strength ω_1^o. The crystal is then rotated about the c' axis, which roughly corresponds to the z axis of both molecules, and Fig. 18 gives the nutation frequencies as a function of

Table I. Durene Crystal Structure

$P2_1/a$ $a_o=11.57$ $b_o=5.77$ $c_o=7.03$ $\beta=113°\ 18'$

GENERAL POSITIONS (in unit cell dimensions)

	a	b	c
1	0.188	0.314	0.267
2	0.093	0.157	0.127
3	0.037	-0.005	0.212
4	-0.055	-0.162	0.090
5	-0.108	-0.325	0.194

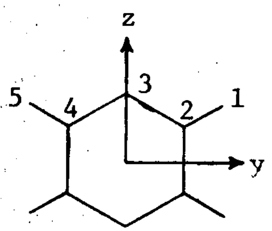

Direction Cosines for Molecule 1

$$\begin{array}{c c}
\begin{matrix} x_1 & y_{-1} & z_1 \end{matrix} & \\
\left[\begin{matrix} 0.7459 & -0.6619 & 0.0739 \\ 0.6552 & 0.7492 & 0.0973 \\ -0.1168 & -0.0207 & 0.9929 \end{matrix}\right] & \begin{matrix} a \\ b \\ c' \end{matrix}
\end{array}$$

Molecule 2

$$\begin{array}{c c}
\begin{matrix} x_2 & y_2 & z_2 \end{matrix} & \\
\left[\begin{matrix} -0.7459 & -0.6619 & -0.0739 \\ 0.6552 & -0.7492 & 0.0973 \\ -0.1168 & 0.0207 & 0.9929 \end{matrix}\right] & \begin{matrix} a \\ b \\ c' \end{matrix}
\end{array}$$

Between 1 and 2

$$\begin{array}{c c}
\begin{matrix} x_1 & y_1 & z_1 \end{matrix} & \\
\left[\begin{matrix} -0.1237 & -0.9918 & 0.0274 \\ 0.9918 & -0.1225 & 0.0356 \\ -0.0274 & 0.0356 & 0.9991 \end{matrix}\right] & \begin{matrix} x_2 \\ y_2 \\ z_2 \end{matrix}
\end{array}$$

Associated Angles

$$\left[\begin{matrix} 97.1 & 172.7 & 88.4 \\ 7.3 & 97.0 & 88.0 \\ 91.6 & 88.0 & 2.4 \end{matrix}\right]$$

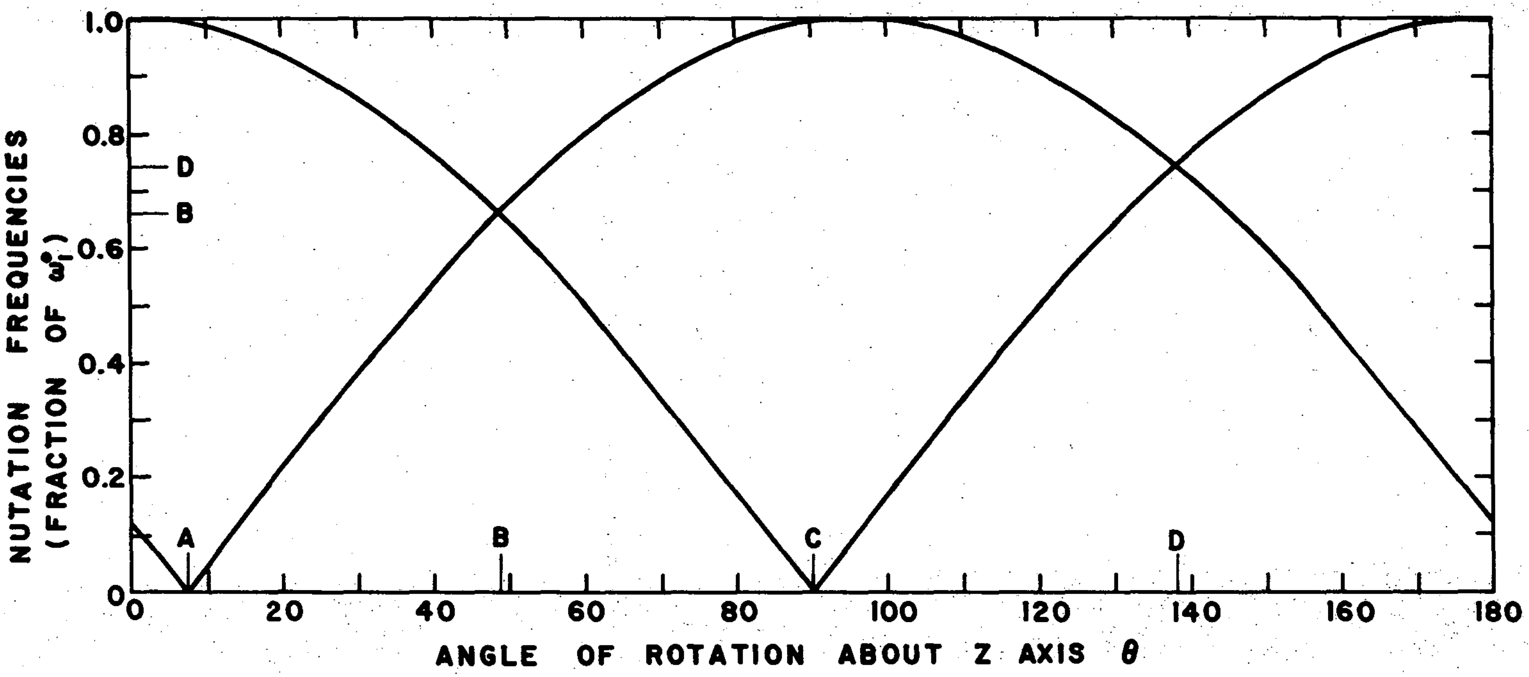

XBL 755-6284

Fig. 18. Transient nutation frequencies expected from a molecule doped in durene as a function of the angle of rotation about the z axis of the molecule ~c' axis of the crystal. Points A-D exhibit only a single nutation frequency.

the angle of rotation, θ. As the crystal is rotated, the two nutation frequencies reflect the respective projections of the polarized driving field direction on the x axis of each molecule in the unit cell, Eq. (36).

The observed transient nutation resulting from the contributions of these two nutation frequencies would exhibit a characteristic "beat" pattern. This is exemplified in curve (a) Fig. 19 which is a plot of the function

$$f(t) = -e^{-t/.3} (\cos 10\pi t + \cos 5\pi t) \tag{109}$$

in which one nutation frequency was arbitrarily chosen to be twice the other. Curve (b) is the Fourier transform power spectrum of curve (a) and of course reflects the two frequency components that were introduced into curve (a). In taking the Fourier transform of (a), the data were purposely "phase-shifted" by starting at the position indicated by the arrow, and an incorrect baseline was artificially introduced to simulate experimental conditions. These factors have the effect of introducing a false zero frequency component and distorting the lineshapes. Since experimental data never begins right at the "top" of the cosine function, this apparent phase shift introduces both absorbtive and dispersive (real and imaginary) components in the Fourier transform necessitating the use of the power spectrum which is the absolute value of the complex Fourier coefficients.

An experimental optically detected transient nutation that reflects this orientational dependence is given in Fig. 20(a) and its Fourier transform is given in (b). Here four, rather than the expected two

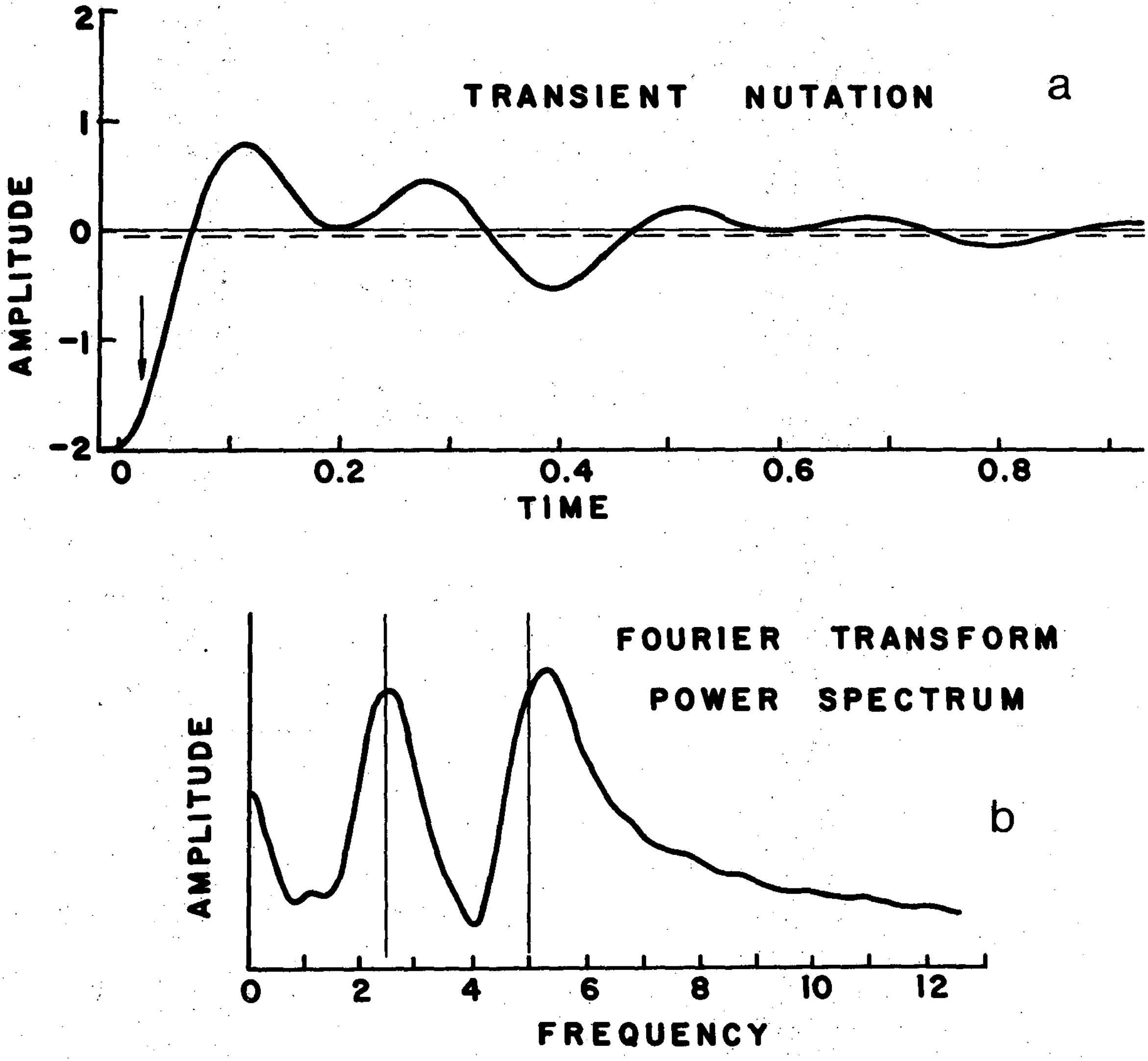

XBL 755-6285

Fig. 19. Top: Transient nutation resulting from the superposition of 2.5 and 5 Hz nutations. An arbitrary damping factor has been added to simulate experimental conditions.
Bottom: Fourier transform power spectrum of top trace reflecting the two nutation frequencies. Experimental conditions were again simulated by starting the Fourier transform at the point indicated by the arrow and introducing a false baseline indicated by the dashed line.

frequency components are present. This is most likely caused by crystal "twinning" or two different kinds of lattice sites. Curve (c) is the Fourier transform of an experimental transient nutation that reflects the two molecules in the unit cell. It might be mentioned that the transient nutations exhibited in Fig. 10 have single nutation frequencies because the transition is associated with the z axis in TCB, the axes being roughly parallel in the durene unit cell (2.4° from Table I). A slight beating effect may be seen on the on-resonance "tail" of the nutation. For other transitions, a single frequency may be obtained by rotating the crystal to the proper orientation, A-D, as illustrated in Fig. 18. Table II lists the same parameters for TCB crystal as were given in Table I for durene.

The angularly dependent nutation frequencies illustrated in Fig. 18 suggest that the exact directions of the transition moments could be obtained from the Fourier transforms of a set of zero-field transient nutations and knowledge of the crystal structure, much in the same way as is done in high-field EPR measurements of the $\Delta m = \pm 1$ transitions. Thus, in theory the complete anisotropic g-tensor could be mapped out in zero field. Several problems would have to be overcome before this method would prove practicable. First, a linearly polarized, homogeneous, strong driving field would have to be produced either by building a fast response cavity or improving helix design. In addition the microwave driving field device must also contain some kind of goniometer for orienting and rotating the crystal sample with respect to the linearly polarized field. For such purposes an exponential horn arrangement

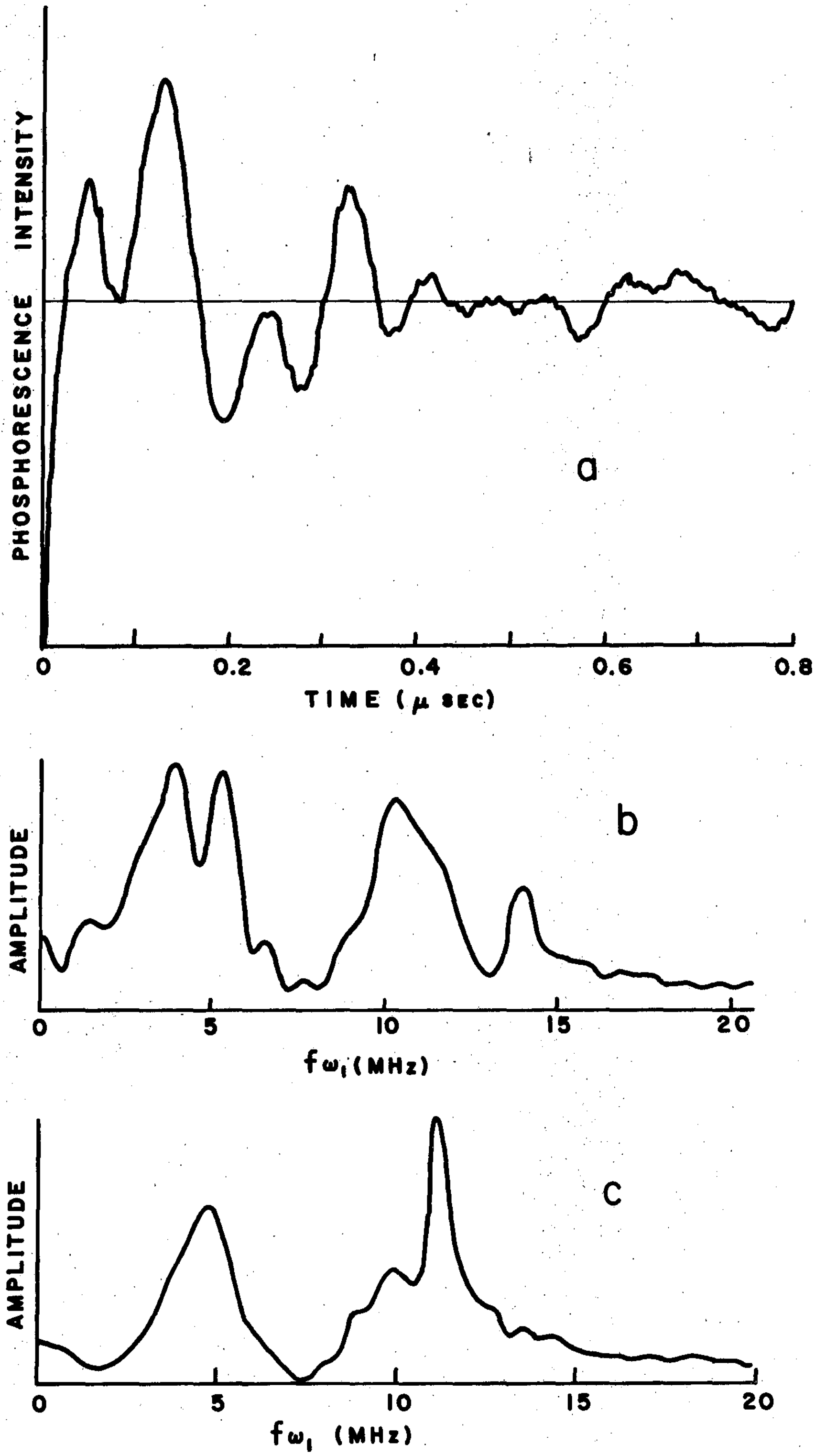

XBL 755-6286

Fig. 20. a) Experimental Transient nutation that reflects several nutation frequencies. b) Fourier transform of this nutation. c) Fourier transform of a transient nutation reflecting the two molecules in the durene unit cell.

Table II. TCB Crystal Structure

$P2_1/a$ $a_o=3.85$ $b_o=10.60$ $c_o=9.73$ $\beta=103.28°$

GENERAL POSITIONS (in unit cell dimensions)

	a	b	c
1	-0.0272	0.2805	0.0915
2	0.4246	0.0690	0.2985
3	0.1680	0.0290	0.1320
4	-0.0113	0.1250	0.0380
5	0.1950	-0.0921	0.0830

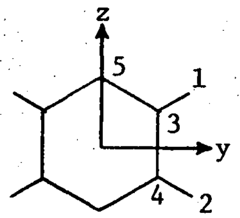

Direction Cosines

$$\begin{array}{cccc} x_1 & y_1 & z_1 & \\ \left[\begin{array}{c} 0.9014 \\ 0.0970 \\ 0.4111 \end{array}\right. & \begin{array}{c} 0.2319 \\ 0.7086 \\ -0.7101 \end{array} & \left.\begin{array}{c} -0.3602 \\ 0.6989 \\ 0.5717 \end{array}\right] & \begin{array}{c} a \\ b \\ c' \end{array} \end{array}$$

$$\begin{array}{cccc} x_2 & y_2 & z_2 & \\ \left[\begin{array}{c} -0.9014 \\ 0.0969 \\ 0.4112 \end{array}\right. & \begin{array}{c} 0.2320 \\ -0.7087 \\ 0.7099 \end{array} & \left.\begin{array}{c} 0.3602 \\ 0.6989 \\ 0.5718 \end{array}\right] & \begin{array}{c} a \\ b \\ c' \end{array} \end{array}$$

Between Molecules

$$\begin{array}{cccc} x_1 & y_1 & z_1 & \\ \left[\begin{array}{c} -0.8885 \\ -0.3287 \\ 0.3293 \end{array}\right. & \begin{array}{c} 0.3287 \\ -0.0043 \\ 0.9426 \end{array} & \left.\begin{array}{c} -0.3294 \\ 0.9426 \\ -0.0082 \end{array}\right] & \begin{array}{c} x_2 \\ y_2 \\ z_2 \end{array} \end{array}$$

Associated Angles

$$\begin{bmatrix} 153.1 & 70.8 & 109.3 \\ 109.2 & 90.2 & 19.5 \\ 70.7 & 19.5 & 90.4 \end{bmatrix}$$

introduced by El-Sayed et al.[75] for polarized studies might prove most practical, although field strengths would present a problem. The zero field transitions must not contain multiplet structure with different f values, for this would also create a spectrum of nutation frequencies. Of course in theory this consideration may be taken care of by calculation.

As a final remark it should be noted that the intensities of the nutation frequency spectrum would reflect the number of molecules contributing to a particular frequency only if the molecules are excited uniformly. The effects of singlet absorbtion selection rules, the polarization of the exciting light, excitation mechanisms, and the geometry of the optical viewing apparatus all play a part in the intensity contributions to the Fourier transform peaks. For example, the crystal may be excited by linearly polarized light propagating along the x axis in the laboratory with the phosphorescence viewed along the y axis. The only molecules that can be "seen" by the spectrometer are those molecules whose singlet transitions may be excited by the x-propagating light and, in addition, have the proper phosphorescence polarization to allow y-propagation to the spectrometer. The intensity will be weighted according to the appropriate projections. To complicate things further, the crystal will have depolarization effects, and, for doped systems, additional consideration must be given to the situation in which the host is excited and transfers excitation to guest traps via polarization selection rules. This latter "problem" may be used to advantage in the study of exciton trapping by effectively isolating translationally inequivalent exciton chains with the transient nutation and selective optical excitation.

G. Experimental Methods and Techniques

In the following section, details of the experimental apparatus used to measure coherence in excited states by optical detection are presented, and the general set-up for a pulse spectrometer and the methods used to obtain coherence information are discussed.

1. Apparatus

The conversion of a cw optically detected magnetic resonance spectrometer to a pulse spectrometer is quite simple because the optical detection feature of the instrument completely avoids "cavity" and detection system overload problems encountered in conventional ESR pulse spectrometers. Only a pulse generator, a fast microwave switch device, and a high power microwave amplifier are required in addition to the normal cw setup. The experimental details of the cw spectrometer have been described elsewhere.[76] A block diagram of the pulse spectrometer is given in Fig. 21.

The heart of the pulse spectrometer lies in the pulse sequence unit, which generally consists of a device constructed from transistor-transistor logic integrated circuit chips. These devices are quite easy to design, simple to build, and are exceedingly reliable as far as "homemade" equipment is concerned. Logic circuit diagrams for a number of these devices are illustrated in Figs. 22-24. For experiments such as the Carr-Purcell train,[41] it is necessary to sweep the probe pulse linearly in time relative to the strobe pulse at pulse separations

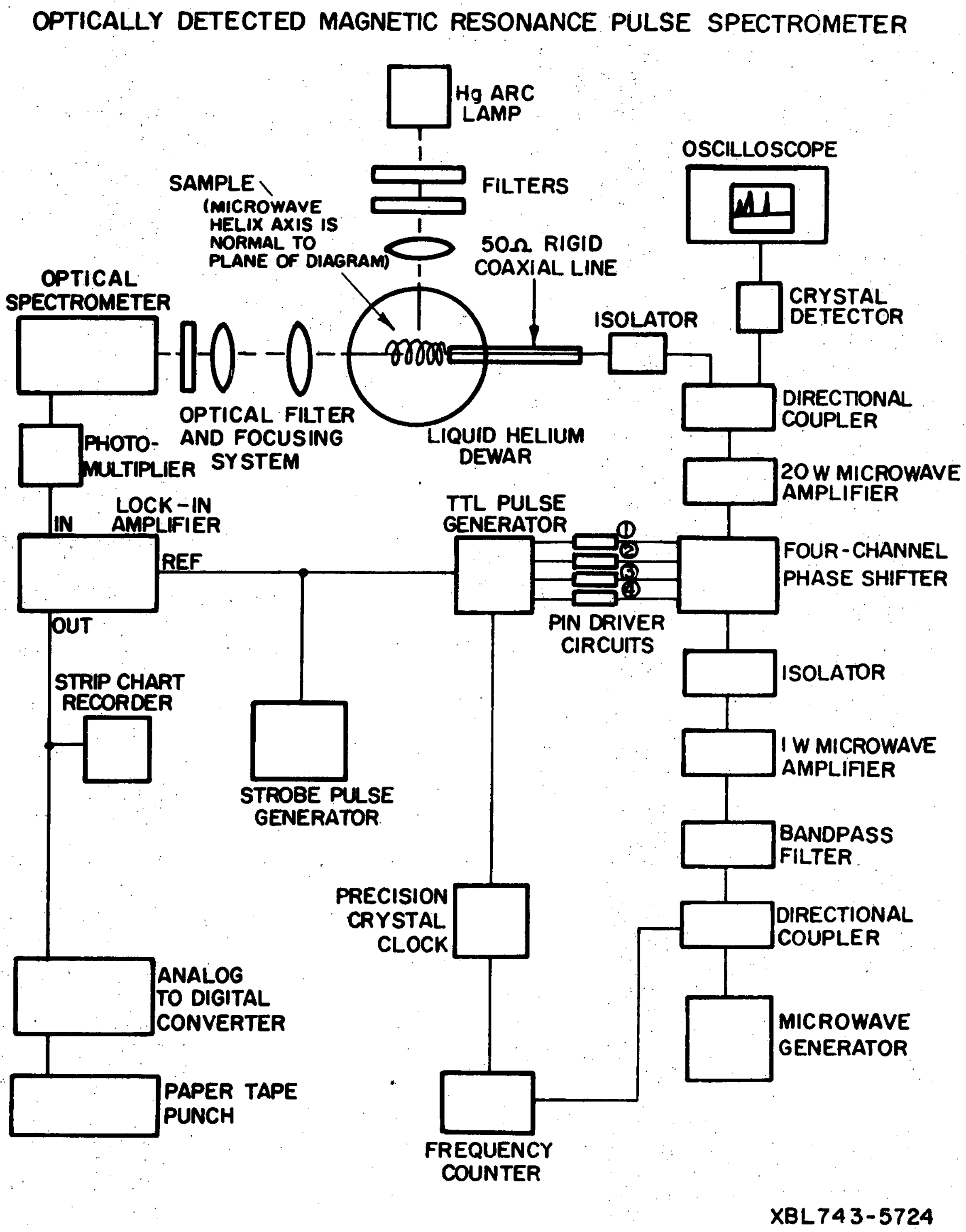

Fig. 21. Block diagram of an optically detected magnetic resonance pulse spectrometer.

of several hundred microseconds. The jitter in this interval must be less than 10 nsec for accurate recording of echoes. A device with this capability is shown in Fig. 22. The strobe pulse opens a gate that allows a train of pulses produced by the 1 MHz crystal clock to pass through. The lower part of the circuit takes only the first pulse in the train and produces a "zero-time" pulse. The upper part of the circuit keeps track of the number of pulses, spaced 1 μsec in time, by counting down from a number preset with six decade thumb switches. When the counter reaches zero, a pulse is produced, thus providing a digital time delay from 0 to 1 sec in steps of 1 μsec. This delayed pulse shuts the gate before any more pulses arrive at the counter, reloads the counter, and activates a monostable multivibrator having a precision 10-turn variable resistor and several possible capacitors in the timing circuit. This allows one of several continuously variable delay ranges to be added to the digital delay. The zero-time pulse circuit utilizes the same capacitance timing circuits without the variable resistor plus an additional delay labelled "trim" so that the two pulses can be overlapped in time, should it become necessary. The center circuit produces a variable pulse that ranges from zero to the maximum time determined by the variable resistor-capacitor combination and is valuable for producing transient nutations. A synchronous clock motor attached to the variable resistor provides a convenient way to sweep linearly in time.

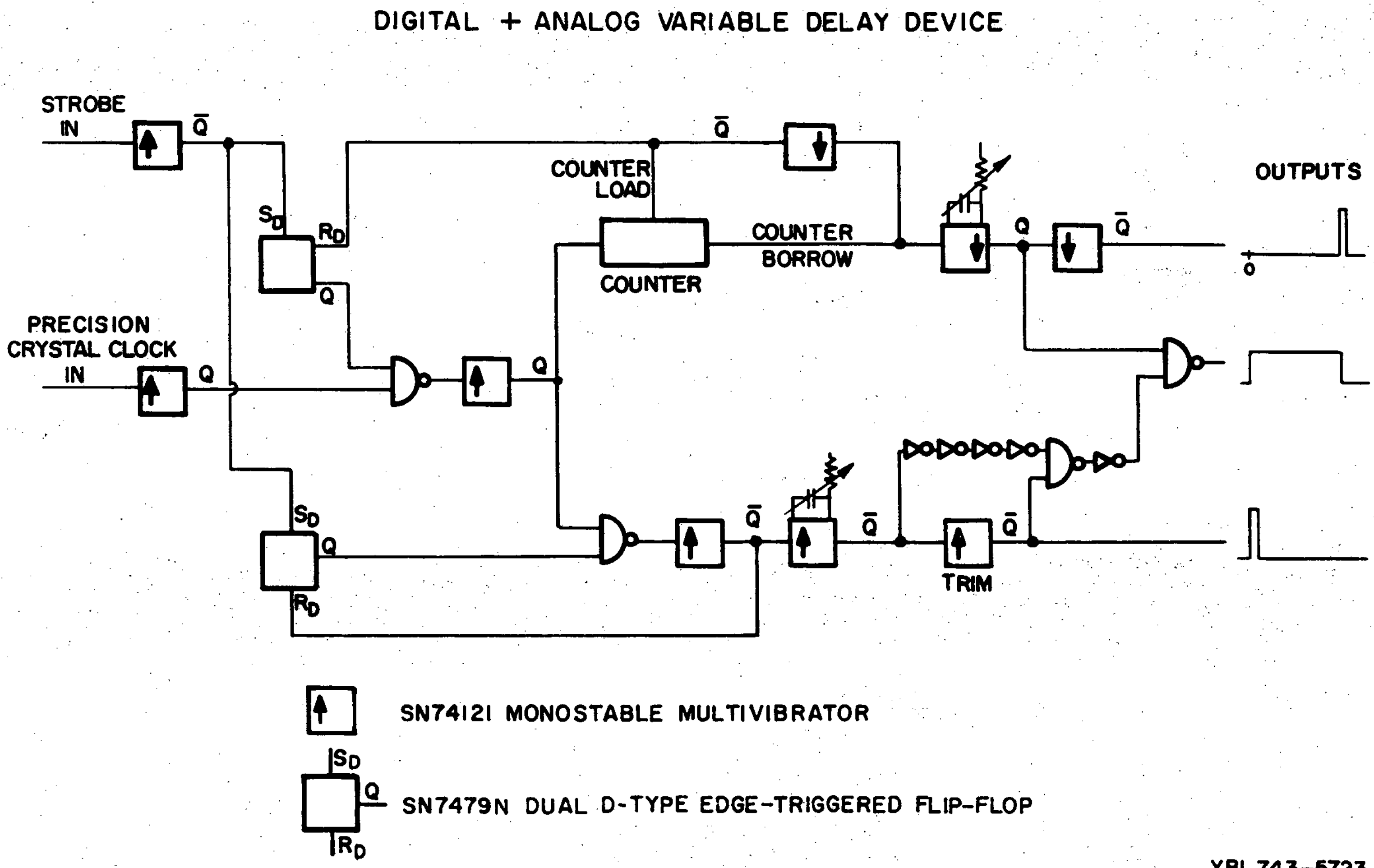

XBL 743-5723

Fig. 22. Schematic diagram of a digital plus variable delay device capable of producing two pulses with highly reproducible pulse separation.

Figure 23 illustrates circuits for a transient nutation and a probe pulse echo shape. As in the previous circuit, the time base is controlled by a variable resistor combined with a SN74121 monostable multivibrator.

The echo maximum decay curve pictured in Fig. 14 can be convieniently measured by constructing the circuit illustrated in Fig. 24. This circuit maintains a symmetrical time interval between the three pulses, insuring that the probe pulse stays on the echo maximum. The device picks out three pulses from a pulse oscillator whose period may be expanded linearly with a variable resistor.

Table III gives descriptive information on the equipment pictured in Fig. 2. It is important to use high isolation PIN diodes such as Hewlett Packard 33124A. Often, two or more of these diodes are placed in series in order to prevent feedthrough which would cause partial or total saturation of the microwave transition when the switch is in the off position. The PIN diodes are controlled by the pulse generator output into a DM 8830N buffer in conjunction with a National Semiconductor Corporation DH0035C PIN diode switch driver using the circuit given in the driver data sheet. This particular system provides relatively clean pulses with rise times on the order of 15 nsec.

Flexibility in the pulse sequences used is made possible by the four-channel phase shifter illustrated in Fig. 25. Each of the PIN diode switches is controlled by a separate driver. Thus, any part of the pulse sequence may be phase shifted by 0°, 90°, 180°, or 270°. This is essential for experiments such as the Carr-Purcell echo train

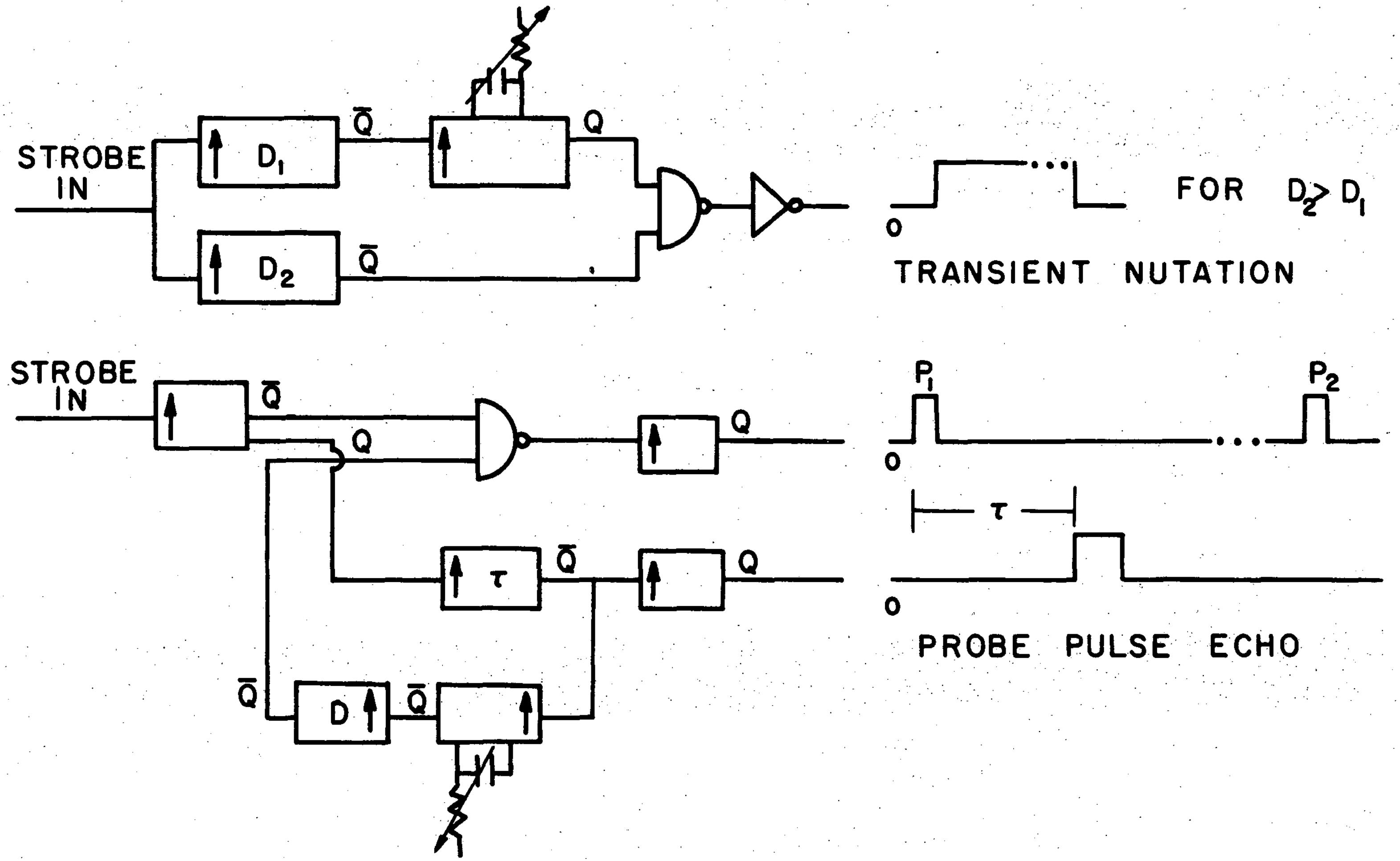

XBL 755-6287

Fig. 23. Schematic diagrams for a transient nutation pulse device that starts at zero and sweeps linearly in time, and a linearly swept device that maps out the echo shape.

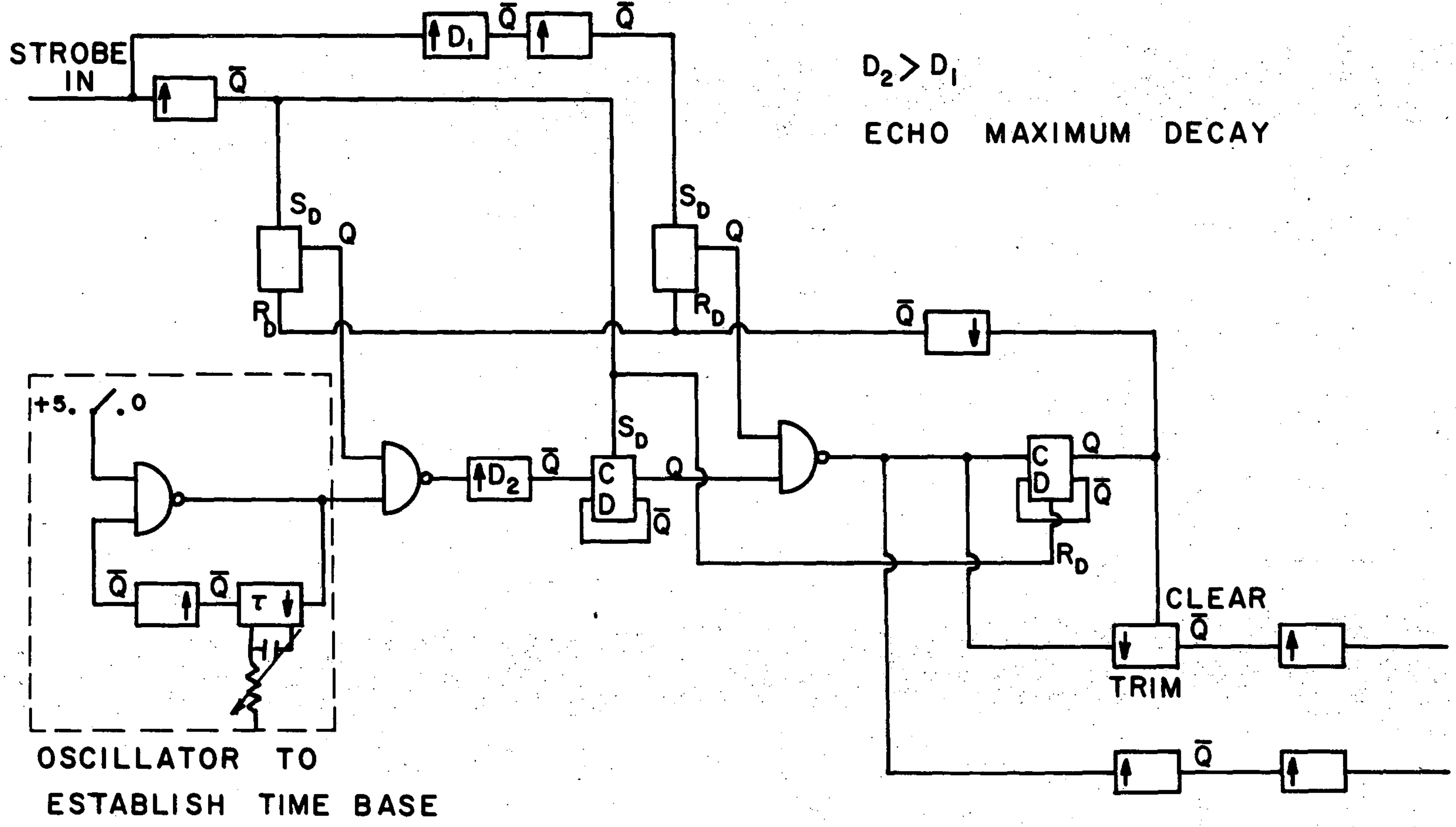

XBL 755-6288

Fig. 24. Schematic diagram of a device that will map out the optically detected echo maximum decay by creating a symmetrically displaced three pulse sequence, $\pi/2$, τ, π, τ, $\pi/2$, where τ is lengthened in a linear fashion.

Table III. Details on the Equipment represented in Figs. 21 and 25.

Figure 21 Equipment

Hg arc lamp: PEK 100 watt high pressure.

Filters: 4 cm H_2O, 2800 Å or 3100 Å Schott interference.

Spectrometer: Jarrell-Ash 3/4 meter Czerny-Turner.

Photomultiplier: EMI 6256S with cooled (-20°C) housing.

Lock-in amplifier: PAR model HR-8.

Oscilloscope: Tektronix 454.

50 Ω rigid coaxial line: Micro Delay Division, Uniform Tubes, Inc.

Isolators, directional couplers, bandpass filters: Hewlett-Packard (HP) and Narda Corporation.

Microwave generator: HP 8690B sweep oscillator with plug-ins.

Frequency counter: HP 5245L with plug-ins.

Precision crystal clock: obtained from frequency counter standard.

1 watt and 20 watt microwave amplifiers: Varian TWT with separate high voltage floating power supplies.

PIN driver circuits: see text.

Recording devices: Roytron paper tape punch, HP 7100B strip chart recorder. The analog to digital converter, strobe pulse generator and pulse generator were constructed from transistor-transistor logic devices.

Figure 25 Equipment

Hybrid tees: Anaren Corporation.

Constant impedance adjustable lines: General Radio 874-LK10L

Variable attenuators: Narda model 792FF.

PIN diodes: HP 33124A high isolation (often two or more of these diodes are placed in series in order to reduce microwave leakage in the "off" configuration).

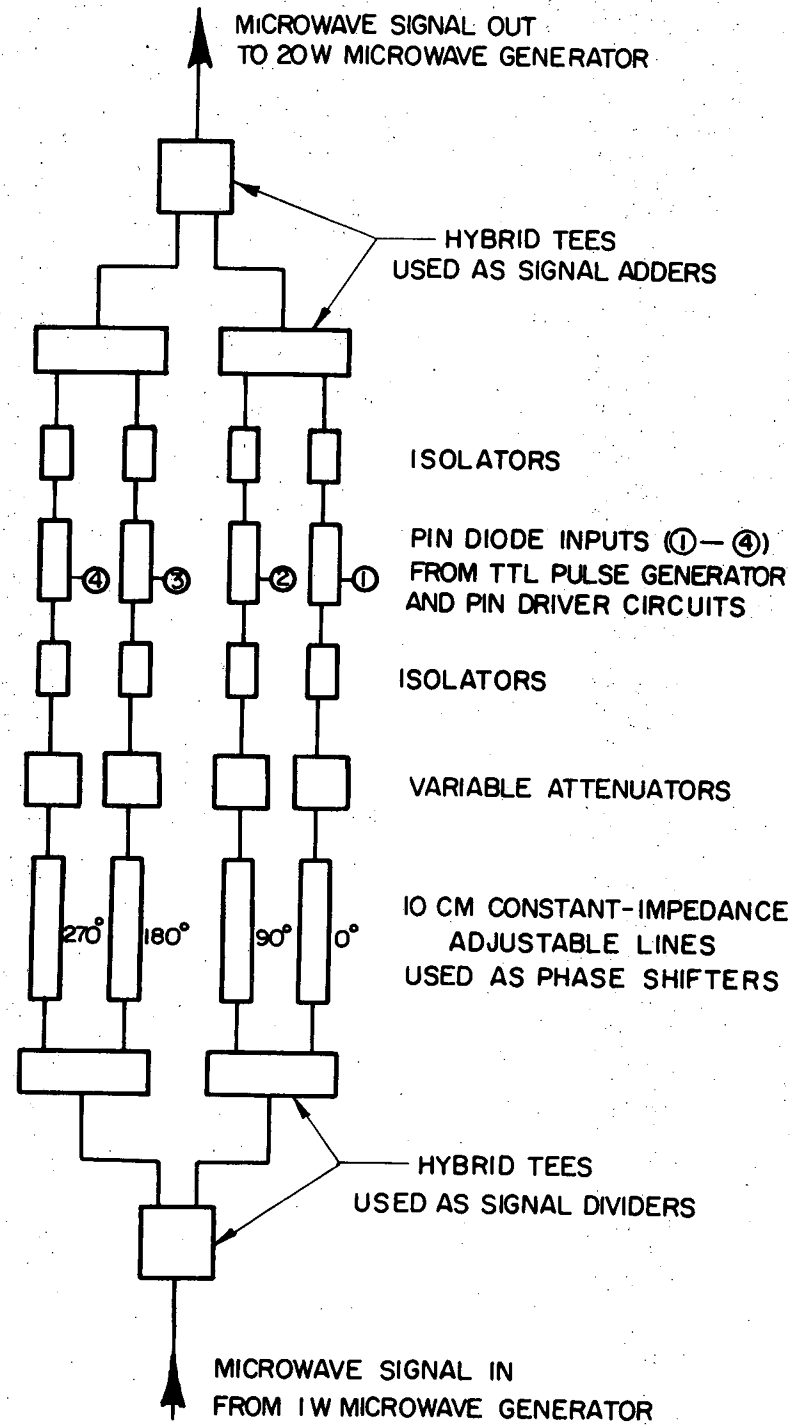

XBL743-5725

Fig. 25. Block diagram of the four-channel phase shifter.

with the Meiboom-Gill modification,[71] in which the π refocussing pulses are phase shifted by 90° from the initial $\pi/2$ pulse. Multiple phases are also required for spin locking[42] and adiabatic demagnetization in the rotating frame.[77] Phase adjustments are made by observing the response of a crystal diode detector to the output of the network when separate channels are switched on individually and to the resultant signal when two channels are opened concurrently and added together.

The procedure is as follows: the individual signals from two channels being compared are equalized by adjusting the variable attenuators in the lines. Combining two signals phase shifted by 180° produces zero detector output, and 0° phase shift produces the maximum combined output which varies from 2-4 times the output due to individual channels, depending on the total incident power and the response characteristics of the crystal. A 90° phase shift produces an intermediate signal. In three-channel experiments, an accurate 90° phase shift can be obtained by adjusting the phase of the signal in question, A, relative to two other signals, B and C, which are set to be 180° out of phase. One merely adjusts the phase of A until the crystal detector responds equally to A + B and A + C. In two-channel experiments, the 90° phase shift can be achieved by setting the length of the adjustable line halfway between 0° and 180° positions. Alternatively, the ODMR echo or spin lock signal itself, whose amplitude will be phase sensitive, can be used to set the phases.

2. Sample Preparation

Compounds of 1,2,4,5 tetrachlorobenzene (TCB) and 1,2,4,5 tetramethylbenzene (durene) were purified by extensive zone refining (~300 passes). Deuterated TCB was synthesized by five exchanges with concentrated D_2SO_4 at 150°C under a nitrogen atmosphere.[78] The concentrated D_2SO_4 was made by distilling a stoichiometric amount of SO_3 into 99.98% D_2O under nitrogen.[79] The d_2 TCB was then zone refined in the same fashion as TCB and durene. Other compounds were obtained commercially except for 2,3, dibromoquinoxaline, which was synthesized and purified by Dr. Robert Chen.

All samples were prepared by growing single crystals in a Bridgman furnace, and a combination of cleaving and cutting were used to form the crystal to a size that could be inserted inside a slow wave helix.

3. Methods

The methods used to measure coherence optically can be divided into two parts. This division is based on the relative time scale of the experiments. For pulse sequences, such as the spin echo, that last times much less than the lifetimes of the states, a lock-in amplifier is used to monitor the final value of the phosphorescence. Experiments that involve sequences that last for times on the same order or longer than the triplet state lifetimes, such as the spin locking experiment, are best recorded as transient waveforms on a digital CAT.

For short sequences the procedure is as follows: The optical spectrometer is set on one of the lines in the phosphorescence spectrum, and the microwave sweeper is tuned to the appropriate resonance frequency associated with one of the triplet state transitions. A strobe pulse generator, which can be a square wave, is used to initiate a pulse sequence device and also serves as a reference frequency for the lock-in amplifier. The reference frequency is largely determined by the triplet state lifetime, the period being roughly determined as five times the average of the lifetimes of the states involved. Since the pulse sequence lasts only on the order of microseconds, it is reasonable to neglect changes in phosphorescence during the sequence. Thus, on the timescale of milliseconds, the entire pulse sequence is completed "instantly," and the final value of the phosphorescence, which is proportional to the coherence remaining in the ensemble at the time the probe pulse was applied, will decay towards the steady-state value present in the absence of microwaves. The strobe then initiates another sequence, and this repetitive signal may be fed into the lock-in amplifier resulting in a DC signal that is proportional to the coherent component at the time the probe pulse was applied. If the probe pulse is now swept slowly, the DC signal from the lock-in will trace out an echo shape, transient nutation, or whatever experiment is being done. Figure 26 illustrates the actual "spikes" that are fed into the lock-in amplifier. In some situations it is advantageous to eliminate a large baseline by performing a two part series that results in "on echo maximum", "off echo maximum" and monitor at half

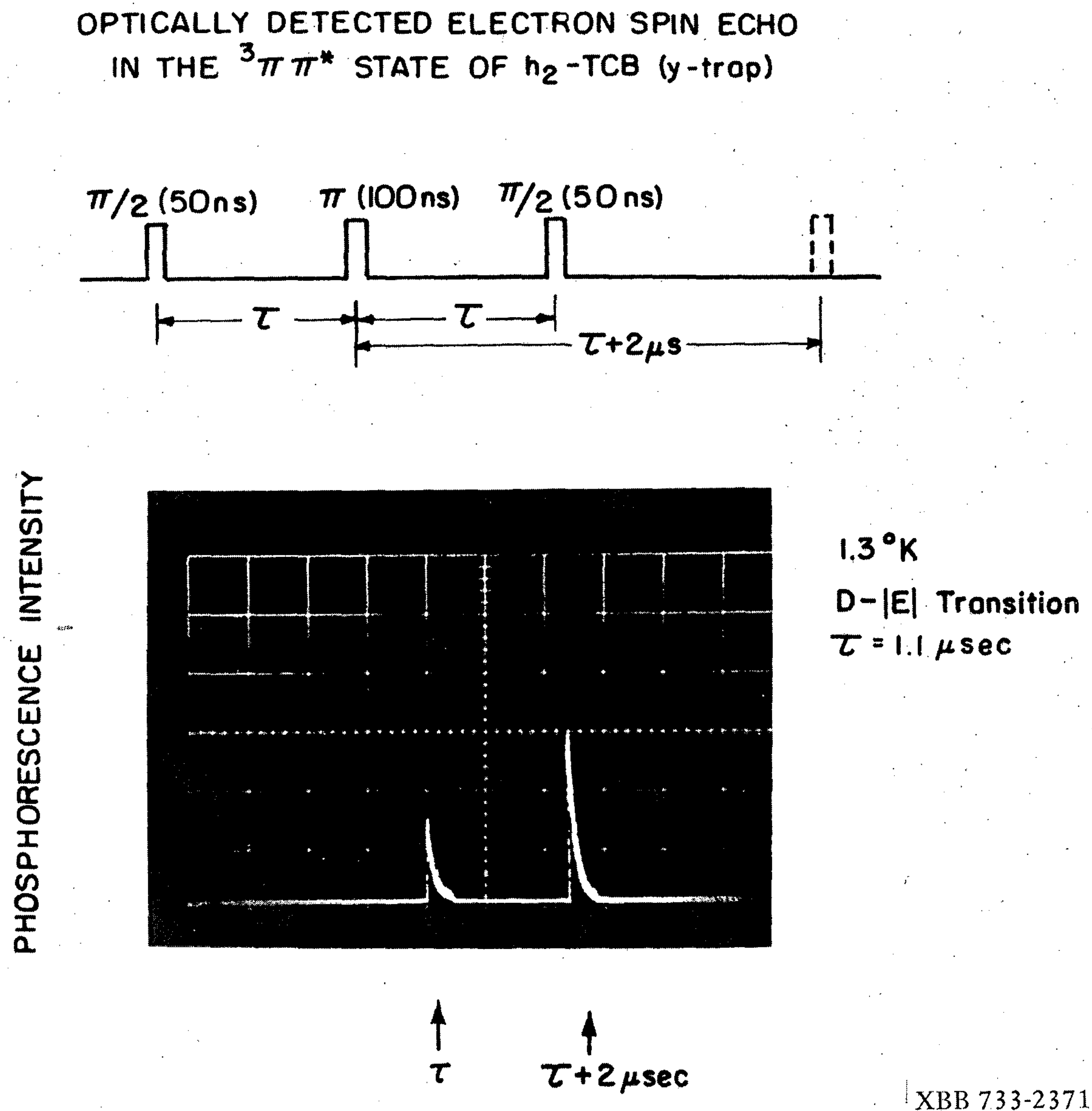

XBB 733-2371

Fig. 26. Photomultiplier output observed in an optically detected spin echo experiment. The first spike is observed when the three pulses are equally spaced, so that the probe pulse occurs at the rephasing time, τ, after the π refocussing pulse, i.e., on the echo maximum. The second spike is seen when the probe pulse is applied off maximum at τ + 2 μsec. The two spikes result from separate three pulse sequences, applied several hundred milliseconds apart.

the strobe frequency.

The long pulse sequences are done in a similar fashion except that the repetitive transient response is recorded on a time averaging computer rather than being fed into a lock-in amplifier. The forms in Fig. 17 were recorded in this fashion.

It might be noted that the first step in any coherence experiment is to perform a transient nutation. This insures that the system is coherently coupled and provides the necessary times for $\pi/2$, π, etc. pulses. Often times it is useful to employ an in-line "trombone" impedence matching device in order to couple the helix most efficiently to the microwaves. Optimum conditions may be determined by adjusting the lock in signal to a maximum for a pulse time $\omega_1 t < \pi/2$, since in this case the signal will always increase if the driving field power is increased.

APPENDIX A

Evaluation of the Exponential Matrix

The exponential matrix resulting from the general solution to Eq. (69) given in Eq. (79) is of the form exp(At) where the matrix A is given by the 4×4 matrix

$$A = \begin{bmatrix} -K_y & \frac{if\omega_1}{2} & \frac{-if\omega_1}{2} & \frac{1}{T_x} \\ \frac{if\omega_1}{2} & -K_A - i\Delta\omega & -K_D & \frac{if\omega_1}{2} \\ \frac{-if\omega_1}{2} & -K_D & -K_A + i\Delta\omega & \frac{if\omega_1}{2} \\ \frac{1}{T_y} & \frac{-if\omega_1}{2} & \frac{if\omega_1}{2} & -K_x \end{bmatrix}$$

The Theorem

Theorem 2 from Putzer[52] is easiest to use in this case and will be repeated here. For an n×n matrix, A,

$$e^{At} = \sum_{j=0}^{n-1} r_{j+1}(t)P_j$$

where

$$P_o = n\times n \text{ identity matrix, } I$$

$$P_j = \prod_{k=1}^{j} (A-\lambda_k I) \qquad j=1,\ldots n$$

$r_1(t)$, ... $r_n(t)$ is the solution of the triangular system

$$\dot{r}_1 = \lambda_1 r_1$$

$$\dot{r}_j = r_{j-1} + \lambda_j r_j \quad j=2,\ldots n$$

initial conditions $r_1(0)=1 \quad r_j(0)=0 \quad j\neq 1$

and $\lambda_1,\ldots\lambda_n$ are the eigenvalues of the matrix A. It is worth mentioning several special cases of theorem 2.

(1) All eigenvalues degenerate $\lambda_1=\lambda_2=\ldots\lambda_n=\lambda$

$$e^{At} = e^{\lambda t}\sum_{k=0}^{n-1} \frac{t^k}{k!}(A-\lambda I)^k$$

(2) All eigenvalues distinct $\lambda_1\neq\lambda_2\neq\ldots\lambda$

$$e^{At} = \sum_{k=1}^{n} e^{\lambda_k t} L_k \qquad \text{where} \qquad L_k = \prod_{\substack{j=1\\ j\neq k}}^{n}\left(\frac{A-\lambda_j I}{\lambda_k-\lambda_j}\right)$$

note that any 2×2 matrix satisfies either (1) or (2). In particular the Hermitian matrix

$$H = \begin{bmatrix} a & b \\ b^* & c \end{bmatrix}$$

has the explicit exponential form

$$e^{iHt} = e^{i\alpha t}\begin{bmatrix} \cos\omega t + i\,\frac{(a-\alpha)}{\omega}\sin\omega t & \frac{ib}{\omega}\sin\omega t \\ \frac{ib^*}{\omega}\sin\omega t & \cos\omega t + \frac{i(c-\alpha)}{\omega}\sin\omega t \end{bmatrix}$$

where

$$\alpha = \frac{a+c}{2}$$

$$\omega = \sqrt{\alpha^2+bb^*-ac}$$

if $\omega=0$ the matrix collapses to the proper form by observing that $\lim_{\omega\to 0} \sin\omega t/\omega = t$. This is useful for evaluating the unitary operators U and S Eq. (15) and Eq. (19).

For the 4×4 matrix the problem breaks up into three main groups: solution of the eigenvalue problem, calculation of the $r_j(t)$, and calculation of P_j.

Eigenvalue Problem

The characteristic equation for the matrix A yields a fourth order polynomial in λ.

$$\lambda^4 + C_3\lambda^3 + C_2\lambda^2 + C_1\lambda + C_o = 0$$

where the coefficients are given by

$$\begin{aligned}
C_3 &= K_x + K_y + 2K_A \\
C_2 &= K_A^2 - K_D^2 + \Delta\omega^2 + 2K_A(K_x+K_y) + K_xK_y - 1/(T_xT_y) + f^2\omega_1^2 \\
C_1 &= (K_x+K_y)(K_A^2-K_D^2+\Delta\omega^2) + 2K_A(K_xK_y - 1/(T_xT_y)) \\
&\quad + \frac{f^2\omega_1^2}{2}[2(K_A + K_D) + (K_x - 1/T_x) + (K_y - 1/T_y)] \\
C_o &= (K_xK_y-1/(T_xT_y))(K_A^2-K_D^2+\Delta\omega^2) + (f^2\omega_1^2/2)[(K_x-1/T_x) + (K_y-1/T_y)]
\end{aligned}$$

Since the coefficients are all real, the quartic equation may be solved by the following algorithm: first solve the cubic

$$y^3 - C_2y^2 + (C_1C_3-4C_o)y - C_3^2C_o - 4C_2C_0 - C_1^2 = 0$$

using any root of y find $R = \sqrt{C_3^2/4 - C_2+y}$

if $R \neq 0$

$$D = \frac{1}{2}\sqrt{\frac{C_3^2}{2} - C_2 - y + \frac{4C_2C_3 - 8C_1 - C_3^3}{4R}}$$

$$E = \frac{1}{2}\sqrt{\frac{C_3^2}{2} - C_2 - y - \frac{4C_2C_3 - 8C_1 - C_3^3}{4R}}$$

if $R=0$

$$D = \frac{1}{2}\sqrt{\frac{3C_3^2}{4} - 2C_2 + 2\sqrt{y^2 - 4C_o}}$$

$$E = \frac{1}{2}\sqrt{\frac{3C_3^2}{4} - 2C_2 - 2\sqrt{y^2 - 4C_o}}$$

and the roots are

$$\lambda_1 = -C_3/4 + R/2 + D \qquad \lambda_3 = -C_3/4 - R/2 + E$$

$$\lambda_2 = -C_3/4 + R/2 - D \qquad \lambda_4 = -C_3/4 - R/2 - E$$

Once the eigenvalues are obtained, they must be classified according to the five possible cases

Case (1) $\lambda_1, \lambda_2, \lambda_3, \lambda_4$

(2) $\lambda_1, \lambda_1, \lambda_2, \lambda_3$

(3) $\lambda_1, \lambda_1, \lambda_2, \lambda_2$

(4) $\lambda_1, \lambda_1, \lambda_1, \lambda_2$

(5) $\lambda_1, \lambda_1, \lambda_1, \lambda_1$

Calculation of the $r_j(t)$

The calculation for each r_j always involves a first order differential equation of the form

$$\dot{r} - \lambda r = f(t)$$

which has the general solution

$$r = e^{\lambda t} \int_o^t f(t')e^{-\lambda t'}\, dt'$$

and the various r_j are obtained through successive integration. The problem falls naturally into the five cases listed above and the results are summarized in the following Table.

r_1	Case (1) - (5) $r_1 = e^{\lambda_1 t}$
r_2	(1) $r_2 = (e^{\lambda_1 t} - e^{\lambda_2 t})/(\lambda_1-\lambda_2)$
	(2) - (5) $r_2 = te^{\lambda_1 t}$
r_3	(1) $r_3 = (e^{\lambda_1 t}-e^{\lambda_3 t})/[(\lambda_1-\lambda_2)(\lambda_1-\lambda_3)] - (e^{\lambda_2 t}-e^{\lambda_3 t})/[(\lambda_1-\lambda_2)(\lambda_2-\lambda_3)]$
	(2),(3) $r_3 = te^{\lambda_1 t}/(\lambda_1-\lambda_2) + (e^{\lambda_2 t} - e^{\lambda_1 t})/(\lambda_1-\lambda_2)^2$
	(4),(5) $r_3 = t^2e^{\lambda_1 t}/2$
r_4	(1) $r_4=(e^{\lambda_1 t}-e^{\lambda_4 t})/[(\lambda_1-\lambda_2)(\lambda_1-\lambda_3)(\lambda_1-\lambda_4)]-(e^{\lambda_3 t}-e^{\lambda_4 t})/[(\lambda_1-\lambda_2)(\lambda_1-\lambda_3)(\lambda_3-\lambda_4)]$ $-(e^{\lambda_2 t}-e^{\lambda_4 t})/[(\lambda_1-\lambda_2)(\lambda_2-\lambda_3)(\lambda_2-\lambda_4)]+(e^{\lambda_3 t}-e^{\lambda_4 t})/[(\lambda_1-\lambda_2)(\lambda_2-\lambda_3)(\lambda_3-\lambda_4)]$
	(2) $r_4 = te^{\lambda_1 t}/[(\lambda_1-\lambda_2)(\lambda_1-\lambda_3)] + (e^{\lambda_2 t}-e^{\lambda_3 t})/[(\lambda_1-\lambda_2)^2(\lambda_2-\lambda_3)]$ $- (e^{\lambda_1 t}-e^{\lambda_3 t})/[(\lambda_1-\lambda_2)^2(\lambda_1-\lambda_3)] - (e^{\lambda_1 t}-e^{\lambda_3 t})/[(\lambda_1-\lambda_2)(\lambda_1-\lambda_3)^2]$
	(3) $r_4 = t(e^{\lambda_1 t}+e^{\lambda_2 t})/(\lambda_1-\lambda_2)^2 + 2(e^{\lambda_2 t}-e^{\lambda_1 t})/(\lambda_1-\lambda_2)^3$
	(4) $r_4 = t^2e^{\lambda_1 t}/[2(\lambda_1-\lambda_2)] - te^{\lambda_1 t}/(\lambda_1-\lambda_2)^2 + (e^{\lambda_1 t}-e^{\lambda_2 t})/(\lambda_1-\lambda_2)^3$
	(5) $r_4 = t^3e^{\lambda_1 t}/6$

Calculation of the P_j

The following table summarizes the procedure for each case. First define the matrix B_j

$$B_j \equiv (A-\lambda_j I)$$

then for each case the P_j are given by

Case	P_o	P_1	P_2	P_3
(1)	I	B_1	B_2B_1	$B_3B_2B_1$
(2)			B_1^2	$B_2B_1^2$
(3)				
(4)				B_1^3
(5)				

and finally the exponential matrix is given by

$$e^{-iLt} = e^{At} = r_1P_o + r_2P_1 + r_3P_2 + r_4P_3$$

APPENDIX B

Computer Program for General Solutions

The program follows very closely the treatment outlined in Appendix A, and is liberally interspersed with comment cards that describe what is being done. It should be noted that the inhomogeneous lineshape integration is time consuming by its very nature and a relatively small number of isochromats have been taken (N=24) as a result. This limits the accuracy to about 7% so care must be excercised when "new effects" are discovered with the program.

A problem is present in the quartic solution subprogram that is a result of round-off errors. It is the author's belief that this subprogram should be replaced with another method for determining the roots of a polynomial in order that it will behave for all magnitudes of the coefficients. As the program stands now it will work for quantities of order unity or higher and the parameters should be scaled to conform to this restriction.

```
      PROGRAM RELAX(INPUT,OUTPUT)
      DIMENSION RTIME(4,100),SR(805)
      DIMENSION R(6),AY(10,10),P(10,10,10),RHOO(10),RHOS(10),ROOT(10),
     1 B2(10,10),B3(10,10),AR(10),EVO(10,10),RHO(10)
      COMPLEX AY,P,RHOO,RHOS,ROOT,B2,B3,AR,EVO,RHO,ZERO,TYME,EI,EII,
     *   EIII,EIV,LI,LII,LIII,LIV,SAYI,SAYII
      COMMON /SHP/ BEE,CANORM,N,T2S
      DATA PIE/1721 6220 7732 5042 0550 B/

C   CALCULATES R-VECTOR COMPONENTS WITH FEEDING,DECAY,AND RELAXATION PARAMETERS
C    USES EITHER REGULAR OR MODIFIED BLOCH EQUATIONS

C   DATA IS READ IN AS FOLLOWS

C     FIRST CARD  8E10.0  PHYSICAL PROPERTIES
C        XK=DECAY CONSTANT FROM LOWER LEVEL
C        YK=DECAY CONSTANT FROM UPPER LEVEL
C        FX=FEEDING RATE TO LOWER LEVEL
C        FY=FEEDING RATE TO UPPER LEVEL
C        T2=HOMOGENEOUS RELAXATION TIME
C        T2S=INHOMOGENEOUS RELAXATION TIME
C            IF T2S=0 INTEGRATION OVER INHOMOGENEOUS LINE IS NOT PERFORMED
C        TX=LIFETIME FOR DECAY FROM LOWER TO UPPER LEVEL
C        TY=LIFETIME FOR DECAY FROM UPPER TO LOWER LEVEL
C        FOR CONVIENIENCE, ZERO VALUES OF THE TIME PARAMETERS IMPLIES THAT
C          THEIR RECIPROCALS ARE ZERO. ANY NUMBER OF PULSE CONDITONS MAY FOLLOW
C           --A NEGATIVE VALUE FOR XK TERMINATES THE PROGRAM.
C     SECOND CARD  I2,8X,5E10.0,I2  PULSE CONDITIONS
C        INIT NEGATIVE ALLOWS COMPONENTS TO BE READ IN
C        INIT ZERO CALCULATES INITIAL STEADY-STATE VALUES FROM FEEDING AND
C          DECAY PARAMETERS. RONE AND RTWO ARE SET TO ZERO
C        INIT POSITIVE USES R-VALUES FROM PREVICUS PULSE AND PHASE-SHIFTS
C          THE DRIVING FIELD BY PHI*PIE
C        WI=DRIVING FIELD FREQUENCY IN HZ. NEGATIVE VALUE CAUSES NEW SET OF
C          PHYSICAL PROPERTIES TO BE READ IN
C        DELW=AMOUNT OFF RESONANCE IN HZ
C        TINT=TIME INTERVAL. PRINTOUT WILL GIVE STATUS OF SYSTEM EVERY TINT
C        TSTOP=TOTAL LENGTH OF PULSE. PRINTS EVERY TINT UNTIL TSTOP IS REACHED
C          IF TINT=TSTOP ONLY THE INITIAL AND FINAL R-VECTOR COMPONENTS ARE
C          PRINTED. THEFINAL VALUES ARE RETAINED FOR THE NEXT PULSE.
C        PHI=PHASE SHIFT ANGLE (PHI*PIE)(FOR 90 DEGREE PHASE SHIFT PHI=0.5)
C        MOD=0 IMPLIES THAT T2 ALONG THE DRIVING FIELD DIRECTION IS ZERO(MODIFIO
C        MOD=OTHERWISE IMPLIES NORMAL BLOCH EQUATIONS
C     THIRD CARD (IF NECESSARY) INITIAL VALUES OF R COMPONENTS
C        RONE,RTWO,RX,RY  4E10.0
C   THUS CARDS ARE AS FOLLOWS PHYS PROP,PULSE COND,(INIT VAL),PULSE,(INIT VAL)..
C     ..PHYS PROP,ETC
C  **IMPORTANT** TO TERMINATE THE PROGRAM NEGATIVE VALUES FOR WI AND XK MUST BE
C     READ IN AS THE LAST TWO CARDS IN THE DATA SET


      ZERO=CMPLX(0.,0.)

C   SET UP THE FIRST P MATRIX WHICH IS THE IDENTITY MATRIX
```

```
      DO 101 J=1,4
      P(1,J,J)=CMPLX(1.,0.)
      JJ=J+1
      IF(JJ.GT.4)GO TO 101
      DO 102 K=JJ,4
      P(1,K,J)=ZERO
      P(1,J,K)=ZERO
  102 CONTINUE
  101 CONTINUE
C    READ IN PHYSICAL PROPERTIES AND ESTABLISH CONSTANTS TO BE USED

    9 READ 10,XK,YK,FX,FY,T2,T2S,TX,TY
      IF(XK)1,2,2
    2 TT2=0.
      TTX=0.
      TTY=0.
      TEE=0.
      TAU=0.
      IF(T2.NE.0.)TT2=1./T2
      IF(TX.NE.0.)TTX=1./TX
      IF(TY.NE.0.)TTY=1./TY
      AK=(XK+YK)/2.
      BIGKY=YK+TTY
      BIGKX=XK+TTX
      IF(AK.NE.0..OR.TT2.NE.0.)TEE=1./(AK+TT2)
      IF((YK.NE.0..AND.TTX.NE.0.).OR.(XK.NE.0..AND.TTY.NE.0.)
     *  .OR.(XK.NE.0..AND.YK.NE.0.))TAU=AK/(XK*YK+YK*TTX+XK*TTY)
      SAVEX=FX
      SAVEY=FY
      PRINT 50,XK,YK,FX,FY
      PRINT 70,T2,T2S,TX,TY
      PRINT 100,TEE,TAU

C   ESTABLISH NORMALIZATION FACTOR FOR SHAPE FUNCTION
C    FUNCTIONS SUBROUTINE SHAPE CAN BE AN EMPIRICAL OR ANALYTICAL SHAPE
C    THAT RETURNS A VALUE FOR EACH J

      BEE=12.
      N=24
      KINT=2*N+1
      NUM=N-1
      CANORM=1.
      IF(T2S.EQ.0.)GO TO 43
      ANORM=0.
      DO 41 J=1,KINT
      ANORM=ANORM+SHAPE(J)
   41 CONTINUE
      CANORM=1./ANORM
   43 CONTINUE

C   READ IN PULSE CONDITIONS AND ESTABLISH INITIAL VALUES. SR STORES THE R--
C    VECTOR COMPONENT VALUES FOR EACH ISOCHROMAT.

  222 READ 20,INIT,WI,DELW,TINT,TSTOP,PHI,MOD
      IF(WI)9,8,13
```

```
   13 IF(MOD)8,11,8
   11 TT2E=0.
      GO TO 12
    8 TT2E=TT2
   12 CONTINUE
      IF(T2S.EQ.0.)KINT=1
      IF(INIT)3,4,5
    3 READ 10,R(1),R(2),R(3),R(4)
      GO TO 6
    4 R(1)=0.
      R(2)=0.

C     TAKE CARE OF PATHOLOGICAL CASES

      R(3)=0.
      R(4)=0.
      IF(AK.EQ.0.)GO TO 301
      IF(XK.EQ.0.)GO TO 302
      IF(YK.EQ.0.)GO TO 303
      R(3)=(FX*BIGKY+FY*TTY)*TAU/AK
      R(4)=(FY*BIGKX+FX*TTX)*TAU/AK
      GO TO 301
  302 IF(TTX.NE.0.)R(3)=FY*TTY/(TTX*YK)
      R(4)=FY/YK
      GO TO 301
  303 IF(TTY.NE.0.)R(4)=FX*TTX/(TTY*XK)
      R(3)=FX/XK
  301 CONTINUE

    6 DO 21 J=1,KINT
      JJ=4*(J-1)
      S=SHAPE(J)
      DO 22 K=1,4
      SR(JJ+K)=R(K)*S
   22 CONTINUE
   21 CONTINUE
      GO TO 26
    5 IF(PHI.EQ.0.)GO TO 26
      ANG=PHI*PIE
      CO=COS(ANG)
      SI=SIN(ANG)
      DO 23 J=1,KINT
      JJ=4*(J-1)
      RI=SR(JJ+1)*CO+SR(JJ+2)*SI
      RII=SR(JJ+2)*CO-SR(JJ+1)*SI
      SR(JJ+1)=RI
      SR(JJ+2)=RII
   23 CONTINUE
   26  PRINT 40,WI,DELW,TINT,TSTOP,PHI
      IF(MOD)24,25,24
   25 PRINT 80
      GO TO 27
   24 PRINT 90
   27 PRINT 60
      WI=2.*PIE*WI
      SDELW=2.*PIE*DELW
```

```
      BIGKA=AK+(TT2E+TT2)/2.
      BIGKD=(TT2E-TT2)/2.
      WISQ=WI*WI
      PLUS=BIGKX+BIGKY
      TIMES=BIGKX*BIGKY-TTX*TTY
      APD=BIGKA+BIGKD

C   SET UP PART OF THE A MATRIX FOR THE LIOUVILLE OPERATOR

      AY(1,1)=CMPLX(-BIGKY,0.)
      AY(1,4)=CMPLX(TTX,0.)
      AY(2,2)=CMPLX(-BIGKA,0.)
      AY(2,3)=CMPLX(-BIGKD,0.)
      AY(3,2)=AY(2,3)
      AY(3,3)=AY(2,2)
      AY(4,1)=CMPLX(TTY,0.)
      AY(4,4)=CMPLX(-BIGKX,0.)
      WW=WI/2.
      AY(1,2)=CMPLX(0.,WW)
      AY(1,3)=CMPLX(0.,-WW)
      AY(2,1)=AY(1,2)
      AY(2,4)=AY(1,3)
      AY(3,1)=AY(1,3)
      AY(3,4)=AY(1,2)
      AY(4,2)=AY(1,3)
      AY(4,3)=AY(1,2)
      SAYI=AY(2,2)
      SAYII=AY(3,3)

C   CALCULATE PART OF THE COEFFICIENTS

      CIII=BIGKX+BIGKY+2.*BIGKA
      SCII=2.*BIGKA*PLUS+TIMES+WISQ
      SCI=2.*BIGKA*TIMES+WISQ*(2.*APD+PLUS-TTX-TTY)/2.
      SCO=WISQ*APD*(PLUS-TTX-TTY)/2.

C    NITTY-GRITTY COMPUTATION. IF KINT=1, INTEGRATION OVER THE LORENTZ LINE IS
C   NOT PERFORMED (ONLY ONE PASS THRU LOOP 28). THE COMPLETE TIME DEVELOPMENT
C   FOR EACH ISOCHROMAT IS COMPUTED IN INTERVALS OF TINT TO A TOTAL TIME TSTOP
C   AND IS STORED IN THE TWO DIMENSIONAL ARRAY RTIME(K,KT). K SUBSCRIPT DEFINES
C   THE R-VECTOR COMPONENT AND KT DEFINES THE INTERVAL IN TIME. THEN ANOTHER
C   ISOCHROMAT IS TAKEN, CALCULATED, AND ADDEED TO RTIME

      DO 28 J=1,KINT
      JJ=4*(J-1)

C   INITIALIZE TIME FOR EACH ISOCHROMAT

      KT=0
      DELW=SDELW
      IF(T2S.GT.0.)DELW=SDELW+BEE*FLOAT(J-N-1)/(FLOAT(N)*T2S)
      FX=SAVEX*SHAPE(J)
      FY=SAVEY*SHAPE(J)

C  PULL ISOCHROMAT INITIAL VALUE FROM STORAGE AND PUT INTO INITIAL
C  DENSITY MATRIX
```

```
      RHOO(1)=CMPLX(SR(JJ+4),0.)
      RHOO(2)=(CMPLX(SR(JJ+1),-SR(JJ+2)))/(2.,0.)
      RHOO(3)=CONJG(RHOO(2))
      RHOO(4)=CMPLX(SR(JJ+3),0.)
      R(1)=SR(JJ+1)
      R(2)=SR(JJ+2)
      R(3)=SR(JJ+3)
      R(4)=SR(JJ+4)

C    FINISH THE A MATRIX

      AY(2,2)=SAYI+CMPLX(0.,-DELW)
      AY(3,3)=SAYII+CMPLX(0.,DELW)

C    FINISH CALCULATION OF COEFFICIENTS

      REP=BIGKA*BIGKA-BIGKD*BIGKD+DELW*DELW
      CII=SCII+REP
      CI=SCI+PLUS*REP
      CO=SCO+TIMES*REP

C   CALCULATE THE STEADY STATE DENSITY MATRIX
C     THREE CASES TO CONSIDER
C     CO IS ZERO BECAUSE THERE IS NO FEEDING

      DO 304 JNF=1,4
      RHOS(JNF)=ZERO
  304 CONTINUE
      IF(FX.EQ.0..AND.FY.EQ.0.)GO TO 307

C     NO DRIVING FIELD

      IF(WI.NE.0.)GO TO 306
      IF(XK.EQ.0.)GO TO 311
      IF(YK.EQ.0.)GO TO 312
      RHOS(1)=(FY*BIGKX+FX*TTX)*TAU/AK
      RHOS(4)=(FX*BIGKY+FY*TTY)*TAU/AK
      GO TO 307
  311 IF(TTX.NE.0.)RHOS(4)=FY*TTY/(TTX*YK)
      RHOS(1)=FY/YK
      GO TO 307
  312 IF(TTY.NE.0.)RHOS(1)=FX*TTX/(TTY*XK)
      RHOS(4)=FX/XK
      GO TO 307

C     CO IS NOT ZERO

  306 A=((FX*BIGKY+FY*TTY)*REP+WISQ*APD*(FY+FX)/2.)/CO
      RHOS(4)=CMPLX(A,0.)
      A=((FY*BIGKX+FX*TTX)*REP+WISQ*APD*(FY+FX)/2.)/CO
      RHOS(1)=CMPLX(A,0.)
      A=FY*(BIGKX-TTY)-FX*(BIGKY-TTX)
      B=A*WI*DELW/(2.*CO)
      C=A*WI*APD/(2.*CO)
      RHOS(2)=CMPLX(B,C)
```

```
      RHOS(3)=CONJG(RHOS(2))
  307 CONTINUE

C   FIND EIGENVALUES OF THE CHARACTERISTIC EQUATION

      CALL QUARTIC(CIII,CII,CI,CO,ROOT)

C   ORDER DEGENERACIES AND DETERMINE CASE NUMBER
C     NCASE=1 FOUR DISTINCT ROOTS 1,2,3,4
C     NCASE=2 THREE ROOTS 1,1,2,3
C     NCASE=3 TWO ROOTS 1,1,2,2
C     NCASE=4 TWO ROOTS 1,1,1,2
C     NCASE=5 ONE ROOT 1,1,1,1
C     ROOTS ARE ORDERED, HIGHEST DEGENERACY FIRST, DEGENERACIES NOT REPEATED

      CALL DEGEN(ROOT,NCASE)

C   WE ARE NOW IN A POSITION TO CALCULATE THE EXPONENTIAL OPERATOR
C   CALCULATE THE B MATRICIES

      DO 105 KK=1,4
      DO 106 KKK=1,4
      P(2,KK,KKK)=AY(KK,KKK)
      IF(KK.EQ.KKK) P(2,KK,KKK)=P(2,KK,KKK)-ROOT(1)
      IF(NCASE.GT.3)GO TO 106
      B2(KK,KKK)=AY(KK,KKK)
      IF(KK.EQ.KKK) B2(KK,KKK)=B2(KK,KKK)-ROOT(2)
      IF(NCASE.NE.1)GO TO 106
      B3(KK,KKK)=AY(KK,KKK)
      IF(KK.EQ.KKK) B3(KK,KKK)=B3(KK,KKK)-ROOT(3)
  106 CONTINUE
  105 CONTINUE

C   CALCULATE THE P MATRICIES

      DO 107 KP=1,2
      DO 108 KK=1,4
      DO 109 KKK=1,4
      IF(KP.EQ.2)GO TO 111
      P(3,KK,KKK)=ZERO
      GO TO 112
  111 P(4,KK,KKK)=ZERO
  112 DO 113 KDUM=1,4
      IF(KP.EQ.2)GO TO 114
      IF(NCASE.EQ.1)GO TO 115
      P(3,KK,KKK)=P(3,KK,KKK)+P(2,KK,KDUM)*P(2,KDUM,KKK)
      GO TO 113
  115 P(3,KK,KKK)=P(3,KK,KKK)+B2(KK,KDUM)*P(2,KDUM,KKK)
      GO TO 113
  114 CONTINUE
      GO TO(116,117,117,118,118),NCASE
  116 P(4,KK,KKK)=P(4,KK,KKK)+B3(KK,KDUM)*P(3,KDUM,KKK)
      GO TO 113
  117 P(4,KK,KKK)=P(4,KK,KKK)+B2(KK,KDUM)*P(3,KDUM,KKK)
      GO TO 113
  118 P(4,KK,KKK)=P(4,KK,KKK)+P(2,KK,KDUM)*P(3,KDUM,KKK)
```

```
  113 CONTINUE
  109 CONTINUE
  108 CONTINUE
  107 CONTINUE
C THIS BEGINS THE TIME DEVELOPMENT LOOP
   31 KT=KT+1
      TIME=FLOAT(KT)*TINT
      DO 32 K=1,4
      IF(J.NE.1)GO TO 72
   71 RTIME(K,KT)=R(K)
      GO TO 32
   72 RTIME(K,KT)=RTIME(K,KT)+R(K)
   32 CONTINUE
C   TEST TO SEE IF TSTOP HAS BEEN REACHED
      IF(TIME.GT.TSTOP)GO TO 33
C   CALCULATE COMPLEX EXPONENTIALS TO BE USED AND ABBREVIATE EIGENVALUES
      TYME=CMPLX(TIME,0.)
      LI=ROOT(1)
      EI=CEXP(LI*TYME)
      IF(NCASE.EQ.5)GO TO 121
      LII=ROOT(2)
      EII=CEXP(LII*TYME)
      IF(NCASE.GT.2)GO TO 121
      LIII=ROOT(3)
      EIII=CEXP(LIII*TYME)
      IF(NCASE.GT.1)GO TO 121
      LIV=ROOT(4)
      EIV=CEXP(LIV*TYME)
  121 CONTINUE
C   CALCULATE PUTZERS R VALUES
      AR(1)=EI
      IF(NCASE.EQ.1)GO TO 122
      AR(2)=TYME*EI
      GO TO 123
  122 AR(2)=(EI-EII)/(LI-LII)
  123 CONTINUE
      GO TO(124,125,125,126,126),NCASE
  124 AR(3)=((EI-EIII)/(LI-LIII)-(EII-EIII)/(LII-LIII))/(LI-LII)
      GO TO 127
  125 AR(3)=(TYME*EI+(EII-EI)/(LI-LII))/(LI-LII)
      GO TO 127
  126 AR(3)=TYME*AR(2)/CMPLX(2.,0.)
  127 CONTINUE
      GO TO(128,129,131,132,133),NCASE
  128 AR(4)=((EI-EIV)/((LI-LIII)*(LI-LIV))-(EIII-EIV)/((LI-LIII)
     * *(LIII-LIV))-(EII-EIV)/((LII-LIII)*(LII-LIV))+(EIII-EIV)/
     * ((LII-LIII)*(LIII-LIV)))/(LI-LII)
      GO TO 134
```

```
  129 AR(4)=(TYME*EI/(LI-LIII)+(EII-EIII)/((LI-LII)*(LII-LIII))
     * -(EI-EIII)/((LI-LII)*(LI-LIII))-(EI-EIII)/((LI-LIII)*(LI-LIII)))
     *  /(LI-LII)
      GO TO 134
  131 AR(4)=(TYME*(EI+EII)+CMPLX(2.,0.)*(EII-EI)/(LI-LII))/((LI-LII)
     * *(LI-LII))
      GO TO 134
  132 AR(4)=(TYME*TYME*EI/CMPLX(2.,0.)-TYME*EI/(LI-LII)+(EI-EII)/((LI-
     * LII)*(LI-LII)))/(LI-LII)
      GO TO 134
  133 AR(4)=TYME*TYME*TYME*EI/CMPLX(6.,0.)
  134 CONTINUE

C  THE FINAL FORM FOR THE EXPONENTIAL MATRIX MAY NOW BE CALCULATED

      DO 135 KK=1,4
      DO 136 KKK=1,4
      EVO(KK,KKK)=ZERO
      DO 137 KDUM=1,4
      EVO(KK,KKK)=EVO(KK,KKK)+AR(KDUM)*P(KDUM,KK,KKK)
  137 CONTINUE
  136 CONTINUE
  135 CONTINUE

C   COMPUTE DENSITY MATRIX

      DO 141 KK=1,4
      RHO(KK)=ZERO
      DO 142 KDUM=1,4
      RHO(KK)=RHO(KK)+EVO(KK,KDUM)*(RHOO(KDUM)-RHOS(KDUM))
  142 CONTINUE
      RHO(KK)=RHO(KK)+RHOS(KK)
  141 CONTINUE

C   CONVERT TO R VECTOR COMPONENTS

      R(1)=2.*REAL(RHO(2))
      R(2)=2.*AIMAG(RHO(3))
      R(3)=REAL(RHO(4))
      R(4)=REAL(RHO(1))
      GO TO 31

C   END OF TIME DEVELOPMENT LOOP. STORE FINAL VALUES OF COMPONENTS IN SR FOR
C    NEXT PULSE CONDITION.

   33 DO 34 K=1,4
      SR(JJ+K)=R(K)
   34 CONTINUE
   28 CONTINUE

C   PRINT OUT STORED, INTEGRATED VALUES AND READ IN ANOTHER PULSE CONDITION

      DO 35 J=1,KT
      RTHREE=RTIME(4,J)-RTIME(3,J)
      TOT=RTIME(4,J)+RTIME(3,J)
      TIME=TINT*FLOAT(J-1)
```

```
      PRINT 30,TIME,(RTIME(K,J),K=1,4),RTHREE,TOT
   35 CONTINUE
      GO TO 222
    1 CONTINUE
   10 FORMAT(8E10.0)
   20 FORMAT(I10,5E10.0,I10)
   30 FORMAT(15X,E9.3,5X,6(E10.3,4X))
   40 FORMAT(//,10X,*PULSE CONDITIONS  WI=*,E8.2,*  DELW=*,E8.2,*  TINT=
     * *,E8.2,*  TSTOP=*,E8.2,*  PHI=*,E8.2,//)
   50 FORMAT(////,10X,*FEEDING AND DECAY PARAMETERS  XK=*,E8.2,*  YK=*,
     * E8.2,*  FX=*,E8.2,*  FY=*,E8.2)
   60 FORMAT(22X,*T*,11X,*RONE*,10X,*RTWO*,11X,*RX*,12X,*RY*,12X,
     * *R3*,9X,*TOT POP*,/)
   70 FORMAT(/,10X,*RELAXATION PARAMETERS  T2=*,E8.2,*  T2S=*,E8.2,
     *  *  TX=*,E8.2,*  TY=*,E8.2,/)
   80 FORMAT(10X,*MODIFIED BLOCH EQUATIONS USED*,//)
   90 FORMAT(10X,*NORMAL BLOCH EQUATIONS USED*,//)
100   FORMAT(10X,*EFFECTIVE RELAXATICN PARAMETERS  T=*,E8.2,*  TAU=*,
     1  E8.2,/)
      END
```

```
      SUBROUTINE QUARTIC(CIII,CII,CI,CO,ROOT)
      DIMENSION ROOT(10)
      DOUBLE PRECISION A3,A2,A1,A0,DUM,DUMI,DUMII,DUMIII,DUMIV,DUMV,
     *  A,B,C,RR,RI,DR,DI,ER,EI
      COMPLEX ROOT,CR
      COMMON /CLAM/ RR,RI,DR,DI,ER,EI,A3,A2,A1,A0
      A3=DBLE(CIII)
      A2=DBLE(CII)
      A1=DBLE(CI)
      A0=DBLE(CO)
C    REMOVE ZERO ROOTS
    1 DO 4 J=1,4
      ROOT(J)=(0.,0.)
    4 CONTINUE
      IF(CII.EQ.0..AND.CI.EQ.0..AND.CO.EQ.0.)GO TO 3
      IF(CI.EQ.0..AND.CO.EQ.0.)GO TO 5
      IF(CO.EQ.0.)GO TO 6
      GO TO 7
    3 ROOT(4)=CMPLX(-CIII,0.)
      RETURN
    5 CALL QUAD(A3,A2,DUM,DUMI,DUMII,DUMIII)
      ROOT(3)=CMPLX(SNGL(DUM),SNGL(DUMI))
      ROOT(4)=CMPLX(SNGL(DUMII),SNGL(DUMIII))
      RETURN
    6 CALL CUBIC(A3,A2,A1,DUM,DUMI,DUMII,DUMIII,DUMIV,KASE)
      ROOT(1)=CMPLX(SNGL(DUM),0.)
      ROOT(2)=CMPLX(SNGL(DUMI),SNGL(DUMII))
      ROOT(3)=CMPLX(SNGL(DUMIII),SNGL(DUMIV))
      RETURN

C    GENERAL QUARTIC
    7 CONTINUE
      A=-A2
      B=A1*A3-4.D0*A0
      C=4.D0*A0*A2-A1*A1-A0*A3*A3
      CALL CUBIC(A,B,C,DUM,DUMI,DUMIII,DUMII,DUMIV,KASE)
      DUMV=0.D0
      CALL RDE(DUM,DUMV,ROOT)
      RETURN
      END
```

```
      SUBROUTINE CUBIC(A2,A1,A0,X1,X2R,X2I,X3R,X3I,KASE)
      DOUBLE PRECISION A2,A1,A0,X1,X2R,X2I,X3R,X3I,R,D,RE,YM,S1,S2
     *   ,ANG,THIRD,SIXTH
      THIRD=1.D0/3.D0
      SIXTH=1.D0/6.D0
      R=(A2*(4.5D0*A1-A2*A2)-13.5D0*A0)/27.D0
      D=(A0*(27.D0*A0-18.D0*A1*A2+4.D0*A2*A2*A2)+A1*A1*(4.D0*A1
     *   -A2*A2))/108.D0
      IF(D)1,2,3
    1 S2=DSQRT(-D)
      KASE=-1
      S1=DEXP(SIXTH*DLOG(R*R-D))
      ANG=DATAN2(S2,R)/3.D0
      RE=S1*DCOS(ANG)
      YM=S1*DSIN(ANG)*DSQRT(3.D0)
      S2=A2/3.D0
      X1=2.D0*RE-S2
      X2R=-RE-S2+YM
      X2I=0.D0
      X3R=-RE-S2-YM
      X3I=0.D0
      RETURN
    2 KASE=0
      IF(R)4,14,9
    9 S1=DEXP(THIRD*DLOG(R))
      GO TO 5
    4 S1=-DEXP(THIRD*DLOG(-R))
      GO TO 5
   14 S1=0.D0
    5 S2=A2/3.D0
      X1=2.D0*S1-S2
      X2R=-S1-S2
      X2I=0.D0
      X3R=X2R
      X3I=0.D0
      RETURN
    3 S1=R+DSQRT(D)
      KASE=1
      S2=R-DSQRT(D)
      IF(S1)6,15,12
   12 S1=DEXP(THIRD*DLOG(S1))
      GO TO 11
   15 S1=0.D0
   11 IF(S2)7,16,13
   13 S2=DEXP(THIRD*DLOG(S2))
      GO TO 8
    6 S1=-DEXP(THIRD*DLOG(-S1))
    7 S2=-DEXP(THIRD*DLOG(-S2))
      GO TO 8
   16 S2=0.D0
    8 D=A2/3.D0
      X1=S1+S2-D
      X2R=-(S1+S2)/2.D0-D
      X2I=DSQRT(3.D0)*(S1-S2)/2.D0
      X3R=X2R
      X3I=-X2I
```

```
      RETURN
      END
```

```
      SUBROUTINE MATCH(A,B,NOPE)
      COMPLEX A,B
      AR=REAL(A)
      BR=REAL(B)
      AI=AIMAG(A)
      BI=AIMAG(B)
      NOPE=1
      IF(ABS(AR-BR).GT.1.E-08.OR.ABS(AI-BI).GT.1.E-08)NOPE=0
      RETURN
      END
```

```
      FUNCTION SHAPE(J)
      COMMON /SHP/ BEE,CANORM,N,T2S
      FACT=1.
      IF(T2S.GT.0.)FACT=1.+BEE*BEE*FLOAT((J-N-1)*(J-N-1))/FLOAT(N*N)
      SHAPE=CANORM/FACT
      RETURN
      END
```

```
      SUBROUTINE DSQC(X,Y)
      DOUBLE PRECISION X,Y,ANG,R
      IF(X.EQ.0.D0.AND.Y.EQ.0.D0)RETURN
      IF(Y.EQ.0.D0)GO TO 2
      R=DEXP(.25D0*DLOG(X*X+Y*Y))
      ANG=DATAN2(Y,X)/2.D0
      X=R*DCOS(ANG)
      Y=R*DSIN(ANG)
      RETURN
    2 IF(X.GT.0.D0)GO TO 3
      Y=DSQRT(-X)
      X=0.D0
      RETURN
    3 X=DSQRT(X)
      RETURN
      END
```

```
      SUBROUTINE RDF(YR,YI,ROOT)
      DIMENSION ROOT(10)
      DOUBLE PRECISION RR,RI,DR,DI,ER,EI,YR,YI,A3,A2,A1,A0,DUM,DUMI
      COMPLEX ROOT,CR
      COMMON /CLAM/ RR,RI,DR,DI,ER,EI,A3,A2,A1,A0
      RR=A3*A3/4.D0-A2+YR
      RI=YI
      CALL DSQC(RR,RI)
      DUMI=DABS(A3)+DABS(A2)+DABS(A1)+DABS(A0)
      SUM=SNGL(DUMI)
      IF((SNGL(RR+RI)+SUM)-SUM.EQ.0.)GO TO 1
      DUM=(A3*(4.D0*A2-A3*A3)-8.D0*A1)/(4.D0*(RR*RR+RI*RI))
      DR=A3*A3/2.D0-A2-YR+RR*DUM
      DI=-RI*DUM-YI
      ER=A3*A3/2.D0-A2-YR-RR*DUM
      EI=RI*DUM-YI
      GO TO 2
    1 RR=0.D0
      RI=0.D0
      DUM=YR*YR-YI*YI-4.D0*A0
      DUMI=2.D0*YR*YI
      CALL DSQC(DUM,DUMI)
      DR=3.D0*A3*A3/4.D0-2.D0*(A2-DUM)
      DI=2.D0*DUMI
      ER=3.D0*A3*A3/4.D0-2.D0*(A2+DUM)
      EI=-2.D0*DUMI
    2 CALL DSQC(DR,DI)
      CALL DSQC(ER,EI)
      RR=RR/2.D0
      RI=RI/2.D0
      DR=DR/2.D0
      DI=DI/2.D0
      ER=ER/2.D0
      EI=EI/2.D0
      DUM=-A3/4.D0
      ROOT(1)=CMPLX(SNGL(DUM+RR+DR),SNGL(RI+DI))
      ROOT(2)=CMPLX(SNGL(DUM+RR-DR),SNGL(RI-DI))
      ROOT(3)=CMPLX(SNGL(DUM-RR+ER),SNGL(-RI+EI))
      ROOT(4)=CMPLX(SNGL(DUM-RR-ER),SNGL(-RI-EI))
      IF(SUM.EQ.0.)RETURN
      DO 3 K=1,4
      SAVER=REAL(ROOT(K))
      A=SAVER/SUM
      SAVEI=AIMAG(ROOT(K))
      B=SAVEI/SUM
      IF(ABS(A).LT.1.E-06)SAVER=0.
      IF(ABS(B).LT.1.E-06)SAVEI=0.
      ROOT(K)=CMPLX(SAVER,SAVEI)
    3 CONTINUE
      RETURN
      END
```

```
      SUBROUTINE DEGEN(ROOT,NCASE)
      DIMENSION ROOT(10),MARK(4)
      COMPLEX ROOT,SAVE,A,B
      KPASS=0
      MATCHM=1
      LOCK=5
      NCASE=5
      NDEG=0
    3 NMARK=0
      K=MATCHM
    2 K=K+1
      IF(K.EQ.LOCK)GO TO 1
      A=ROOT(K)
      B=ROOT(MATCHM)
      CALL MATCH(A,B,NOPE)
      IF(NOPE.EQ.0)GO TO 2
      NMARK=NMARK+1
      NDEG=NDEG+1
      MARK(NMARK)=K
      GO TO 2
    1 KPASS=KPASS+1
      IF(KPASS.GE.2)GO TO 8
      IF(NDEG.EQ.3)RETURN
      NCASE=4
      IF(NDEG.EQ.0)GO TO 5
    9 DO 6 J=1,NMARK
      KDUM=MARK(NMARK-J+1)
      IF(KDUM.EQ.LOCK-J)GO TO 6
      SAVE=ROOT(KDUM)
      ROOT(KDUM)=ROOT(LOCK-J)
      ROOT(LOCK-J)=SAVE
    6 CONTINUE
      MATCHM=MATCHM+1
      LOCK=LOCK-NMARK
      IF(NDEG.EQ.2)RETURN
      GO TO 7
    5 SAVE=ROOT(MATCHM)
      ROOT(MATCHM)=ROOT(LOCK-1)
      ROOT(LOCK-1)=SAVE
    7 CONTINUE
      GO TO 3
    8 NCASE=3
      IF((NDEG.EQ.2).AND.(NMARK.EQ.1))RETURN
      NCASE=4
      IF(NDEG.EQ.2)GO TO 9
      NCASE=2
      IF((NMARK.EQ.0).AND.(NDEG.EQ.1))RETURN
       NDEG=2
      IF(NMARK.EQ.1)GO TO 9
      NCASE=1
      A=ROOT(2)
      B=ROOT(3)
      CALL MATCH(A,B,NOPE)
      IF(NOPE.EQ.0)RETURN
      NCASE=2
      SAVE=ROOT(1)
```

```
      ROOT(1)=ROOT(2)
      ROOT(2)=SAVE
      ROOT(3)=ROOT(4)
      RETURN
      END


      SUBROUTINE QUAD(A1,A0,X1R,X1I,X2R,X2I)
      DOUBLE PRECISION A1,A0,X1R,X1I,X2R,X2I,D
     *    ,ROUND
      ROUND=(DABS(A1)+DABS(A0))/2.D0
      D=(A1*A1-4.D0*A0)/4.D0
      IF((ROUND+D)-ROUND)1,2,3
    1 D=DSQRT(-D)
      X1R=-A1/2.D0
      X1I=D
      X2R=X1R
      X2I=-D
      RETURN
    2 X1R=-A1/2.D0
      X1I=0.D0
      X2R=X1R
      X2I=0.D0
      RETURN
    3 X1R=-A1/2.D0+DSQRT(D)
      X1I=0.D0
      X2R=-A1/2.D0-DSQRT(D)
      X2I=0.D0
      RETURN
      END
```

APPENDIX C

The following tables list the unitary time evolution operator $S_{ij}(\theta,\phi)$ corresponding to a pulse involving the ij transition in the zero field triplet state spin sublevels, on resonance for $\theta = \pi/2$ and $\theta = \pi$, and with phase ϕ. Also listed are the results of applying Eq. (19) to a general hermitian matrix, A, utilizing the pulse matricies $S_{ij}(\theta,\phi)$.

$S_{xy}\ (\theta,\phi)$ - xy transition

PHASE ϕ	$\theta = \pi/2$	$\theta = \pi$
	$\vert z\rangle \quad \vert y\rangle \quad \vert x\rangle$	$\vert z\rangle \quad \vert y\rangle \quad \vert x\rangle$
0°	$\begin{bmatrix} 1 & 0 & 0 \\ 0 & \frac{\sqrt{2}}{2} & -\frac{\sqrt{2}}{2} \\ 0 & \frac{\sqrt{2}}{2} & \frac{\sqrt{2}}{2} \end{bmatrix}$	$\begin{bmatrix} 1 & 0 & 0 \\ 0 & 0 & -1 \\ 0 & 1 & 0 \end{bmatrix}$
90°	$\begin{bmatrix} 1 & 0 & 0 \\ 0 & \frac{\sqrt{2}}{2} & i\frac{\sqrt{2}}{2} \\ 0 & i\frac{\sqrt{2}}{2} & \frac{\sqrt{2}}{2} \end{bmatrix}$	$\begin{bmatrix} 1 & 0 & 0 \\ 0 & 0 & i \\ 0 & i & 0 \end{bmatrix}$
180°	$\begin{bmatrix} 1 & 0 & 0 \\ 0 & \frac{\sqrt{2}}{2} & \frac{\sqrt{2}}{2} \\ 0 & -\frac{\sqrt{2}}{2} & \frac{\sqrt{2}}{2} \end{bmatrix}$	$\begin{bmatrix} 1 & 0 & 0 \\ 0 & 0 & 1 \\ 0 & -1 & 0 \end{bmatrix}$
270°	$\begin{bmatrix} 1 & 0 & 0 \\ 0 & \frac{\sqrt{2}}{2} & -i\frac{\sqrt{2}}{2} \\ 0 & -i\frac{\sqrt{2}}{2} & \frac{\sqrt{2}}{2} \end{bmatrix}$	$\begin{bmatrix} 1 & 0 & 0 \\ 0 & 0 & -i \\ 0 & -i & 0 \end{bmatrix}$

S_{xz} (θ,ϕ) - xz transition

PHASE ϕ	$\theta = \pi/2$	$\theta = \pi$
	$\begin{array}{ccc} \|z\rangle & \|y\rangle & \|x\rangle \end{array}$	$\begin{array}{ccc} \|z\rangle & \|y\rangle & \|x\rangle \end{array}$
0°	$\begin{bmatrix} \frac{\sqrt{2}}{2} & 0 & \frac{\sqrt{2}}{2} \\ 0 & 1 & 0 \\ -\frac{\sqrt{2}}{2} & 0 & \frac{\sqrt{2}}{2} \end{bmatrix}$	$\begin{bmatrix} 0 & 0 & 1 \\ 0 & 1 & 0 \\ -1 & 0 & 0 \end{bmatrix}$
90°	$\begin{bmatrix} \frac{\sqrt{2}}{2} & 0 & -i\frac{\sqrt{2}}{2} \\ 0 & 1 & 0 \\ -i\frac{\sqrt{2}}{2} & 0 & \frac{\sqrt{2}}{2} \end{bmatrix}$	$\begin{bmatrix} 0 & 0 & -i \\ 0 & 1 & 0 \\ -i & 0 & 0 \end{bmatrix}$
180°	$\begin{bmatrix} \frac{\sqrt{2}}{2} & 0 & -\frac{\sqrt{2}}{2} \\ 0 & 1 & 0 \\ \frac{\sqrt{2}}{2} & 0 & \frac{\sqrt{2}}{2} \end{bmatrix}$	$\begin{bmatrix} 0 & 0 & -1 \\ 0 & 1 & 0 \\ 1 & 0 & 0 \end{bmatrix}$
270°	$\begin{bmatrix} \frac{\sqrt{2}}{2} & 0 & i\frac{\sqrt{2}}{2} \\ 0 & 1 & 0 \\ i\frac{\sqrt{2}}{2} & 0 & \frac{\sqrt{2}}{2} \end{bmatrix}$	$\begin{bmatrix} 0 & 0 & i \\ 0 & 1 & 0 \\ i & 0 & 0 \end{bmatrix}$

$S_{yz}(\theta,\phi)$ - yz transition

PHASE ϕ	$\theta = \pi/2$	$\theta = \pi$
	$\begin{array}{ccc} \vert z\rangle & \vert y\rangle & \vert x\rangle \end{array}$	$\begin{array}{ccc} \vert z\rangle & \vert y\rangle & \vert x\rangle \end{array}$
0°	$\begin{bmatrix} \frac{\sqrt{2}}{2} & -\frac{\sqrt{2}}{2} & 0 \\ \frac{\sqrt{2}}{2} & \frac{\sqrt{2}}{2} & 0 \\ 0 & 0 & 1 \end{bmatrix}$	$\begin{bmatrix} 0 & -1 & 0 \\ 1 & 0 & 0 \\ 0 & 0 & 1 \end{bmatrix}$
90°	$\begin{bmatrix} \frac{\sqrt{2}}{2} & i\frac{\sqrt{2}}{2} & 0 \\ i\frac{\sqrt{2}}{2} & \frac{\sqrt{2}}{2} & 0 \\ 0 & 0 & 1 \end{bmatrix}$	$\begin{bmatrix} 0 & i & 0 \\ i & 0 & 0 \\ 0 & 0 & 1 \end{bmatrix}$
180°	$\begin{bmatrix} \frac{\sqrt{2}}{2} & \frac{\sqrt{2}}{2} & 0 \\ -\frac{\sqrt{2}}{2} & \frac{\sqrt{2}}{2} & 0 \\ 0 & 0 & 1 \end{bmatrix}$	$\begin{bmatrix} 0 & 1 & 0 \\ -1 & 0 & 0 \\ 0 & 0 & 1 \end{bmatrix}$
270°	$\begin{bmatrix} \frac{\sqrt{2}}{2} & -i\frac{\sqrt{2}}{2} & 0 \\ -i\frac{\sqrt{2}}{2} & \frac{\sqrt{2}}{2} & 0 \\ 0 & 0 & 1 \end{bmatrix}$	$\begin{bmatrix} 0 & -i & 0 \\ -i & 0 & 0 \\ 0 & 0 & 1 \end{bmatrix}$

(θ,ϕ)	$A^{*xy}(\theta,\phi)$ - xy transition
$(\pi/2,0°)$	$\begin{bmatrix} A^*_{zz} & \frac{\sqrt{2}}{2}(A^*_{zy}+A^*_{zx}) & \frac{\sqrt{2}}{2}(A^*_{zx}-A^*_{zy}) \\ \frac{\sqrt{2}}{2}(A^*_{yz}+A^*_{xz}) & \frac{1}{2}(A^*_{xx}+A^*_{yy})+\mathrm{Re}A^*_{yx} & \frac{1}{2}(A^*_{xx}-A^*_{yy})+i\mathrm{Im}A^*_{yx} \\ \frac{\sqrt{2}}{2}(A^*_{xz}-A^*_{yz}) & \frac{1}{2}(A^*_{xx}-A^*_{yy})-i\mathrm{Im}A^*_{yx} & \frac{1}{2}(A^*_{xx}+A^*_{yy})-\mathrm{Re}A^*_{yx} \end{bmatrix}$
$(\pi,0°)$	$\begin{bmatrix} A^*_{zz} & A^*_{zx} & -A^*_{zy} \\ A^*_{xz} & A^*_{xx} & -A^*_{xy} \\ -A^*_{yz} & -A^*_{yx} & A^*_{yy} \end{bmatrix}$
$(\pi/2,90°)$	$\begin{bmatrix} A^*_{zz} & \frac{\sqrt{2}}{2}(A^*_{zy}+iA^*_{zx}) & \frac{\sqrt{2}}{2}(A^*_{zx}+iA^*_{zy}) \\ \frac{\sqrt{2}}{2}(A^*_{yz}-iA^*_{xz}) & \frac{1}{2}(A^*_{xx}+A^*_{yy})-\mathrm{Im}A^*_{yx} & \frac{i}{2}(A^*_{yy}-A^*_{xx})+\mathrm{Re}A^*_{yx} \\ \frac{\sqrt{2}}{2}(A^*_{xz}-iA^*_{yz}) & \frac{i}{2}(A^*_{xx}-A^*_{yy})+\mathrm{Re}A^*_{yx} & \frac{1}{2}(A^*_{xx}+A^*_{yy})+\mathrm{Im}A^*_{yx} \end{bmatrix}$
$(\pi,90°)$	$\begin{bmatrix} A^*_{zz} & +iA^*_{zx} & +iA^*_{zy} \\ -iA^*_{xz} & A^*_{xx} & A^*_{xy} \\ -iA^*_{yz} & A^*_{yx} & A^*_{yy} \end{bmatrix}$

(θ,ϕ)	$A^{*xy}(\theta,\phi)$ - xy transition
$(\pi/2,180°)$	$\begin{bmatrix} A^{*}_{zz} & \frac{\sqrt{2}}{2}(A^{*}_{zy} - A^{*}_{zx}) & \frac{\sqrt{2}}{2}(A^{*}_{zy} + A^{*}_{zx} \\ \frac{\sqrt{2}}{2}(A^{*}_{yz} - A^{*}_{xz}) & \frac{1}{2}(A^{*}_{yy} + A^{*}_{xx}) - \mathrm{Re}A^{*}_{yx} & \frac{1}{2}(A^{*}_{yy} - A^{*}_{xx}) + i\mathrm{Im}A^{*}_{yx} \\ \frac{\sqrt{2}}{2}(A^{*}_{yz} + A^{*}_{xz}) & \frac{1}{2}(A^{*}_{yy} - A^{*}_{xx}) - i\mathrm{Im}A^{*}_{yx} & \frac{1}{2}(A^{*}_{yy} + A^{*}_{xx}) + \mathrm{Re}A^{*}_{yx} \end{bmatrix}$
$(\pi,180°)$	$\begin{bmatrix} A^{*}_{zz} & -A^{*}_{zx} & A^{*}_{zy} \\ -A^{*}_{xz} & A^{*}_{xx} & -A^{*}_{xy} \\ A^{*}_{yz} & -A^{*}_{yx} & A^{*}_{yy} \end{bmatrix}$
$(\pi/2,270°)$	$\begin{bmatrix} A^{*}_{zz} & \frac{\sqrt{2}}{2}(A^{*}_{zy} - iA^{*}_{zx}) & \frac{\sqrt{2}}{2}(A^{*}_{zx} - iA^{*}_{zy}) \\ \frac{\sqrt{2}}{2}(A^{*}_{yz} + iA^{*}_{xz}) & \frac{1}{2}(A^{*}_{yy} + A^{*}_{xx}) + \mathrm{Im}A^{*}_{yx} & \frac{i}{2}(A^{*}_{xx} - A^{*}_{yy}) + \mathrm{Re}A^{*}_{yx} \\ \frac{\sqrt{2}}{2}(A^{*}_{xz} + iA^{*}_{yz}) & \frac{i}{2}(A^{*}_{yy} - A^{*}_{xx}) + \mathrm{Re}A^{*}_{yx} & \frac{1}{2}(A^{*}_{yy} + A^{*}_{xx}) - \mathrm{Im}A^{*}_{yx} \end{bmatrix}$
$(\pi,270°)$	$\begin{bmatrix} A^{*}_{zz} & -iA^{*}_{zx} & -iA^{*}_{zy} \\ iA^{*}_{xz} & A^{*}_{xx} & A^{*}_{xy} \\ iA^{*}_{yz} & A^{*}_{yx} & A^{*}_{yy} \end{bmatrix}$

(θ,ϕ)	$A^{*xz}\ (\theta,\phi)$ - xz transition
$(\pi/2,0°)$	$\begin{bmatrix} \frac{1}{2}(A^*_{zz} + A^*_{xx}) - \mathrm{Re}A^*_{xz} & \frac{\sqrt{2}}{2}(A^*_{zy} - A^*_{xy}) & \frac{1}{2}(A^*_{zz} - A^*_{xx}) - i\mathrm{Im}A^*_{xz} \\ \frac{\sqrt{2}}{2}(A^*_{yz} - A^*_{yx}) & A^*_{yy} & \frac{\sqrt{2}}{2}(A^*_{yz} + A^*_{yx}) \\ \frac{1}{2}(A^*_{zz} - A^*_{xx}) + i\mathrm{Im}A^*_{xz} & \frac{\sqrt{2}}{2}(A^*_{zy} + A^*_{xy}) & \frac{1}{2}(A^*_{zz} + A^*_{xx}) + \mathrm{Re}A^*_{xz} \end{bmatrix}$
$(\pi,0°)$	$\begin{bmatrix} A^*_{xx} & -A^*_{xy} & -A^*_{xz} \\ -A^*_{yx} & A^*_{yy} & A^*_{yz} \\ -A^*_{zx} & A^*_{zy} & A^*_{zz} \end{bmatrix}$
$(\pi/2,90°)$	$\begin{bmatrix} \frac{1}{2}(A^*_{zz} + A^*_{xx}) - \mathrm{Im}A^*_{xz} & \frac{\sqrt{2}}{2}(A^*_{zy} + iA^*_{xy}) & \frac{i}{2}(A^*_{xx} - A^*_{zz}) + \mathrm{Re}A^*_{xz} \\ \frac{\sqrt{2}}{2}(A^*_{yz} - iA^*_{yx}) & A^*_{yy} & \frac{\sqrt{2}}{2}(A^*_{yx} - iA^*_{yz}) \\ \frac{i}{2}(A^*_{zz} - A^*_{xx}) + \mathrm{Re}A^*_{xz} & \frac{\sqrt{2}}{2}(A^*_{xy} + iA^*_{zy}) & \frac{1}{2}(A^*_{zz} + A^*_{xx}) + \mathrm{Im}A^*_{xz} \end{bmatrix}$
$(\pi,90°)$	$\begin{bmatrix} A^*_{xx} & iA^*_{xy} & A^*_{xz} \\ -iA^*_{yx} & A^*_{yy} & -iA^*_{yz} \\ A^*_{zx} & iA^*_{zy} & A^*_{zz} \end{bmatrix}$

(θ,ϕ)	$A^{*xz}\ (\theta,\phi)$ - xz transition
$(\pi/2,180°)$	$\begin{bmatrix} \frac{1}{2}(A^*_{zz} + A^*_{xx}) + \mathrm{Re}A^*_{xz} & \frac{\sqrt{2}}{2}(A^*_{zy} + A^*_{xy}) & \frac{1}{2}(A^*_{xx} - A^*_{zz}) - i\mathrm{Im}A^*_{xz} \\ \frac{\sqrt{2}}{2}(A^*_{yz} + A^*_{yx}) & A^*_{yy} & \frac{\sqrt{2}}{2}(A^*_{yx} - A^*_{yz}) \\ \frac{1}{2}(A^*_{xx} - A^*_{zz}) + i\mathrm{Im}A^*_{xz} & \frac{\sqrt{2}}{2}(A^*_{xy} - A^*_{zy}) & \frac{1}{2}(A^*_{zz} + A^*_{xx}) - \mathrm{Re}A^*_{xz} \end{bmatrix}$
$(\pi,180°)$	$\begin{bmatrix} A^*_{xx} & A^*_{xy} & -A^*_{xz} \\ A^*_{yx} & A^*_{yy} & -A^*_{yz} \\ -A^*_{zx} & -A^*_{zy} & A^*_{zz} \end{bmatrix}$
$(\pi/2,270°)$	$\begin{bmatrix} \frac{1}{2}(A^*_{zz} + A^*_{xx}) + \mathrm{Im}A^*_{xz} & \frac{\sqrt{2}}{2}(A^*_{zy} - iA^*_{xy}) & \frac{i}{2}(A^*_{zz} - A^*_{xx}) + \mathrm{Re}A^*_{xz} \\ \frac{\sqrt{2}}{2}(A^*_{yz} + iA^*_{yx}) & A^*_{yy} & \frac{\sqrt{2}}{2}(A^*_{yx} + iA^*_{yz}) \\ \frac{i}{2}(A^*_{xx} - A^*_{zz}) + \mathrm{Re}A^*_{xz} & \frac{\sqrt{2}}{2}(A^*_{xy} - iA^*_{zy}) & \frac{1}{2}(A^*_{zz} + A^*_{xx}) - \mathrm{Im}A^*_{xz} \end{bmatrix}$
$(\pi,270°)$	$\begin{bmatrix} A^*_{xx} & -iA^*_{xy} & A^*_{xz} \\ iA^*_{yx} & A^*_{yy} & iA^*_{yz} \\ A^*_{zx} & -iA^*_{zy} & A^*_{zz} \end{bmatrix}$

(θ,ϕ)	$A^{*yz}(\theta,\phi)$ - yz transition
$(\pi/2,0°)$	$\begin{bmatrix} \frac{1}{2}(A^*_{zz}+A^*_{yy})+\mathrm{Re}A^*_{zy} & \frac{1}{2}(A^*_{yy}-A^*_{zz})+i\mathrm{Im}A^*_{zy} & \frac{\sqrt{2}}{2}(A^*_{zx}+A^*_{yx}) \\ \frac{1}{2}(A^*_{yy}-A^*_{zz})-i\mathrm{Im}A^*_{zy} & \frac{1}{2}(A^*_{zz}+A^*_{yy})-\mathrm{Re}A^*_{zy} & \frac{\sqrt{2}}{2}(A^*_{yx}-A^*_{zx}) \\ \frac{\sqrt{2}}{2}(A^*_{xz}+A^*_{xy}) & \frac{\sqrt{2}}{2}(A^*_{xy}-A^*_{xz}) & A^*_{xx} \end{bmatrix}$
$(\pi,0°)$	$\begin{bmatrix} A^*_{yy} & -A^*_{yz} & A^*_{yx} \\ -A^*_{zy} & A^*_{zz} & -A^*_{zx} \\ A^*_{xy} & -A^*_{xz} & A^*_{xx} \end{bmatrix}$
$(\pi/2,90°)$	$\begin{bmatrix} \frac{1}{2}(A^*_{zz}+A^*_{yy})-\mathrm{Im}A^*_{zy} & \frac{i}{2}(A^*_{zz}-A^*_{yy})+\mathrm{Re}A^*_{zy} & \frac{\sqrt{2}}{2}(A^*_{zx}-iA^*_{yx}) \\ \frac{i}{2}(A^*_{yy}-A^*_{zz})+\mathrm{Re}A^*_{zy} & \frac{1}{2}(A^*_{zz}+A^*_{yy})+\mathrm{Im}A^*_{zy} & \frac{\sqrt{2}}{2}(A^*_{yx}-iA^*_{zx}) \\ \frac{\sqrt{2}}{2}(A^*_{xz}+iA^*_{xy}) & \frac{\sqrt{2}}{2}(A^*_{xy}+iA^*_{xz}) & A^*_{xx} \end{bmatrix}$
$(\pi,90°)$	$\begin{bmatrix} A^*_{yy} & A^*_{yz} & -iA^*_{yx} \\ A^*_{zy} & A^*_{zz} & -iA^*_{zx} \\ iA^*_{xy} & iA^*_{xz} & A^*_{xx} \end{bmatrix}$

(θ,ϕ)	$A^{*yz}(\theta,\phi)$ - yz transition
$(\pi/2,180°)$	$\begin{bmatrix} \frac{1}{2}(A^*_{zz}+A^*_{yy})-\mathrm{Re}A^*_{zy} & \frac{1}{2}(A^*_{zz}-A^*_{yy})+i\mathrm{Im}A^*_{zy} & \frac{\sqrt{2}}{2}(A^*_{zx}-A^*_{yx}) \\ \frac{1}{2}(A^*_{zz}-A^*_{yy})-i\mathrm{Im}A^*_{zy} & \frac{1}{2}(A^*_{zz}+A^*_{yy})+\mathrm{Re}A^*_{zy} & \frac{\sqrt{2}}{2}(A^*_{zx}+A^*_{yx}) \\ \frac{\sqrt{2}}{2}(A^*_{xz}-A^*_{xy}) & \frac{\sqrt{2}}{2}(A^*_{xz}+A^*_{xy}) & A^*_{xx} \end{bmatrix}$
$(\pi,180°)$	$\begin{bmatrix} A^*_{yy} & -A^*_{yz} & -A^*_{yx} \\ -A^*_{zy} & A^*_{zz} & A^*_{zx} \\ -A^*_{xy} & A^*_{xz} & A^*_{xx} \end{bmatrix}$
$(\pi/2,270°)$	$\begin{bmatrix} \frac{1}{2}(A^*_{zz}+A^*_{yy})+\mathrm{Im}A^*_{zy} & \frac{i}{2}(A^*_{yy}-A^*_{zz})+\mathrm{Re}A^*_{zy} & \frac{\sqrt{2}}{2}(A^*_{zx}+iA^*_{yx}) \\ \frac{i}{2}(A^*_{zz}-A^*_{yy})+\mathrm{Re}A^*_{zy} & \frac{1}{2}(A^*_{zz}+A^*_{yy})-\mathrm{Im}A^*_{zy} & \frac{\sqrt{2}}{2}(A^*_{yx}+iA^*_{zx}) \\ \frac{\sqrt{2}}{2}(A^*_{xz}-iA^*_{xy}) & \frac{\sqrt{2}}{2}(A^*_{xy}-iA^*_{xz}) & A^*_{xx} \end{bmatrix}$
$(\pi,270°)$	$\begin{bmatrix} A^*_{yy} & A^*_{yz} & iA^*_{yx} \\ A^*_{zy} & A^*_{zz} & iA^*_{zx} \\ -iA^*_{xy} & -iA^*_{xz} & A^*_{xx} \end{bmatrix}$

ACKNOWLEDGEMENTS

I am indebted to Professor Charles B. Harris for providing me with stimulation and countless suggestions that guided me through experimental and theoretical difficulties.

I should also like to thank my friends in the research group for discussions and diversions that made the tedious times more bearable. In particular I wish to thank M. D. Fayer for conversations that led to a number of the conceptualizations presented in this work, and to M. T. Lewellyn for carefully proofreading the initial drafts. Support for this work was due partly to the Inorganic Materials Research Division of the Lawrence Berkeley Laboratory under the auspices of the U. S. Energy Research and Development Administration and partly by a Standard Oil Fellowship for the year 1973-1974.

REFERENCES

1. J. Brossel and A. Kastler, Compt. Rend 229, 1213 (1949).
2. J. Brossel and F. Bitter, Phys. Rev. 86, 308 (1952).
3. S. Geshwind, R. Collins, and A. Schalow, Phys. Rev. Lett. 3, 545 (1959).
4. S. Geshwind, G. Devlin, R. Cohen, and S. Chinn, Phys. Rev. 137, A1087 (1965).
5. M. Sharnoff, J. Chem. Phys 46, 3263 (1967).
6. A. Kwiram, Chem. Phys. Lett., 1, 272 (1967).
7. C. Hutchison and B. Mangum, J. Chem. Phys. 29, 952 (1958).
8. C. Hutchison and B. Mangum, J. Chem. Phys. 34, 908 (1961).
9. J. Schmidt, I. Hesselmann, M. DeGroot & J. van der Waals, Chem. Phys. Lett. 1, 434 (1967).
10. D. Tinti, M. ElSayed, A. Maki, and C. Harris, Chem. Phys. Lett. 3. 343 (1969).
11. C. Harris, D. Tinti, M. ElSayed, and A. Maki, Chem. Phys. Lett. 4, 409 (1969).
12. T. Kuan, D. Tinti, and M. ElSayed, Chem. Phys. Lett. 4, 507 (1970).
13. A. Kwirim, M.T.P. International Review of Science, Phys. Chem. Series I, Vol 4, p 271-316; Ed. C. McDowell, Butterworth Pub. Co. (1972).
14. M. ElSayed, Accts. Chem. Res 4, 23 (1971).
15. A. Denison, Mag. Res. Rev. 2, 1 (1973).
16. S. McGlynn, T. Azumi, and M. Kinoshita, Molecular Spectroscopy of the Triplet State, Prentice Hall, New Jersey, (1969).

17. A. Carrington and A. McLachlan, Introduction to Magnetic Resonance, Harper & Row, N.Y. (1967) Ch. 8.

18. J. van der Waals and M. de Groot, The Triplet State.

19. M. de Groot, I. Hesselmann, J. van der Waals, Mol. Phys. 12, 259 (1967).

20. W. Breiland and C. Harris, Chem. Phys. Lett. 18, 309 (1973).

21. C. Harris, J. Chem. Phys. 54, 972 (1971).

22. J. Schmidt, W. Van Dorp, and J. van der Waals, Chem. Phys. Lett 8, 345 (1971).

23. J. Schmidt, Chem. Phys. Lett. 14, 411 (1972).

24. W. Breiland, C. Harris, and A. Pines, Phys. Rev. Lett. 30, 158 (1973).

25. U. Fano. Rev. Mod. Phys., 29, 74 (1957).

26. D. ter Haar, Rep. Prog. Phys. 24, 304 (1961).

27. R. Feynman, F. Vernon, and R. Hellwarth, J. Appl. Phys. 28, 49 (1957).

28. H. Margenau and G. Murphy, The Mathematics of Physics and Chemistry, D. Van Nostrand Co., Ltd., New Jersey, (1956), p 570.

29. A. Abragam, The Principles of Nuclear Magnetism, Oxford U.P., London, (1961).

30. N. Kurnit, I. Abella, and S. Hartmann, Phys. Rev. Lett. 13, 567 (1964).

31. I. Abella, N. Kurnit, and S. Hartmann, Phys. Rev., 141, 391 (1966).

32. This is referred to as the "Rotating Field Approximation" by papers relating to laser studies, and consequences of its neglect are discussed with respect to magnetic resonance by Ref(33).

33. F. Bloch and A. Siegert, Phys. Rev. 57, 522 (1940).

34. I. Rabi, N. Ramsey, and J. Schwinger, Rev. Mod. Phys. 26, 167 (1954).

35. H. Torrey, Phys. Rev. 76, 1059 (1949).

36. T. Dyke, G. Tomasevich, W. Klemperer, and W. Falconer, J. Chem. Phys. 57, 2277 (1972).

37. U. Fano, Phys. Rev., 90, 577 (1953).

38. F. Bloch, Phys. Rev. 70, 460 (1946).

39. A. Redfield, Phys. Rev. 98, 1787 (1955).

40. E. Hahn, Phys. Rev. 80, 580 (1950).

41. H. Carr and E. Purcell, Phys. Rev., 94, 630 (1954).

42. I. Solomon, C. R. Acad. Sci. 248, 92 (1959).

43. D. Douglas, G. Jones, J. Chem. Phys. 45, 956 (1966).

44. R. Ernst and W. Anderson, Rev. Sci. Instr. 37, 93 (1966).

45. C. Closs, J. Amer. Chem. Soc. 91, 4552 (1969).

46. F. Adrian, J. Chem. Phys. 54, 3912 (1971); 54, 3918 (1971).

47. R. Brewer and R. Shoemaker, Phys. Rev. Lett. 27, 631 (1971).

48. A. Icsevgi and W. Lamb, Jr., Phys. Rev. 185, 517 (1969).

49. See for example 112-114, 118-121 in Supplementary References.

50. See for Example 58-61.

51. W. Weisskopf and E. Wigner, Z. Phys. 63, 54 (1930).

52. E. Putzer, Amer. Math. Monthly 73, 2 (1966).

53. R. Zwanzig, Physica 30, 1109 (1964).

54. R. Dicke, Phys. Rev. 93, 99 (1954).

55. See the section on "Superradiance" in the Supplementary References.

56. D. McClure, J. Chem. Phys. 20, 682 (1952).

57. A. Albrecht, J. Chem. Phys. 38, 354 (1963).

58. T. Carver and R. Partridge, Am. J. Phys. 34, 339 (1966).

59. W. Bell and A. Bloom, Phys. Rev. 107, 1559 (1957).

60. L. Chase, Phys. Rev. Lett. 21, 888 (1968).

61. J. Dodd and G. Series, Proc. Roy. Soc. (LONDON) A263, 353 (1961).

62. M. Bixon, J. Jortner, and Y. Dothan, Mol. Phys. 17, 109 (1969).

63. R. Webb, Rev. Sci. Instr. 33, 732.

64. T. Cheng and N. Hirota, J. Chem. Phys. 56, 5019 (1972).

65. M. El-Sayed, J. Chem. Phys. 52, 6438 (1970).

66. D. Tinti and M. El-Sayed, J. Chem. Phys. 54, 2529 (1971).

67. A. Shain and M. Sharnoff, J. Chem. Phys. 59, 2335 (1973).

68. C. Harris and R. Hoover, J. Chem. Phys. 56, 2199 (1972).

69. D. Schweitzer, J. Zuclich, and A. Maki, Mol. Phys. 25, 193 (1973).

70. O. Kalman and M. El-Sayed, J. Chem. Phys., 54, 4414 (1971).

71. S. Meiboom and D. Gill, Rev. Sci. Instr. 29, 688 (1958).

72. M. Fayer and C. Harris, Chem. Phys. Lett. 25, 149 (1974).

73. I. Solomon, Phys. Rev. Lett. 2, 301 (1959).

74. R. Wyckoff, Crystal Structures Interscience Publ. New York, V. 6, p. 350.

75. M. El-Sayed, E. Gossett, and M. Leung, Chem. Phys. Lett. 21, 20 (1973).

76. M. Buckley and C. Harris, J. Chem. Phys. 56, 137 (1972).

77. C. Slichter and W. Holton, Phys. Rev. 122, 1701 (1961).

78. R. Renaud, D. Kovachic, and L. Leitch, Can. J. Chem. 39 21 (1961).

79. A. Best and C. Wilson, J. Chem. Soc. 235 (1946).

SUPPLEMENTARY REFERENCES

DENSITY MATRIX

Many texts deal with the density matrix from the viewpoint of statistical mechanics in which the diagonal elements are weighted by Boltzmann factors. In this kind of treatment the matrix is by definition diagonal which implies that equilibrium thermodynamics is being employed. By considering the projection operator form given in Eq(3) one is doing nothing more than rewriting the Schrodinger Equation in a different form. However, by adding relaxation one essentially combines the two forms creating a "non-equilibrium thermodynamics". This relatively new way of viewing the density matrix is well covered in Refs. 25, 26, and by McWeeny. Dicke and Wittke give a good elementary description of the statistical density matrix. Reference 53 gives a clear explanation of the Liouville or superoperator approach, and Banwell and Primas give extensive treatment to superoperator algebra.

80. R. McWeeny, Rev. Mod. Phys. 32, 335 (1960).

81. R. Dicke and J. Wittke, Introduction to Quantum Mechanics, Addison-Wesley Publishing Co., Reading, Mass. p 331.

83. C. Banwell and H. Primas, Mol. Phys. 6, 225 (1963).

TWO-LEVEL SYSTEMS

Merzbacher gives a good elementary treatment of a two-level system. The treatment by Jaynes is interesting since he essentially applies a superoperator approach that is tantamount to the two dimensional representation of the rotation operator, Ref. 28. Shirley, Salwen, Franken, Franzen et al, and Delory treat basic quantum mechanics with emphasis on

interference effects. References 58-62 also deal with this problem. Wells and Glauber are not elementary treatments.

84. E. Merzbacher, Quantum Mechanics, John Wiley & Sons, N. Y. (1970) p. 276.

85. I. Rabi, Phys. Rev. 51, 652 (1937).

86. F. Bloch and I. Rabi, Rev. Mod. Phys. 17, 237 (1945).

87. N. Bloembergen and R. Pound, Phys. Rev. 95, 8 (1954).

88. E. Jaynes, Phys. Rev. 98, 1099 (1955).

89. I. Senitzky, Phys Rev. 119, 670 (1960); 124, 642 (1961); 131, 2827 (1963); 134, A816 (1964); 137, A1635 (1965); 142, 277 (1966).

90. J. Shirley, Phys. Rev. 138, B979 (1965).

91. S. Kukolich, Phys. Rev. 138, A1322 (1965).

92. A. Ben-Reuven and S. Kukolich, Chem. Phys. Lett. 23, 376 (1973).

93. H. Salwen, Phys. Rev., 99, 1274 (1955).

94. P. Franken, Phys. Rev., 121, 508 (1961).

95. W. Franzen, and M. Alam, Phys. Rev. 133, A460 (1964).

96. J. Delory and C. Tric, Chem. Phys., 3, 54 (1974).

97. W. Wells, Ann. of Phys. 12, 1 (1961).

98. R. Glauber, Phys. Rev. 130, 2529 (1963).

99. R. Glauber, Phys. Rev. 131, 2766 (1963).

EARLY MASER THEORY

The work by Lamb is particularly good. See Ref. 27 also.

100. J. Gordon, H. Zeiger, and C. Townes, Phys. Rev. 99, 1264 (1955).

101. A. Javan, Phys. Rev. 107, 1579 (1957).

102. L. Davis, Proc. IEEE 51, 76 (1963).

103. E. Jaynes and F. Cummings, Proc. IEEE 51, 89 (1963).

104. A. Yariv and J. Gordon, Proc. IEEE, 51, 4 (1963).

105. T. Maiman, Phys. Rev. 123, 1145 (1961); 123, 1151 (1961).

106. W. Lamb, Jr., Phys. Rev. 134, A1429 (1964).

NON-LINEAR INTERACTIONS OF LIGHT WITH MATTER

107. A. Javan and A. Szöke, Phys. Rev. 137, A536 (1965).

108. J. Parks and A. Javan, Phys. Rev. 139, A1351 (1965).

109. H. Schlossberg and A. Javan, Phys. Rev. 150, 267 (1966).

110. J. Giordmaine and W. Kaiser, Phys. Rev. 144, 676 (1966).

111. E. Lu, Phys. Rev. A. 8, 1053 (1973).

112. J. Stone, E. Thiele, and M. Goodman, J. Chem. Phys. 59, 2909 (1973).

113. M. Ducloy, Phys. Rev. A, 8, 1844 (1973).

114. B. Mollow, Phys. Rev. A, 8, 1949 (1973).

115. S. McCall and E. Hahn, Phys. Rev. Lett. 18, 908.

116. I. Asher, A. Hopf, and L. Kie, Phys. Rev. A, 8, 396.

117. J. Diels and E. Hahn, Phys. Rev. A, 8, 1084.

LASER AMPLIFIERS (REF 48 ALSO)

118. L. Frantz and J. Nodvik, J. App. Phys. 34, 2346 (1963).

119. J. Wittke and P. Warter, J. App. Phys. 35, 1668 (1964).

120. F. Arecchi and R. Bonifacio, IEEE J. Quantum Elec. QE 1, 169 (1965).

121. F. Hopf and M. Scully, Phys. Rev. 179, 399 (1969).

PHOTON ECHOES (REF 30, 31 ALSO)

122. J. Gordon, C. Wang, C. Patel, R. Slusher, W. Tomlinson, Phys. Rev. 179, 294 (1969).

123. R. Brewer and R. Shoemaker, Phys. Rev. Lett. 27, 631 (1971).

124. P. Liao and S. Hartmann, Optics Commun., 8, 310 (1973).

SUPERRADIANCE

This list is by no means complete and represents more or less a scattered sampling of the field. Dicke's paper (Ref54) was virtually ignored until high power laser pulses were experimentally practicable. The major interest among physicists today is the so-called Dicke Decay in which an originally inverted state spontaneously evolves into a superradiant state. This phenomena has been confused with amplified spontaneous emission experimentally and much of the arguments are caught up in semantics.[129] Buley et al., Bonifacio et al.,[128] and Friedberg et al. offer the closest explanation with respect to the vector model.

125. E. Buley and F. Cummings, Phys. Rev. 134, A1454 (1964).
126. V. Ernst and P. Stehle, Phys. Rev. 176, 1456 (1968).
127. J. Eberly and N. Rehler, Phys. Lett. 29A, 142 (1969).
128. R. Bonifacio, D. Kim, and M. Scully, Phys. Rev. 187, 441 (1969).
129. L. Allen and G. Peters, Phys. Lett. 31A, 95 (1970).
130. J. Eberly and N. Rehler, Phys. Rev. A, 2, 1607 (1970).
131. R. Bonifacio, P. Schwendimann, and F. Haake, Phys. Rev. A, 4, 302 (1971); 4, 854 (1971).
132. W. Gamble, C. Bowden, R. Hartmann, L. Narducci and J. Castle, J. Mag. Res. 14, 358 (1974).
133. R. Jodoin and L. Mandel, Phys. Rev. A, 9, 873 (1974).
134. R. Picard and C. Willis, Phys. Rev. A, 8, 1536 (1973).
135. P. Lee, Y. Lee, and C. Chang, Phys. Rev. A, 8, 1722 (1973).
136. A. Flusberg, R. Friedberg, and S. Hartmann, Phys. Rev. A, 10, 1904 (1974).
137. R. Jodoin, and L. Mandel, Phys. Rev. A, 10, 1898 (1974).

138. R. Friedberg and S. Hartmann, Phys. Rev. A, 10, 1728 (1974).

139. G. Banfi and R. Bonifacio, Phys. Rev. Lett. 33, 1259 (1974).

AMPLIFIED SPONTANEOUS EMISSION

The first reference more or less covers all their previous work.

140. L. Allen and G. Peters, Phys. Rev. A, 8, 2031 (1973).

141. L. Allen and G. Peters, J. Phys. A, 4, 238 (1971); 4, 377 (1971); 4, 564 (1971); 5, 546 (1972); 5, 695 (1972).

PULSED MAGNETIC RESONANCE

Farrar and Becker offer the best introduction to this subject and the review by Mansfield is also good. Mims[146] treats the interesting case of "Intermediate" microwave power and its effect on the echo shapes, a situation often encountered in electron spin resonance. The author has observed "beats" on the echo maximum decay 148 and 150 for pure TCB crystals and for 1,2 dichloroquinoxaline and 1,2 dibromoquinoxaline (1%) in durene.

142. T. Farrar and E. Becker, Pulse and Fourier Transform NMR, Academic, New York (1971).

143. P. Mansfield

144. M. Bloom, E. Hahn, and B. Herzog, Phys. Rev. 97, 1699 (1955).

145. A. Bloom, Phys. Rev. 98, 1105 (1955).

146. W. Mims, Rev. Sci. Instr., 36, 1472 (1965).

147. W. Mims, Phys. Rev. B, 3, 2840 (1971).

148. L. Rowan, E. Hahn, and W. Mims, Phys. Rev. 137, A61 (1965).

149. D. Grischkowsky and S. Hartmann, Phys. Rev. B, 2, 60 (1970).

150. W. Mims, Phys. Rev. B, 5, 2409 (1972).

The following are some techniques that may become useful in optically detected magnetic resonance.

151. T. Das and D. Roy, Phys. Rev. 98, 525 (1955).

152. G. Whitfield and A. Redfield, Phys. Rev. 106, 918 (1957).

153. M. Schwab and E. Hahn, J. Chem. Phys. 52, 3152 (1970).

154. H. Kessemeier and W. Rhim, Phys. Rev. B, 5, 761 (1972).

155. N. Boden and M. Mortimer, Chem. Phys. Lett. 21, 538 (1973).

156. M. Goldman, M. Chapellier, and V. Chau, Phys. Rev. 168, 301 (1968).

157. E. Ostroff and J. Waugh, Phys. Rev. Lett. 16, 1097 (1966).

158. J. Waugh, L. Huber, U. Haeberlen, Phys. Rev. Lett. 20, 180 (1968).

159. J. Waugh, C. Wang, L. Huber, R. Vold, J. Chem. Phys. 48, 662 (1968).

160. U. Haeberlen and J. Waugh, Phys. Rev. 175, 453 (1968).

161. W. Rhim, A. Pines, and J. Waugh, Phys. Rev. B 3, 684 (1971).

162. U. Haeberlen, J. Ellett Jr., and J. Waugh, J. Chem. Phys. 55, 53 (1971).

163. M. Mehring, J. Waugh, Phys. Rev. B, 5, 3459 (1972).

164. A. Pines, M. Gibby, J. Waugh, J. Chem. Phys. 59, 569 (1973).

FOURIER TRANSFORM SPECTROSCOPY

In addition to Ref. 44 the following modifications have been proposed.

165. I. Lowe and R. Norberg, Phys. Rev. 107, 46 (1957).

166. R. Ernst, J. Chem. Phys. 45, 3845 (1966).

167. R. Ernst, J. Mag. Res. 1, 7 (1969); 3, 10 (1970); 4, 280 (1971).

168. R. Freeman and H. Hill, J. Chem. Phys. 54, 3367 (1971); 55 1985 (1971).

169. G. Parker, J. Chem. Phys. 58, 3274 (1973).

170. J. Kaplan, J. Chem. Phys. 57, 5615 (1972).

RELAXATION IN MAGNETIC RESONANCE

The classic relaxation papers are given by 171-184.

171. J. Van Vleck, Phys. Rev. 74, 1168 (1948)
172. N. Bloembergen, E. Purcell, and R. Pound, Phys. Rev. 73, 679 (1948).
173. R. Wangsness and F. Bloch, Phys. Rev. 89, 728 (1953).
174. F. Bloch, Phys. Rev. 102, 104 (1956).
175. A. Redfield, IBM J. Res. Dev. 1, 19 (1957).
176. W. Blumberg, Phys. Rev. 119, 79 (1960).
177. P. Anderson, J. Phys. Soc. Japan 9 316 (1954).
178. R. Kubo, K. Tomita, J. Phys. Soc. Japan 9, 888 (1954).
179. R. Kubo, J. Phys. Soc. Japan 9, 935 (1954).
180. H. Torrey, Phys. Rev. 92, 962 (1953).
181. D. Pines, C. Slichter, Phys. Rev. 100, 1014 (1955).
182. H. C. Torrey, Phys. Rev. 104, 563 (1956).
183. N. Bloembergen and P. Sorokin, Phys. Rev. 110, 865 (1958).
184. W. Mims, K. Nassau, and J. McGee, Phys. Rev. 123, 2059 (1961).
185. P. Scott and C. Jeffries, Phys. Rev. 127, 32 (1962); 127, 51 (1962).
186. G. Leppelmeier and E. Hahn, Phys. Rev. 141, 724 (1966).
187. G. Leppelmeier and E. Hahn, Phys. Rev. 142, 179 (1966).

CHEMICALLY INDUCED POLARIZATION

This field is closely related in formalism to ODMR since the chemical creation of an aligned nuclear or electron spin state corresponds to the preferential intersystem crossing into a zero field sublevel. See also 45, 46.

188. P. Atkins, K. McLauchlan, and P. Percival, Mol. Phys. 25, 281 (1973).

189. J. Pedersen, J. Chem. Phys. 59, 2656 (1973).

190. H. Fischer and G. Laroff, Chem. Phys. 3, 217 (1974).

191. P. Atkins, A. Dobbs, and K. McLauchlan, Chem. Phys. Lett. 25, 105 (1974).

EARLY DOUBLE RESONANCE EXPERIMENTS

In addition to Ref. 1, 2, 3, 4, 59, 60, the following are of interest in relation to ODMR.

192. H. Dehmelt, Phys. Rev. 105, 1924 (1957); 105, 1487 (1957).

193. J. Dodd, G. Series, M. Taylor, Proc. Roy. Soc. (LONDON) A273, 41 (1962).

194. J. Dodd, W. Fox, G. Series, and M. Taylor, Proc. Phys. Soc. 74, 789 (1959).

195. D. Hanson, Chem. Phys. Lett. 12, 65 (1971).

TRIPLET STATE KINETIC PARAMETERS

In addition to the methods described in Ref. 64-70 the following contain alternative procedures.

196. T. Azumi and Y. Nakano, J. Chem. Phys. 50, 539 (1969).

197. M. El-Sayed and O. Kalman, J. Chem. Phys. 52, 4903 (1970).

198. M. El-Sayed, J. Chem. Phys. 54, 680 (1971).

199. M. El-Sayed and J. Olmsted III, Chem. Phys. Lett. 11, 568 (1971).

200. J. Schmidt, W. Veeman, and J. van der Waals, Chem. Phys. Lett. 4, 341 (1969).

201. D. Antheunis, J. Schmidt, and J. van der Waals, Chem. Phys. Lett. 6, 255 (1970).

202. J. Schmidt, D. Antheunis and J. van der Waals, Mol. Phys. 22, 1 (1971).

203. C. Winscom and A. Maki, Chem. Phys. Lett. 12, 264 (1971).

RELAXATION OF EXCITED TRIPLET STATES, T_1 MEASUREMENTS

204. P. Fischer and A. Denison, Mol. Phys. 17, 297 (1969).

205. L. Hall, D. Owens, and M. El-Sayed, Mol. Phys. 20, 1025 (1971); 22, 361, (1971).

206. L. Sims, A. Guzzo, and A. Denison, Chem. Phys. Lett 5, 370 (1970).

207. J. Marvani, Chem. Phys. Lett. 7, 29 (1970).

208. J. Wolfe, Chem. Phys. Lett. 10, 212 (1971).

209. R. Hochstrasser and P. Prasad, Chem. Phys. Lett. 9, 113 (1971).

210. U. Konzelmann and M. Schwoerer, Chem. Phys. Lett. 18, 143 (1973).

COHERENCE EXPERIMENTS IN THE TRIPLET STATE

In addition to Refs. 21-24, 68 and 72, the following coherence experiments have been done in the triplet state.

211. C. Van 't Hof, J. Schmidt, P. Verbeek, and J. van der Waals, Chem. Phys. Lett. 21, 437 (1973).

212. H. Brenner, J. Brock, C. Harris, J. Chem. Phys. 60, 4448 (1974).

213. C. Harris, R. Schlupp, and H. Schuch, Phys. Rev. Lett. 30, 1019 (1973).

214. W. Breiland, H. Brenner, and C. Harris, J. Chem. Phys. 60, (1974).

TCB CRYSTAL STRUCTURE

215. C. Dean, M. Pollak, B. Craven, G. Jeffrey, ACTA. Cryst. 11, 710 (1958).

216. G. Gafner and F. Herbstein, ACTA. Cryst. 13, 702 (1960).

217. F. Herbstein, ACTA. Cryst. 18, 997 (1965).

218. T. Strand and H. Cox, Jr., J. Chem. Phys. 44, 2426 (1966).

HELIX DESIGN (SEE REF. 63)

219. M. Pearlman and R. Webb, Rev. Sci. Instr. 38, 1264 (1967).

220. F. Volino, F. Csakvary, and P. Servoz-Gavin, Rev. Sci. Instr. 39, 1660 (1968).

TECHNICAL INFORMATION DIVISION
LAWRENCE BERKELEY LABORATORY
UNIVERSITY OF CALIFORNIA
BERKELEY, CALIFORNIA 94720